

Fluorescence microscopy of colloidal silver nanoparticles immobilized
on a glass surface: Emission spectra, power-law blinking and memory
in the intermittent emission intensity.

Diplomarbeit

zur Erlangung des akademischen Grades
Diplom-Physiker

vorgelegt von
Christian Bläul

geboren am 2. 1. 1982 in Dresden

Institut für Biophysik
Fachrichtung Physik
Fakultät Mathematik und Naturwissenschaften
der Technischen Universität Dresden

2009

1. Gutachter: Prof. Petra Schwille
 2. Gutachter: Prof. Lukas Eng
- Supervisor: Dr. Eugene Petrov

Datum des Einreichens der Arbeit: 23. 4. 2009

Abstract

In this study, the phenomenon of emission blinking, previously observed for semiconductor nanocrystals and organic dye molecules, was investigated for metal nanoparticles. In particular, it was found that the duration of successive on- and off-states are not random but rather show positive auto-correlation; at the same time, anti-correlation between on-durations and successive or preceding off-durations was observed. The distribution of on-durations were found to closely follow a power law, $P(\tau_{\text{on}}) = \tau_{\text{on}}^{-m_{\text{on}}}$, whereas the off-durations τ_{off} showed a power law with an exponential cut-off, $P(\tau_{\text{off}}) = \tau_{\text{off}}^{-m_{\text{off}}} \exp(-\tau_{\text{off}}/\theta_{\text{cut}})$. It was confirmed that ergodicity-breaking does not allow to use fluorescence correlation spectroscopy to study the emission blinking of Ag nanoparticles. Emission spectra showed a broad structureless fluorescence continuum with superimposed surface-enhanced Raman scattering peaks whose intensity and position depended on the particular chemical composition of the local environment.

Kurzfassung

In dieser Diplomarbeit wurde das pulsierende Emissionsverhalten, bisher bei Quantenpunkten und organischen Farbstoffmolekülen beobachtet, bei Ag-Nanopartikeln untersucht. Es wurde festgestellt, dass die Dauer von aufeinander folgenden An- und Aus-Zuständen nicht zufällig, sondern positiv autokorreliert ist. Außerdem sind die Dauer eines An-Zustands mit der des nächsten Aus-Zustands antikorreliert, und umgekehrt. Während die Wahrscheinlichkeitsverteilung $P(\tau_{\text{on}})$ der Länge von An-Zuständen einem Potenzgesetz $P(\tau_{\text{on}}) = \tau_{\text{on}}^{-m_{\text{on}}}$ folgte, zeigten die Längen von Aus-Zuständen ein Potenzgesetz mit einem zusätzlichen exponentiellen Abfall, $P(\tau_{\text{off}}) = \tau_{\text{off}}^{-m_{\text{off}}} \exp(-\tau_{\text{off}}/\theta_{\text{cut}})$. Es wurde bestätigt, dass die Nicht-Ergodizität des Systems es nicht erlaubt, Fluoreszenz-Korrelations-Spektroskopie zur Untersuchung des dynamischen Emissionsverhaltens von Silber-Nanopartikeln zu nutzen. In Emissionsspektren wurde ein breites Fluoreszenzband gefunden, auf dem sich schmale Raman-Bänder befanden, die wahrscheinlich von Molekülen aus der lokale Umgebung erzeugt und durch die Partikeloberfläche verstärkt wurden.

Contents

1. Introduction	7
1. Brief overview on the research of silver nanoparticles	7
2. Emission properties of silver nanoparticles	7
3. Goals of the work	9
2. Fundamentals	10
1. Photophysical concepts	10
2. Statistical concepts	12
3. Experimental techniques	15
3. Materials and methods	18
1. Preparation of colloidal silver nanoparticles	18
2. Sample preparation	18
3. Optical setup for wide-field experiments	19
4. Confocal setup	22
5. Fluorescence lifetime measurements	23
6. Computer simulations	24
7. Experimental data processing	25
8. Power-law exponent estimation	29
4. Sample characterization	35
1. Transmission electron microscopy	35
2. Scanning electron microscopy	36
3. Optical absorption	36
4. Optical microscopy	38
5. Emission spectra and excited-state lifetimes	41
1. Emission spectra of Ag samples	41
2. Fluorescence decay kinetics	45
6. Dynamic emission behavior	48
1. Power law blinking	48
2. Non-constant average state durations	52
3. Reversible intensity decay upon CW excitation	54
4. Fluorescence behavior in different environments	57
5. Experiments with spectrally resolved detection	58
7. Patterns in silver nanoparticle blinking	62
1. Fluorescence correlation spectroscopy of Ag nanoparticles	62
2. On- and off-duration correlations (memory)	67
8. Conclusions	72

Abbreviations and notations used in this work

AOTF	Acousto-optical tunable filter
ACF	Autocorrelation function
CCD	Charge-coupled device
CDF	Cumulative distribution function
CW	Continuous wave
EMCCD	Electron-multiplying charge-coupled device
FWHM	Full width, half maximum
HPLC	High performance liquid chromatography water
MLE	Maximum likelihood estimator
NA	Numerical aperture
NP	Nanoparticle
PSF	Point spread function
PVP	Polyvinylpyrrolidone, $(C_6H_9NO)_n$
QD	Quantum dot
SEM	Scanning electron microscopy
SERS	Surface-enhanced Raman spectroscopy
$\langle \xi \rangle$	Time average of $\xi(t)$, $\langle \xi \rangle = \frac{1}{T} \int_0^T \xi(t) dt$, where T is the observation time
$\bar{\xi}$	Ensemble average of ξ , $\bar{\xi} = \frac{1}{N} \sum_{i=1}^N \xi_i(t)$, where N is the size of the ensemble

1. Introduction

Preliminary results of this work have been published in:

E. P. Petrov, C. Bläul and P. Schwill (2009). Memory in blinking dynamics of silver nanoparticles. In V. E. Borisenko, V. S. Gurin and S. V. Gaponenko, editors, *Physics, Chemistry and Application of Nanostructures*. World Scientific, Singapore.

1.1. Brief overview on the research of silver nanoparticles

In this section, an overview of the field of this thesis is given; the mentioned concepts will be explained in more detail later.

Silver nanoparticles sized from a few to tens of nanometers show interesting optical properties: They have been used decades for Raman spectroscopy of single organic molecules, because these nanoparticles enhance the extremely weak Raman signal of neighboring molecules by several orders of magnitude, via the phenomenon known as surface-enhanced Raman scattering (SERS) [KneippK97, KneippK99]. SERS is routinely used in vibrational spectroscopy.

Silver nanoparticles can also enhance the emission intensity of commonly used dyes by a factor of a few tens, reduce the fluorescence lifetime, increase quantum yields, and increase photostability [Larkin04, Lakowicz06, Chowdhury07]. These effects appear to be due to two reasons, namely, the increased fields near the particles induced by the incident light and coupling of excited-state fluorophores to surface plasmons in the metal particle, which in turn radiates to the far-field [Lakowicz05].

Silver nanoparticles with sizes of about 1 nm and smaller were found to be strongly fluorescent by themselves [Rabin98, Ievlev00, Richards08, Sengupta08]. This makes silver nanoparticles a tool to answer biological questions. Protein-silver-complexes are useful to track proteins [Maliwal03, Narayanan08] and can be employed for imaging of structures and functions of cells [Biju08, YuJ08, Narayanan08]. Contrary to conventional dyes, silver nanoparticles can be detected in both light and electron microscopy. In [LeeK07], 12-nm particles were detected by their fluorescence within living zebrafish. Larger nanoparticles (20-50 nm) can act as a sensor via the efficient collection of Raman and hyper-Raman vibration spectra of specific target molecules in cells [KneippJ06], even in very low concentrations.

On the other hand, recent studies show that Ag nanoparticles can present serious danger to living organisms by causing cytotoxicity, genotoxicity, and cell cycle arrest [AshaRani09] as well as ecotoxicity [Yang09]. This is because without capping, silver nanoparticles can bind covalently to specific lipids, amino acids [Wang05] and to DNA [Yang09]. It was observed that silver nanoparticles were internalized by the cell [LeeK07], lowered the DNA replication fidelity [Chia09] and produced reactive oxygen species [AshaRani09].

1.2. Emission properties of silver nanoparticles

Bulk metals are known to emit weak light caused by electron-hole recombination [Mooradian69] and optically excited electron plasma [Steinmann63]. Silver nanoparticles sized tens of nanometers show

comparably strong emission on their own [Schwille01a, Andersen04], observable with a microscope eyepiece. It was found that the photoemission wavelength is independent of the silver particle size, while the intensity increases sharply with decrease of particle size [Smitha08]. This emission is commonly attributed to fluorescent few-atom Ag_n [Peyser01] clusters or dyes adsorbed to the nanoparticle surface [Futamata07]. The excitation of either can then be transferred to the nanoparticle, where a plasmon is generated that can decay [Lakowicz05, Chowdhury07, Chowdhury08]. .

Usually, the observed emission is time-dependent. Intensity fluctuations upon continuous-wave (CW) excitation are called blinking in this work. Its origin and properties are still not properly understood. In silver systems, blinking was first seen as an intrinsic property for silver island films covered with a layer of AgO [Peyser01]. Later, blinking was studied for individual nanoparticles [Wu08]. Silver nanoparticles were found to fluoresce when grown in polymers such as DNA [Richards08, Sengupta08] or in PVP [Slistan08]. In these surroundings and when kept in oxygen-free environment, silver nanoparticles emit without blinking.

Regarding the blinking phenomenon in silver nanoparticle emission, the explanations given so far include

- (a) Photochemical generation and destruction of fluorescent oligomeric silver atom clusters with different emission colors, from silver oxide [Peyser01, Jacobson05].
- (b) Slow diffusion of an emitting adsorbate on the nanoparticle surface into and out of regions of high electric field enhancement [JiangJ03, Futamata04].

The explanation (b) does not seem plausible because it was found that the emission becomes time-independent in the absence of oxygen [Jacobson06] – it is not obvious how oxygen should interfere with the diffusion. Other than that, a specific molecule adsorbed to the nanoparticle surface does change the observable Raman spectrum, but not the blinking properties [Andersen04]. Blinking was also observed, when no specific molecule was present in the silver particle’s immediate surroundings, pointing towards a mechanism intrinsic to the silver nanoparticles, or alternatively, a photochemically generated emitting molecule or cluster containing Ag. Also, even in experiments with nanoparticles surrounded by molecules at concentrations of hundreds of molecules per silver particle, blinking of the emission was observed [Bjorneld00]. One may expect that, at high concentrations blinking disappears because at high concentration, there is almost always an analyte molecule present in positions with a huge electric field - which is not what was observed.

It has been found experimentally and confirmed theoretically that the local electromagnetic field changes dramatically from point to point on a silver particle or island film surface [Weitz83, Shalaev98, Xu00, Futamata07]. As a consequence, the laser energy is localized in tightly confined spots close to sharp metal peaks or cracks between adjacent particles.

It was found [Maruyama04, Emory06] that Ag nanoparticles that were blinking at room temperature were, when cooled to 77 K, either emitting with a constant intensity or remained dark, suggesting that diffusion of an oligomeric Ag cluster, or chemical reactions play a role. According to [Emory98a], nanoparticles with a given size predominantly emit in a certain wavelength range. In fact, emission wavelength, excitation wavelength and particle size were found to be directly proportional, therefore emphasizing the importance of surface plasmons for the emission. Therefore, for a

given excitation wavelength of 514 nm, high emission levels were only observed for a few percent of silver nanoparticles [Emory98b].

1.3. Goals of the work

The goal of this work was to study the emission properties of colloidal silver nanoparticles deposited on glass substrates. To archive this goal, several problems had to be solved: First, nanoparticles had to be prepared and characterized. Second, appropriate setups had to be chosen and adjusted for spectral analysis, electron microscopy, dynamic emission properties and fluorescence lifetime properties. Later, methods of data analysis had to be developed, to identify single nanoemitters and study their intensity fluctuations.

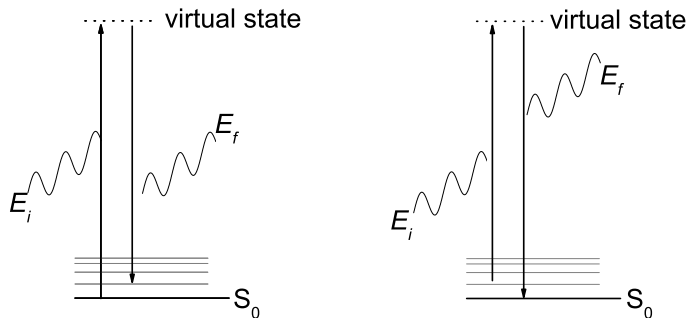


FIG. 1: Illustration of inelastic scattering. The lower horizontal lines represent the ground state S_0 and several vibrational energy states of a molecule. The incoming photon has an energy E_i , the molecule gains an vibrational energy $E_i - E_f$. The process shown in the left is Raman scattering, whereas anti-Raman scattering is shown in the right.

2. Fundamentals

2.1. Photophysical concepts

2.1.1. Luminescence

This general term is used to describe light emission which is not directly related to heat. For this work, the processes fluorescence and chemiluminescence are important.

2.1.2. Raman scattering

Raman scattering is an inelastic optical process during which electromagnetic energy is transferred to or from a molecule. A molecule is Raman-active, if it has bonds that, when bent or stretched, change the polarizability of the molecule. The polarizability determines how much the induced dipole moment of a molecule changes when an external field is applied. The scattering probability, often expressed via the cross section, is proportional to the square of the induced dipole moment.

When a molecule absorbs a photon (energy E_i), one of its electrons is excited to a higher energy state. In case of Raman scattering, this state is said to be virtual because it can take any value, whereas real states for bound electrons have discrete energies. Because the excited state for Raman scattering is virtual, a molecule can scatter any incident electric field, independent of its frequency. After less than a picosecond, the electron relaxes to a real state, and the molecule emits light with a frequency corresponding to the energy difference between the initial and the final real state, as is shown in Fig. 1. If the molecule ends up in a higher vibrational state than before absorbing the photon, the process resulting in a lower-energy (red-shifted) photon is called Stokes scattering. The opposite, called anti-Stokes scattering and is much less pronounced at room temperature.

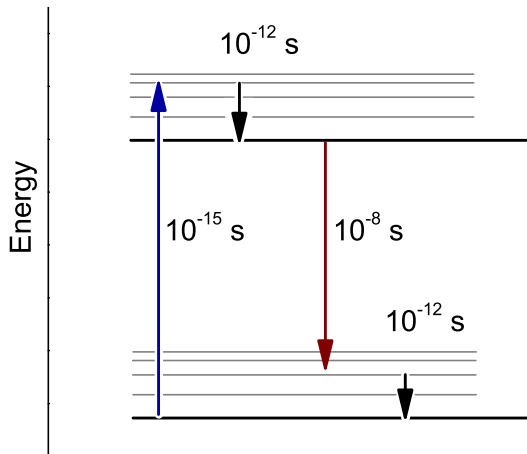


FIG. 2: (a) Simplified Jabłoński diagram. The lower stack of horizontal lines presents the ground state with vibrational levels, the upper stack presents the first excited singlet state with its vibrational levels. Arrows show the four processes belonging to one fluorescence cycle; the typical duration of each process in seconds is written above each arrow. The processes are, from left to right (i) photon absorption, (ii) vibrational relaxation, (iii) fluorescence (iv) vibrational relaxation.

Whereas classical Raman spectroscopy requires rather large molecular ensembles due to the extremely low cross-section (typically $10^{-30} - 10^{-25} \text{ cm}^2/\text{molecule}$ [KneippK99]) of the scattering process, metal surfaces can enhance the scattering intensity [Pettinger81, Fleischmann81]. The experimental application of this phenomenon is called surface-enhanced Raman spectroscopy (SERS), which is sensitive enough for single molecule experiments [KneippK97, Nie97].

2.1.3. Fluorescence

When a molecule absorbs a photon, it is electrically excited. Fluorescence is the spontaneous emission of photons accompanying the relaxation of a molecule, typically from its first excited singlet state S_1 to the ground state S_0 [Valeur06]. A molecule showing fluorescence is called fluorophore. Usually, fluorophores have delocalized electron clouds such as from double bonds, because these have a high absorption cross section. Another system with a high absorption cross section are semiconductor nanocrystals, so-called quantum dots (QDs).

As can be seen in Fig. 2, each electronic state of a molecule consists of additional vibrational levels. When a molecule absorbs light, one of the molecules' electrons is promoted to a higher energy state within $\approx 10^{-15} \text{ s}$. Usually, the new state is a both electronically and vibrationally excited one. After undergoing vibrational relaxation to the first excited state within $10^{-13} - 10^{-11} \text{ s}$, the molecule may emit a quantum of fluorescent light. This usually takes on average $10^{-10} - 10^{-7} \text{ s}$. Other, non-radiative process may change the state of the molecule, such as quenching, intersystem crossing or

internal conversation. These processes reduce the quantum yield, the ratio of the number of absorbed photons to emitted photons.

Silver nanoparticles sized in the order of tens of nanometers are not expected to show significant fluorescence [Kreibig95]. Therefore, unexpectedly bright emission from silver particles attracted much attention.

2.1.4. Plasmons

When exposed to an oscillating electric field, electrons in the conduction band of nanometer-sized metal particles will be driven to oscillate with the same frequency [Link00]. There are two main resonances, surface and volume ones, at which all conduction-band electrons are collectively excited, leading to an in-phase oscillation with the external driving field. Oscillations of free electrons are called plasmons and will continue to exist even after the excitation ceases, due to the restoring force of the net charge of the electrons displaced against the positively charged lattice. Plasmons can decay both by emitting photons at the plasmon's frequency and by heating the material by creating phonons.

Optical extinction of metallic colloids is due to absorption and scattering, whose relative contribution depends on the metal, its size and shape and its surroundings, as can be calculated using Mie theory [Kreibig95]. The scattering component of the extinction is a measure of the extent to which the plasmons can radiate into the far-field [Lakowicz05]. Consider the presence of a fluorophore within a few nanometers distance to a colloid's surface: according to the radiating plasmon (RP) model, the absorption of the colloid will cause fluorescence quenching and the scattering component will cause enhanced fluorescence [Lakowicz05, Horimoto08].

2.2. Statistical concepts

2.2.1. Probability distributions

A distribution describes how likely a certain value of a random variable ξ is. Note that ξ can take values of a certain set; in the following it is assumed that ξ is a real number from the interval $\xi_{\min} \leq \xi \leq \xi_{\max}$. There are several mathematically equivalent ways to define a specific distribution, for example (i) the probability density $P(\xi)$, with the normalization condition $\int_{\xi_{\min}}^{\xi_{\max}} P(\xi) d\xi = 1$ or (ii) the cumulative distribution $F(x) = \int_{\xi_{\min}}^x P(\xi) d\xi$, with $F(\xi_{\min}) = 0$ and $F(\xi_{\max}) = 1$.

2.2.2. Histograms

Histogramming has been used for decades to visualize an experimental data set x . Let $a = \min(x)$ and $b = \max(x)$. Then the data is grouped into bins with intervals

$$\mathcal{T}_i = [e_i, e_{i+1}) = \{x \mid e_i \leq x < e_{i+1}\}, \quad (2.1)$$

defined by a set of bin edges e_i . In order to use the histogram as a rough estimator for the probability density, the discrete number of elements in each bin i has to be divided by $n(e_{i+1} - e_i)$. This estimator is parametric, because it depends on the positions of the edges e_i . Their choice has significant influence on the shape of the histogram and on the possibility to use a histogram as a reliable probability density

estimator [Izenman91]. In this work, unless noted otherwise, the distance between consecutive bin edges, the bin size, was chosen according to the Freedman-Diaconis rule [Freedman81]

$$e_{i+1} - e_i = 2\text{IQR}(x)n^{-1/3}, \quad (2.2)$$

with IQR being the inter-quartile range (the absolute difference of the two values of ξ that satisfy $F(\xi) = 0.75$ and $F(\xi) = 0.25$) and n the number of elements in x .

2.2.3. Power laws

Later in this work, a special probability distribution, known as the power law distribution, will appear. It can be written in the following form:

$$P_m(\xi) = \frac{\xi^{-m}}{A(m)} \quad (2.3)$$

where $m > 0$ is the parameter (“exponent” or “scaling parameter”) of the power law. In case of $m > 1$, the distribution can only be defined for $0 < \xi_{\min} \leq \xi$ since in case where $\xi_{\min} = 0$, normalization is impossible. $A(m)$ is a normalization constant that ensures $\int_{\xi_{\min}}^{\xi_{\max}} P_m(\xi)d\xi = 1$. For the case $m = 1$, both a lower limit ξ_{\min} and an upper limit ξ_{\max} are needed, whereas for $0 < m < 1$, only an upper limit for ξ needs to be introduced, since it is necessary that $\xi \leq \xi_{\max} < \infty$ in order to provide that $P_m(\xi)$ is a probability distribution.

An important property of power law distributions with $m > 1$ is that they are characterized by the so-called heavy tails, therefore large ξ appear frequently in data sets drawn from power law distributions. A heavy-tailed distribution has a significant amount of probability far away from the most probable value—the ξ for which $P(\xi)$ is maximal. For a power law distribution with an exponent $1 < m \leq 2$, even though most numbers ξ drawn from $P_m(\xi)$ are very small, the infrequently drawn large numbers lead to a diverging mean $E[\xi] = \int_{\xi_{\min}}^{\infty} \xi P_m(\xi)d\xi$.

In this work, a power law distribution will be used to model the distributions of time intervals, during which nanoparticle emits light (on-duration) or stays dark (off-duration).

2.2.4. Stochastic processes

When investigating a system, one often observes the change of a physical quantity $f(t)$ over time. In the context of this work, such a quantity will be the emission intensity $I(t)$. A stochastic process is a model that describes the probability structure of $f(t)$ [Shiavi07].

2.2.5. Telegraph process

The telegraph process is a continuous-time stochastic process that switches between two distinct values, which in this work will be used to model the on- and the off-intensity of single emitters of a Ag nanoparticle sample. All properties of such a process depend on the two probability distributions that govern the durations of the stay in the on- and off-state.

2.2.6. Averages

A set of several realizations $I_p(t)$, ($p = 1, 2, 3, \dots, N$) of the same stochastic process is called an ensemble. To estimate properties of the process, one can either average of the ensemble,

$$\overline{f(I)}(t) = \sum_p f(I_p(t)),$$

or over time,

$$\langle f(I) \rangle(p) = \sum_t f(I_p(t)).$$

In the examples above, f is an arbitrary function.

In this work, ensemble averages will be taken by averaging the quantity under investigation (usually, time-dependent emission intensity) over a number of emitters detected in the region of interest. This averaging implies an assumption (not necessarily correct), that all statistical properties of these emitters are governed by identical statistical laws.

2.2.7. Autocorrelation function

In this work, several methods of estimating the properties of a stochastic process will be used, the most important being the autocorrelation function (ACF). In its time-averaging variant, it is defined as

$$g(t_{\text{lag}}) \propto \langle (I(t) - \langle I \rangle)(I(t + t_{\text{lag}}) - \langle I \rangle) \rangle \quad (2.4)$$

and can be used to analyze the presence of memory in the signal. Generally, the value at the origin, $g(0)$, contains an additional contribution of uncorrelated noise, which is not present in $g(t_{\text{lag}} \neq 0)$.

2.2.8. Ergodicity

Statistical properties of the process such as the probability density are, in general, a function of t . If they are not, the process is called stationary. For stationary processes, it is meaningful to extract a statistical property (such as the mean) of just one time series and compare it to the respective property of the process, which is called the ensemble average. A stochastic process is said to be ergodic, if the time average converges to the ensemble average [Shiavi07].

In many measurements of time series, a typical time constant of the process is defined by the decay of the autocorrelation function, Eq. (2.4), to some fraction of its maximum, for example $1/2$ or $1/e$. Measurements longer than, say, 100 times that time constant, are assumed to sample the probability space well enough to characterize the underlying probability distribution, so that the ACF has converged well enough to be used as an estimate of its statistical limit.

If the durations τ of random telegraph process are power law-distributed with an exponent $1 < m < 2$, this is not a valid assumption. Because of the heavy tail of this distribution, events τ with a duration of the order of the acquisition time T are likely to occur. Consequently, the mean $\langle \tau \rangle$ will grow with the duration of the experiment, because large τ will dominate the mean [Brokmann03, Schriefl05, Margolin06]. For this distribution, ensemble averaging $\bar{\tau}$ and temporal averaging $\langle \tau \rangle$ do not coincide [Messin01, Margolin06] even for very long measurement times T and very large ensembles.

It is therefore important to discern the two averaging methods, time averaging and ensemble averaging, and all functions that depend on them, such as the autocorrelation function.

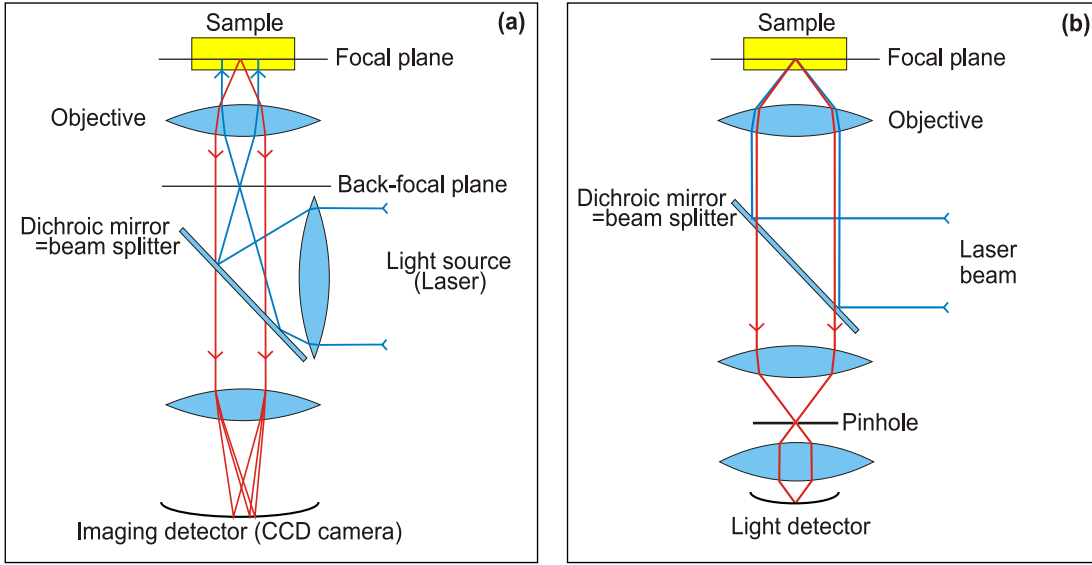


FIG. 3: (a) Illustration of wide-field epi-illumination. (b) Beam path in a confocal setup.

2.3. Experimental techniques

2.3.1. Wide-field light microscopy

A classical transmission microscope uses wide-field illumination, e.g. the whole sample is illuminated by a light source from one side. After scattering by the sample, light is collected by optics on the other side of the sample.

Alternatively, when studying the emission (fluorescence, scattering) by a sample, the sample is illuminated by light coming from the same objective which is used for detection (epi-illumination). In case of the present work, monochromatic laser light was used for illumination. Typically, a dichroic mirror is used to separate excitation and emission light, as can be seen in Fig. 3. In order to obtain optimal contrast, optical emission filters are used to block the remaining Rayleigh scattering from reaching the detector. The detector can be, for example, a human eye or a CCD camera.

The silver nanoparticles imaged in this work were roughly ten times smaller than the wavelength of the light they emit. Therefore they can be approximated by point-like light sources and their image as detected by the CCD chip is not determined by their actual shape, but by the diffraction of the emission light at the optical devices. The spatial pattern detected from a point-like emitter is called point spread function (PSF). Often, a simple approximation of the PSF in the focal plane is used, namely a two-dimensional Gaussian:

$$\text{PSF}(x, y) \propto \exp\left(-\frac{x^2 + y^2}{2\sigma_{\text{PSF}}^2}\right), \quad (2.5)$$

$$\sigma_{\text{PSF}} \approx 0.21 \frac{\lambda_{\text{em}}}{\text{NA}} = 0.21 \frac{\lambda_{\text{em}}}{n \sin \alpha} \quad (2.6)$$

Here, x and y are the Cartesian distances from the optical axis (the axis of symmetry of the objective), NA is the numerical aperture, $NA = n \sin \theta$, a measure of the range of angles the objective accepts light. θ is the maximum convergence semi-angle.

2.3.2. Confocal microscopy

To reach higher resolution and better contrast, only a diffraction-limited spot on the sample is illuminated by a tightly focused laser beam. Likewise, only the scattering and fluorescence emission of the focal spot is detected, because a pinhole is inserted in the detection pathway at the conjugated plane to the excitation pinhole, as is sketched in Fig. 3(b). Mirrors can be used to scan the sample in two spatial dimensions, but at any given time, only one diffraction-limited spot is analyzed.

2.3.3. Videomicroscopy

When studying the collective behavior of the sample, it is advantageous to detect light of a larger area simultaneously. This can be archived with a digital camera, which is a photon detector with many sensitive elements (pixels) placed in a rectangular area, the chip. Photons are converted into electrons that are stored inside the pixels of the chip. After illuminating the chip for some time, the stored electrons have to be detected by electronics in order to transfer the information to a computer. This read-out step is performed by applying a voltage across the chip to drag the electrons from one element to the next, towards an amperemeter whose analog current measurement is converted into a digital signal which is then used. In the following, an image acquired by the camera will be called a frame.

There are several important limitations to versatility of CCDs: (i) Read-out takes time. For this work, a camera with 512x512 pixels was used, and the read-out of the full chip took 31 ms. Experimentally, faster frame-to-frame times desirable. To archive this, one can (a) use the frame transfer mode, which uses a second chip as a temporal storage (b) use only a small region of the chip or (c) treat several pixels as one (binning). Solutions b and c trade temporal against spatial resolution. (ii) Each element contains a capacitor that can hold a certain number of electrons. If this number is exceeded, the additional light signal will either be disregarded or drain into neighboring pixels. The camera used in this could detect up to about 16 000 photons per pixel per frame. (iii) Even though, for the camera used, more than 90% of all photons are converted into electrons, two significant noise sources reduced the image quality, namely dark counts and read-out noise. The manufacturer, Andor, implemented two technical improvements in the hardware used: (a) the chip can be cooled to reduce the noise. For the present work, a temperature of -85°C was used. Additionally, (b) an on-chip electron-multiplier (a tuneable amplification register) was used to dramatically reduce the read-out noise.

2.3.4. Microspectroscopy

To spectrally resolve the image formed by a sample, a spectrometer was coupled to the microscope. Inside of the spectrometer was a reflective grating, that diffracted parallel light into several beams traveling in different directions. The intensity of the beams was detected by a CCD chip. Each of the pixels of the CCD detected light of a certain wavelength range, which is overlapping with the range of the neighboring pixels. The resolution of such a spectrometer depends on the quality of the

grating (regularity, number of grooves) and on the number of pixels that the spectrum is imaged on. One has to account for the spectral and individual sensitivity of the pixels by calibrating the recorded spectrum with a known spectrum.

2.3.5. Fluorescence correlation spectroscopy (FCS)

The temporal correlation of an intensity signal $I(t)$ is a sensitive method to detect changes in the number of molecules or their individual brightness [Schwille01b, Krichevsky02]. In this work, particles were immobilized and diffusion or rotation were not expected. Instead, brightness fluctuations of photophysical or chemical origin were important. The autocorrelation function for an ensemble can be written as

$$g(t, t_{\text{lag}}) = \frac{\overline{(I(t) - \bar{I}(t))(I(t + t_{\text{lag}}) - \bar{I}(t + t_{\text{lag}}))}}{\bar{I}(t) \bar{I}(t + t_{\text{lag}})}, \quad (2.7)$$

with the vertical bar corresponding to ensemble-averaging. In many experimental situations such as fluorophores with constant brightness diffusing in three dimensions, the system is considered to be in equilibrium and the signal is stationary and ergodic. Then, $g(t_{\text{lag}})$ can also be calculated from a single intensity measurement of sufficient length, using

$$g(t_{\text{lag}}) = \frac{\langle\langle I(t)I(t + t_{\text{lag}}) \rangle\rangle}{\langle I(t) \rangle^2} - 1, \quad (2.8)$$

with $\langle \dots \rangle$ denoting time averaging, by assuming that the process stationary and ergodic.

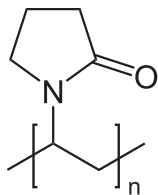


FIG. 4: Polyvinylpyrrolidone, $(C_6H_9NO)_n$

3. Materials and methods

3.1. Preparation of colloidal silver nanoparticles

There exist a number of methods to create nanometer-sized silver particles, including γ -irradiation [Zhu97], electrolysis [Yin03], laser ablation [Mafune00], exploding wires by electric current [Siwach08] and biosynthesis by bacteria [Klaus99] or fungi [Mukherjee01]. Most scientists use the procedure of Lee and Meisel [LeeP82] due to its simplicity and well-known properties. An excellent review on preparation methods and their advantages can be found in [Krutyakov08].

In the present work, nanoparticles were prepared in aqueous solution following the procedure of Lee and Meisel:

$AgNO_3$ (18 mg) was dissolved in 100 mL warm HPLC grade water at $\approx 40^\circ C$, and heated under vigorous stirring, to archive boiling. Upon boiling, a 1% solution of sodium citrate (2 mL) was added rapidly. The solution kept on boiling while being stirred for approximately 90 min, during which the nanoparticles were growing. Subsequently the colloidal sol solution was allowed to cool for 30 minutes in a room-temperature environment. The supernatant of a 3-minute centrifugation step at 13000 g, as suggested in [Hildebrand84], was then filtered using filter paper (#50, Whatman) and filter syringes (0.45 μm , Acrodise) to remove larger aggregates. The resulting stock solution was transparent with a green-yellowish tone. It was kept in darkness at $8^\circ C$ for later use and showed no sign of precipitation.

3.2. Sample preparation

The easiest way to study our Ag nanoparticles appeared to be to let the sol solution dry on a clean coverslide. Depending on the objective, #1 or #1.5 coverslides (Menzel, Braunschweig, Germany) were used. We didn't use any special treatment except for heating on a hotplate (RCT basic, IKA WERKE) for accelerated drying at a temperature of about $65^\circ C$. This way, several droplets were successively dried on the same spot in order to have a higher surface concentration.

For experiments with the amphiphilic polymer polyvinylpyrrolidone (PVP) the following protocol was used: A mixture of Ag nanoparticles and PVP was produced by adding 0.2 g/ml dry PVP

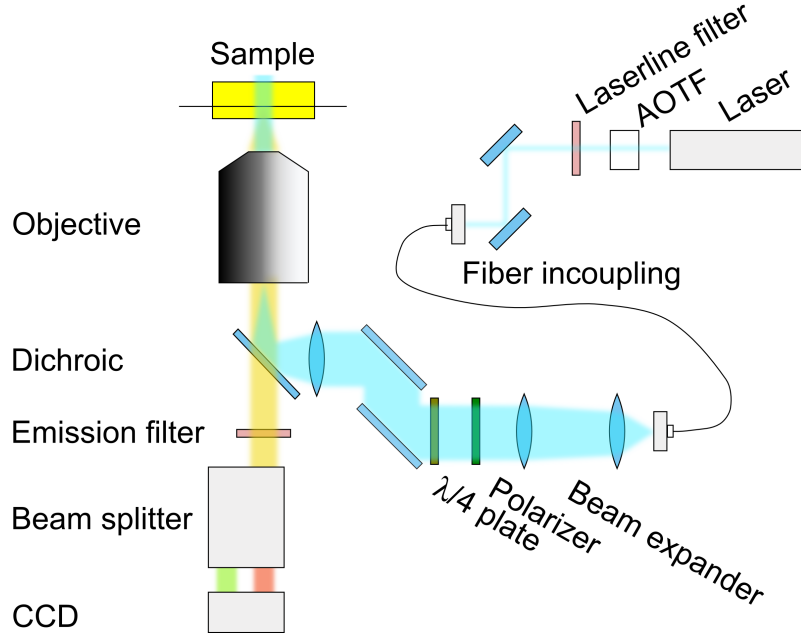


FIG. 5: Illustration of experimental two-color-detection wide-field setup. The sample was excited by laser radiation, the emission signal is split by a beam splitter and focussed on a CCD camera.

(Alfa Aesar, Ward Hill, USA) with a quoted molecular weight of 8000 to the Ag sol stock solution, resulting in a viscous fluid. In a spin-coating deposition procedure, eight droplets of the solution, 2.5 μl each, were successively applied at the coverslide, which rotated at a rate of 7500 rpm.

3.3. Optical setup for wide-field experiments

The $\lambda_{ex} = 488 \text{ nm}$ laser line of an Innova70C-Spectrum multiline Argon/Krypton ion mixed gas laser (Coherent, Cambridgeshire, United Kingdom) was used for sample excitation. The line was selected by an acousto-optical tunable filter (AOTF, AA.MOD.4C, A.A Sa Co., St-Rémy-Lès-Chevreuse, France), which allowed rapid ($< 1 \mu\text{s}$) switching of the relative intensity throughput. After further blocking unwanted laser lines with a OD4 laser line filter (Z488/10, AHF-Analysetechnik, Tübingen, Germany), the light was then coupled into a fiber (Thorlabs, Karlsfeld, Germany), which only transmitted the TEM_{00} mode and allowed for a more flexible setup. A polarizer and a $\lambda/4$ -plate were inserted at this point of the beam path to create circular-polarized light. Subsequently, the beam was expanded by a telescope and, by means of another lens, the light was focused on the back-focal plane of the objective, thereby creating a parallel beam through the sample.

An α Plan-FLUAR 1084-514 1.45 NA 100x oil immersion objective (Zeiss, Oberkochen, Germany) mounted on an Axiovert 200 microscope (Zeiss) was used for most measurements. The filter cube contained a dichroic mirror (495 DCXRV, AHF-Analysetechnik) and a Raman RazorEdge 488 emission filter (AHF-Analysetechnik) to separate the laser light from that emitted by the sample at longer wavelengths, which was collected by the same objective. The microscope had a port to

which a peltier-cooled Andor iXon3 DU897E EMCCD camera (Andor Technology, Belfast, Northern Ireland) with 512x512 pixels was attached. The software package Solis (Andor) was used to acquire videos that were subsequently analyzed using dedicated software written in Matlab (The MathWorks, Natick, USA).

Optionally, a A8509 beam splitter (Hamamatsu Photonics, Japan) was inserted into the detection pathway between microscope and CCD to image red and green spectral components simultaneously, as shown in Fig. 5. The beam splitter was aligned so that half of the CCD pixels were imaging the red component, the other half of the signal passing through the green filter. In order to do so, the oil-immersion objective α Plan APOCHROMAT 100x, NA 1.46 (Zeiss) was used, as it had a smaller chromatic aberration than the previously mentioned objective and allowed for simultaneous focusing in the red and in the green channel. The following filters (AHF-Analysetechnik, Tübingen, Germany) were used: 525/50 HQ in the green and 680/100 HQ in the red channel. Due to the fact that the setup was shared with other scientists, a recalibration of the exact channel mapping was necessary after every measurement. This was done by selecting the sub-pixel position of at least 10 particles visible in both channels, first by hand and then by coupled fitting, allowing one image to be turned and stretched relative to the other.

For microspectroscopy experiments, the laser lines at 488.0 and 514.5 nm and matching laser line filters (AHF-Analysetechnik), were used for the acquisition of spectra. An USB2000 fiber spectrometer (Ocean Optics, Florida, USA) was attached to a microscope port. In this configuration, the light emitted from the full field of view was coupled into the fiber via a lens. Usually, only ensemble measurements were performed, due to relatively low sensitivity. An integration time of 1 s per spectrum was used, and several hundreds of such spectra were averaged to improve the signal-to-noise ratio. Spectra of silver samples were corrected for the wavelength-dependent sensitivity of the spectrometer. For this correction, several Alexa dyes were measured with both the USB2000 and a calibrated Fluorolog-3 spectrofluorometer model FL3-22 (Horiba Jobin Yvon).

3.3.1. Excitation power density at the sample

To calculate the excitation power density at the sample, it is crucial to know the area illuminated by the parallel laser beam. A fluorescent layer was applied on a coverslide using an office text marker. This layer proved to be homogeneous on a length scale of millimeters, when imaged with a CCD camera. Inhomogeneities in the image were mainly caused by laser interference, which was insignificantly time-dependent and strongly influenced by minor position changes of the optical components in the setup. The collected fluorescence showed that the laser intensity has an almost flat profile (see Fig. 6). The effective area was measured to be $54.6 \cdot 10^{-6} \text{ cm}^2$. This number was obtained by approximating the profile with an ellipse (axes of 41.2 and 42.2 μm), shown as dashed lines in Fig. 6. The ellipse was found by minimizing the intensity differences of a five-parameter model (two center coordinates, two axes and ellipse intensity) and the profile picture. Note that the intensity distribution in the sample is not cut as in the CCD image shown, but indeed ellipse-shaped, as was observed via the eyepiece. The eyepiece has a field-of-view of about twice the size than the sample area imaged on the CCD. At the sample, the laser power density did not exceed 8 W/cm^2 at the maximum power setting of the laser, $\approx 2 \text{ W}$ optical power integrated over all laser lines.

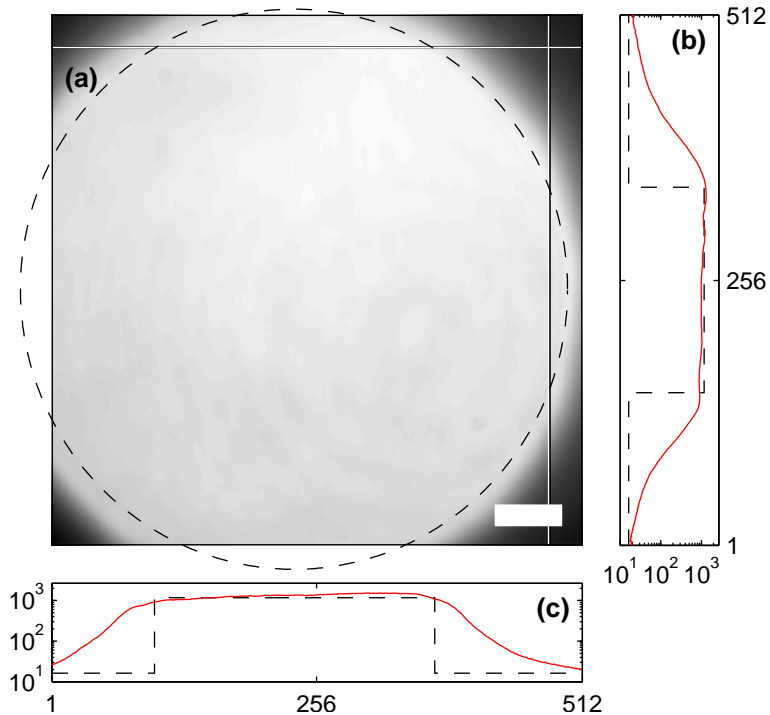


FIG. 6: **(a)** Laser beam intensity profile, measured with a coverslide with a thin fluorescent layer. The image was averaged over 40 s. The bar in the image corresponds to 10 μm . **(b)** Vertical cross section at the line marked in (a). The pixel position is on the x axis, electron counts are on the y axis. The experimental profile is shown in red, the elliptical approximation of equal integrated intensity as dashed black line. **(c)** Horizontal cross section at the line marked in (a). Electron counts are on the x axis, the pixel position is on the y axis.

3.3.2. Excitation light stability

The laser light arriving at the sample did not have a constant power. To quantify the fluctuations, we used a power meter (Newport 841-PE with an attenuated 818-SL head) connected to a computer to record a time series $p(t)$ of the power of at least 10 minutes duration, sampled twice per second. From that series, the ratio of standard deviation

$$\sigma_p = \sqrt{\frac{\sum_{i=1}^n (p_i - \langle p \rangle)^2}{n-1}} \quad (3.1)$$

to the mean

$$\langle p \rangle = \frac{1}{n} \sum_{i=1}^n p_i, \quad (3.2)$$

called the relative root mean square deviation (rRMS), was calculated. The power meter was consecutively fixed at three positions in the beam path. (i) Between the AOTF and the in-coupling to single-mode fiber the stability was $\text{rRMS} = 0.19\%$. The laser power feedback loop was set to an output power of 1 W, the AOTF to 50%. The whole system was switched on 15 minutes before the measurement, therefore the system was probably close but not yet at thermal equilibrium. (ii) Between the telescope and the in-coupling to the microscope, rRMS was 3.37%. This measurement was

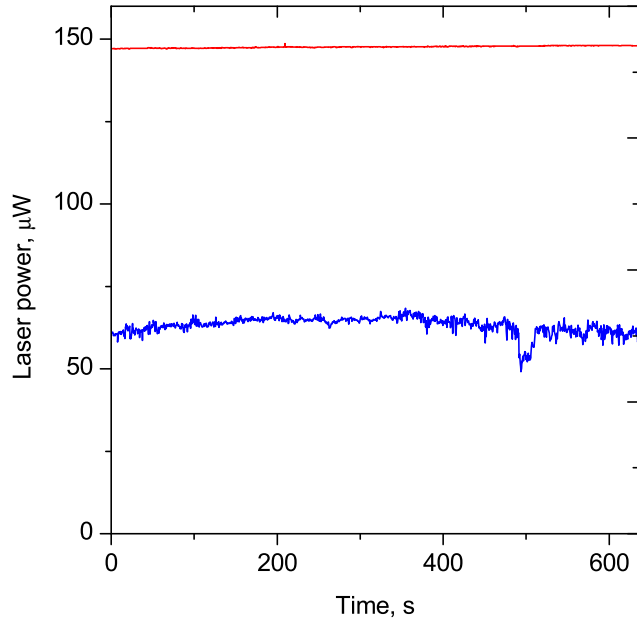


FIG. 7: Laser light power behind the AOTF (—) compared to that of the laser light that passed through the objective (—).

begun 30 minutes after switching the laser on. The large fluctuation amplitude increase was due to the fiber - most likely a result of minimal physical movements that lead to partial interferences. (iii) Above the objective, without immersion oil or sample, the stability was $rRMS = 4.44\%$, as measured one hour after switching the laser on. The even stronger fluctuations can be explained by interference of the main laser light with its weak reflections coming from the microscope body and are shown in Fig. 7.

3.3.3. Determination of the imaging scale

For accurate determination of a physical distance within the sample, the number of pixels per micrometer has to be known. This number can easily be measured by imaging a line grating. For the present work a grating with 600 lines per millimeter (Edmund Industrial Optics) was used. The spatial resolution was $6.4 \text{ pixel}/\mu\text{m}$, as calculated after measuring the distance between 40 lines.

3.4. Confocal setup

We used a laser scanning microscope (LSM 510 ConfoCor 3, Zeiss) to detect the signal of single emission centers on dry silver samples. The water immersion objective C-Apochromat 40x/1.2 W UV-VIS-NIR was used in combination with a pinhole of $70 \mu\text{m}$ diameter, so that the effective area in the focal plane of the confocal laser spot was $1.13 \cdot 10^{-9} \text{ cm}^2$. The 488.0 nm-line of an Argon ion gas laser was used at a power of $1.82 \mu\text{W}$, measured without an objective. No measurements of the size or shape of the excitation volume were performed, but the size can be estimated via Eq. (2.6)

to be in the order of $\sigma_{\text{PSF}} = 85.4$ nm. If the diameter of the excitation area in the focal plane were $4\sigma_{\text{PSF}} = 341$ nm at $1/e^2$ of the maximum intensity, then the power density would be 248 W/cm².

3.5. Fluorescence lifetime measurements

To measure emitter intensity decays on the nanosecond and sub-nanosecond time scales, the time-correlated single photon counting (TCSPC) technique [OConnor84] was used. Since electrons are responsible for all interaction with visible light in a solid state material, a TCSPC experiment tells about the radiative electronic relaxation pathways - in other words some insight into the electronic band structure in the sample. In a TCSPC experiment, the time between the pulse and the first detected photon from many excitation/emission cycles is presented as a histogram to extract the typical lifetime(s) of the emitting system. The detected intensity decay is the convolution of laser pulse shape and the excited system's response to a delta-peak excitation. In a typical fluorescent dye such as Alexa488, this response will be an exponentially decaying function,

$$f(t) = \exp(-t/\tau)$$

with a time constant τ depending on the coupling between the excited state and final energy state of the dye. The electronics used had a fixed number of 4096 channels that corresponded to time bins. Careful selection of the channel width influences both the shortest and the longest detectable arrival times (relative to the pulse). The inverse of the laser repetition rate presents an upper limit of retrievable lifetimes and should be slower than the inverse of the longest expected lifetime. The first two effects are combined to a function called the instrument response (IRF).

Fluorescence decay kinetics were acquired with the confocal microscope using the LSM Upgrade Kit (PicoQuant GmbH, Berlin, Germany). The kit included a 470 nm semiconductor laser, 2 single photon avalanche photodiodes (SPAD) and electronics, that convert the time between pulse and detected photon into a digital number, called a channel. The pulsed laser was controlled by a software, Sepia II. The laser power setting used for the electronic feed back loop was kept fixed to 75%, because a change would influence the shape of the instrument response function. To avoid the pile-up artefact, one has to set the excitation power so that on average, one emission photon (or less) per 100 laser pulses can be expected. The actual power available at the sample was tuned via OD filters and measured with an 841-PE (Newport, Irvine, USA). Without attenuation, measured powers were 1.08 μW or 955 W/cm². Further details of the setup can be found in [Gaertner08]. The IRF was measured by placing a droplet of a strongly scattering liquid, dissolved powdered milk, on the coverslide. During measurements of the IRF, a filter centered at the laser wavelength of 470 nm and a FWHM size of 40 nm ("BP 470/70", AHF-Analysetechnik, Tübingen, Germany) was used, because only the scatter response of the sample can be used to estimate the IRF. All lifetime measurements were carried out using a BP 685/70 bandpass filter (AHF-Analysetechnik) that blocked the potential contribution of Rayleigh scattering.

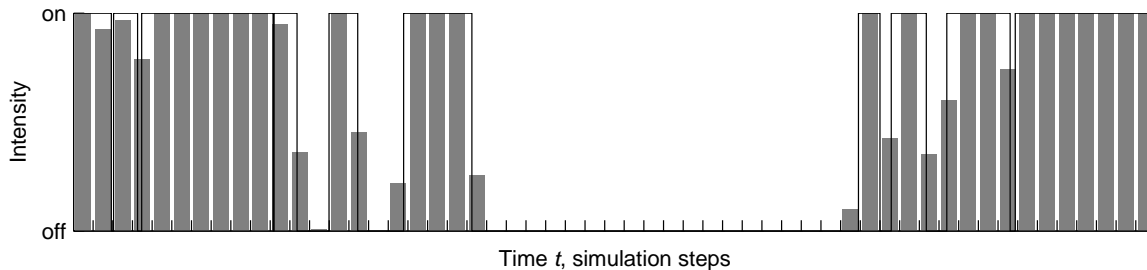


FIG. 8: Simulated continuous-time telegraph process (—) with equal exponential distributions (Eq. (3.3), $t_{\text{decay}} = 3$). For each simulation step, the gray bars correspond to the time fraction spent in the on-state and therefore to the integrated intensity of that time step.

3.6. Computer simulations

The fluctuating intensity $I(t)$ of single emitters was simulated by assuming a simple on/off model. These *in silico* experiments were used to test the reliability of methods that were employed to analyze experimental data such as the power law exponent estimation described in the next section.

To simulate the blinking dynamics, time series $p(t)$ of a continuous-time random telegraph process were generated. This kind of stochastic process jumps between two constant levels, one (on) and zero (off), at random times. The duration $p(t)$ stays at the on-level was drawn from two probability distributions, Ψ_{on} and Ψ_{off} . Two different classes of distributions have been considered, exponentially distributed durations and power law-distributed durations. Let X be a uniformly distributed random number on $[0, 1]$. Then, a random variable Y distributed exponentially,

$$\Psi_x(\tau) = t_{\text{decay}}^{-1} e^{-\tau/t_{\text{decay}}}, \quad (3.3)$$

can be generated by

$$Y = -t_{\text{decay}} \log(X).$$

If both the on- and the off-duration distributions are exponential, then the system will be ergodic [Margolin06]. Power laws $\Psi_x(\tau) = \frac{\tau^{-m_x}}{A(m_x)}$ as discussed on page 13, were generated by [Weisstein06]

$$Y = X^{1/(1-m_x)}.$$

Whereas the telegraph intensity trace $p(t)$ only contains intensities of one and zero, changing at arbitrary times, the binned (integrated) intensity data obtained from CCD measurements of silver nanoparticles $I(t)$ contains arbitrary intensities (within limits), but each frame contains the integrated intensity of a fixed duration. To allow direct comparison with the experimental data, the algorithm has to calculate intermediate intensity levels, that correspond to how long $p(t)$ was in the on-state during that particular time step, as can be seen in Fig. 8. Only the intensity data was used for further calculations. No noise was added to the data simulated with this method.

All computer simulations and data analyses were carried out on a workstation running Windows XP. Unless explicitly specified, dedicated Matlab (MathWorks, Natick, USA) routines, written in the course of the present work, were used for all calculations.

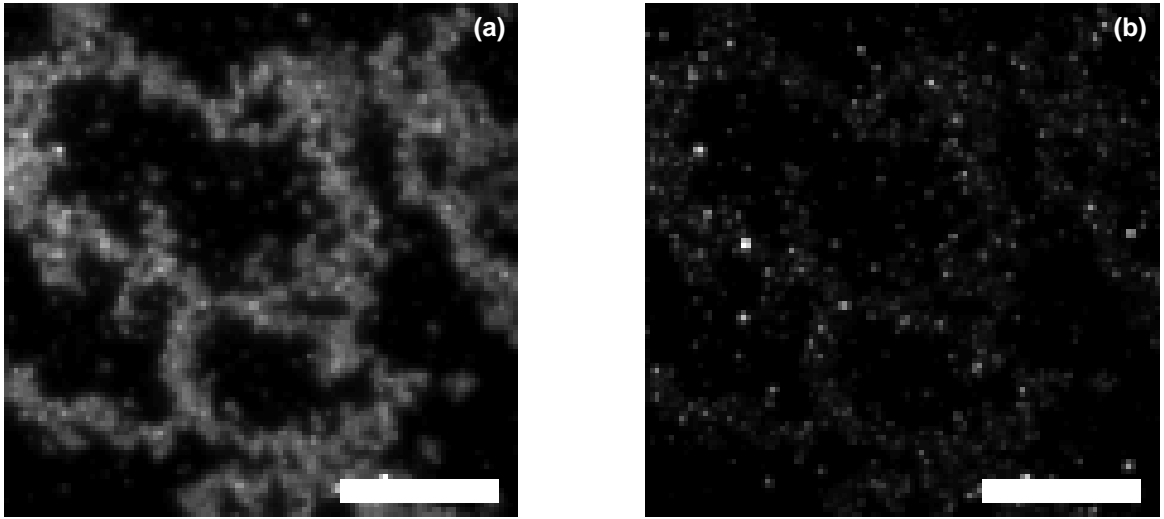


FIG. 9: (a) Mean intensity of a twenty-minute experiment. (b) Standard deviation map of the same experiment. Both are shown on a linear scale

3.7. Experimental data processing

First, the mobility of emitters on dry cover slides was studied, by splitting the recorded data into two-minute slices and averaging the intensity data over these two minutes. For each slice the resulting image was compared to the images of the other slices, using the ability of the human brain to detect slight movements. No such movements were found, in agreement with [Emory06]. There, it was confirmed via repeated atomic force measurements, that the silver nanoparticles are firmly immobilized and do not move or rotate on the time scale of minutes.

3.7.1. Emitter identification

Since the Ag particles were immobilized at the surface of the coverslide, light arriving at each CCD pixel during the course of an experiment can be attributed to one and the same emitter (a particle or a group of particles). Mean and standard deviation of the intensity collected at one CCD pixel over the duration of the experiment were calculated, yielding two pseudo-images (Fig. 9). Local maxima of either were considered to be interesting emitters. The intensity as a function of time of the pixel corresponding to the maxima and its eight direct neighbors was stored. In this work, such an intensity trace will be denoted by $I(t)$. The width of such a region was three pixels, corresponding to 470 nm in the sample focus plane. The diameter of the PSF at a fraction of $1/e^2$ of the maximum intensity can be approximated by Eq. (2.6) to 200 nm at an emission wavelength of 530 nm, therefore a large fraction of the light from the emitter will be detected.

3.7.2. Background subtraction

We assume that the intensity trace can be presented as a sum of three independent components: intensity bursts due to the on-off-emission dynamics of a silver nanoparticle, slowly fluctuating background

and a white noise component due to sources such as photon shot noise (Poisson-distributed), CCD read-out and electron-multiplying noise (both following closely the Gaussian statistic [Schaefer06]).

To separate the intensity bursts from the underlying background, three steps were taken. First, a filtering method developed by Chung and Kennedy [ChungS91] was used. This non-linear filtering allows for background rejection with minimal signal distortion, because it is sensitive to abrupt signal changes and the slowly fluctuating background, whereas it ignores the non-correlated white noise (a discussion on noise source follows in the next section). A moving average filter, which blurs sharp intensity changes, was extended by weights to avoid the blurring:

$$I(t) = \sum_{k=1}^K \frac{1}{k \sum_{k=1}^K (f_k(t) + b_k(t))} \left(f_k(t) \sum_{j=t-k}^{t-1} I(j) + b_k(t) \sum_{j=t+1}^{t+k} I(j) \right)$$

For each data point, the two weights $f_k(t)$ and $b_k(t)$ are calculated by considering the intensities before and after that specific point:

$$f_k(t) = \sum_{j=0}^{M-1} \left(I(t-j) - \sum_{j=t-k-j}^{t-j-1} I(j) \right)^2$$

$$b_k(t) = \sum_{j=0}^{M-1} \left(I(t+j) - \sum_{j=t+k-j}^{t+j-1} I(j) \right)^2$$

The interval to consider is determined by the window size parameters M and K , which have to be chosen empirically. It was found after performing extensive tests that, for the data measured, meaningful results are obtained when M was in the interval of 12...24; K was chosen to be in the interval of 64...120. These numbers had to be varied according to the frame-to-frame time t_{int} , as

$$Mt_{\text{int}} = 0.05 \text{ s}$$

and

$$Kt_{\text{int}} = 1 \text{ s}.$$

As a result of the Chung-Kennedy filtering, an intensity trace that contained both the slowly fluctuating background and the spikes, but not the white noise, was gained and shall be called $I_{\text{CK}}(t)$.

In a following step, the instantaneous spikes in $I_{\text{CK}}(t)$ were removed. Whenever the numerical derivative of $I_{\text{CK}}(t)$ was larger than $L = 8$ intensity units, corresponding to a sudden intensity rise, the values of $I_{\text{CK}}(t)$ after the rise were replaced by the intensity just before the rise, until the signal was again lower or equal to that. The result was subtracted from $I(t)$ to obtain $I_{\text{filt}}(t)$ (Fig. 10 and Fig. 11b), which was then used for determination of on- and off-state durations, as explained below.

3.7.3. Thresholding of intensity traces

One exemplary intensity trace $I(t)$ is presented in Fig. 11, having a noisy baseline with events of much higher intensity. One can assume that the emitter either is in the on-state or does not emit light (off-state) at a given time. In order to discriminate the on- and off-states in the presence of noise, a histogram $H(I)$ of the values in the intensity trace $I(t)$ is used.

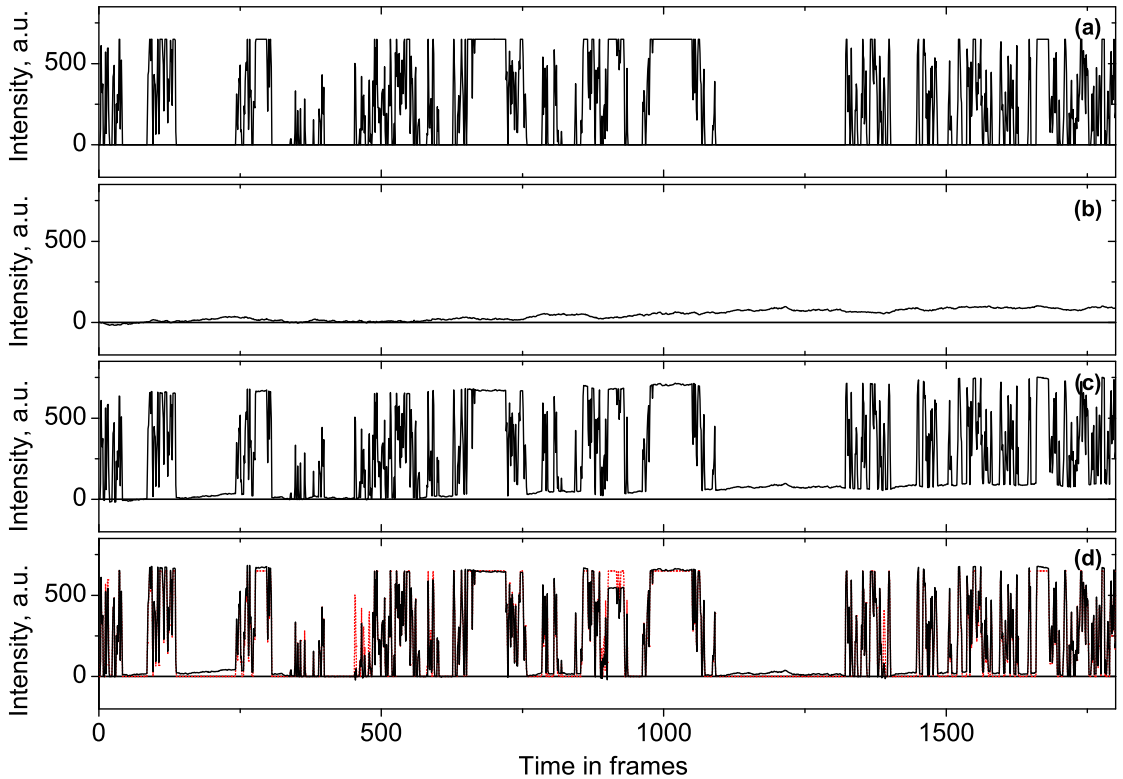


FIG. 10: **(a)** Simulated intensity trace of a power law-driven telegraph process; the amplitude was 650, the off-exponent was $m_{\text{off}} = 1.8$ and the on-exponent was $m_{\text{on}} = 2.0$. **(b)** Background, simulated by an Ornstein-Uhlenbeck process. **(c)** Sum of **(a)** and **(b)** **(d)** Data of **(c)** after applying the background subtraction method explained in the text. The parameters $M = K = 1$ and $L = 78$ were used for the Chung and Kennedy filter [ChungS91].

In most QD experiments, a clear on-intensity level was observed, very well separated from the off-level, which was dominated by noise. This results in a clear dip in the intensity histograms (Fig. 12a), which allows for easy discrimination between the on- and off-levels. This was not the case for the silver samples measured in the present work. It was shown for QD emission, that the dip can be hidden due to the chosen integration time acquisition or histogram bin width [ZhangK06]. Therefore, a range of bin widths was tested, but without identifying a dip. Alternatively, we calculated the boundary between on- and off-state as follows.

The histogram is dominated by frequent low-intensity events and, for many emitters, could be fitted well with a Gaussian (see Fig. 11):

$$H(I) = A \exp\left(-\frac{(I - I_b)^2}{2\sigma_b^2}\right). \quad (3.4)$$

For some emitters, both the visual impression of the threshold and the histogram fit were not convincing. These emitters showed a slowly fluctuating background intensity, for some emitters even with an amplitude comparable to the intensity spikes. In order to be able to analyze these emitters

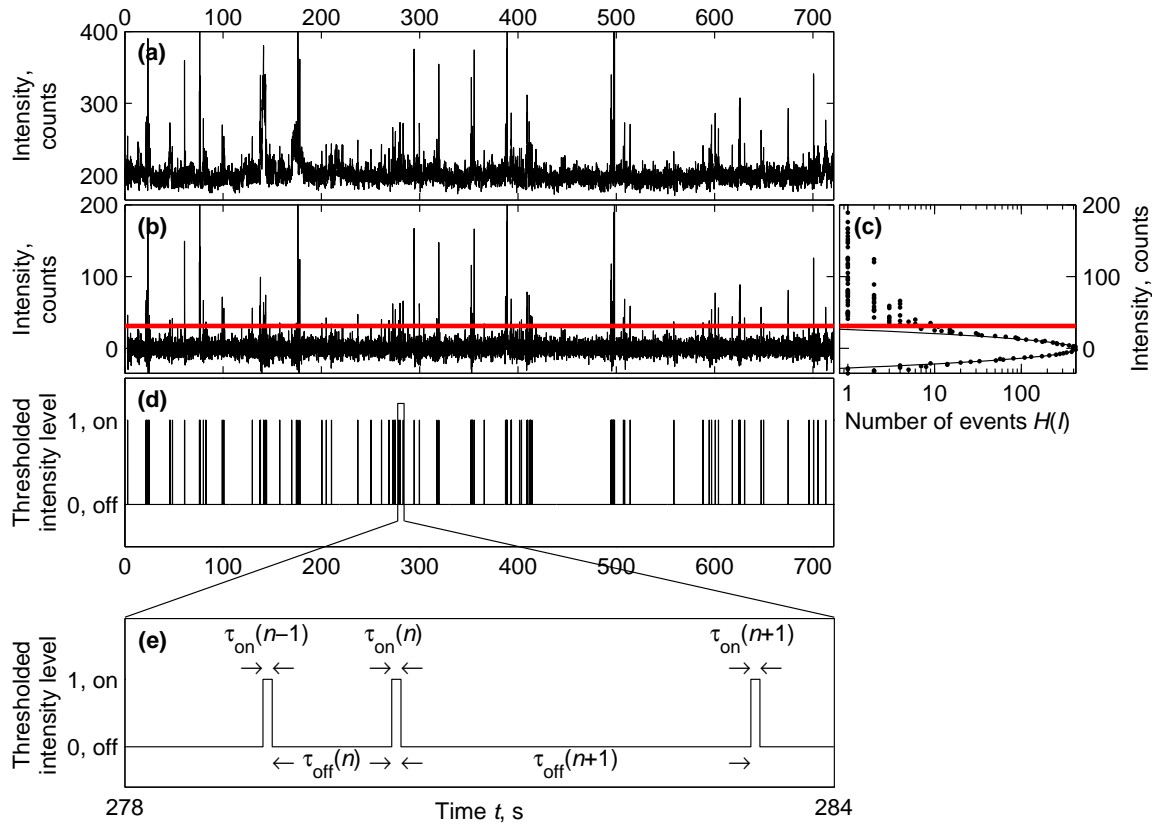


FIG. 11: (a) Typical intensity trace of one emitter, recorded at an image rate of 14 ms, taking an average of 6 images (binning) to improve the signal-to-noise ratio. The laser power was $210 \mu\text{W}$, which corresponds to an excitation power density at the sample of ca. 3.8 W/cm^2 . (b) Intensity trace (a) without the slowly fluctuating background. (c) Frequency histogram of the filtered intensity trace. The Gaussian fit is displayed as a black line, the resulting threshold is drawn in red. The histogram bin width was one count. (d) Result of thresholding: the so-called “telegraph” signal. There are 189 transitions from “on” to “off” in this 12-minute trace. (e) Detail of the telegraph process shown above. Note that the n th off-duration always precedes the n th on-duration.

as well, the slowly fluctuating background was subtracted from the recorded signal of all emitters before calculating the histogram. The effect of this step was checked thoroughly and was found not to influence particle properties such as on-off-duration probability distributions or the “memory” effect described later on. When the background was subtracted as described above, the intensity histogram of about 94% of the emitters could be well fitted to a Gaussian.

The fit yielded the mean level I_b and standard deviation σ_b which were slightly different for each emitter.

A threshold dividing off- and on-events was chosen at $I_b + 4\sigma_b$ on the grounds that the observed blinking properties such as the probability distribution of on- and off-durations did not change for threshold levels from $3\sigma_b$ to $6\sigma_b$, even though the number of events above the threshold decreased for high threshold levels. After thresholding, the on- and off-durations $\tau_{\text{on/off}}(n)$ were calculated. The

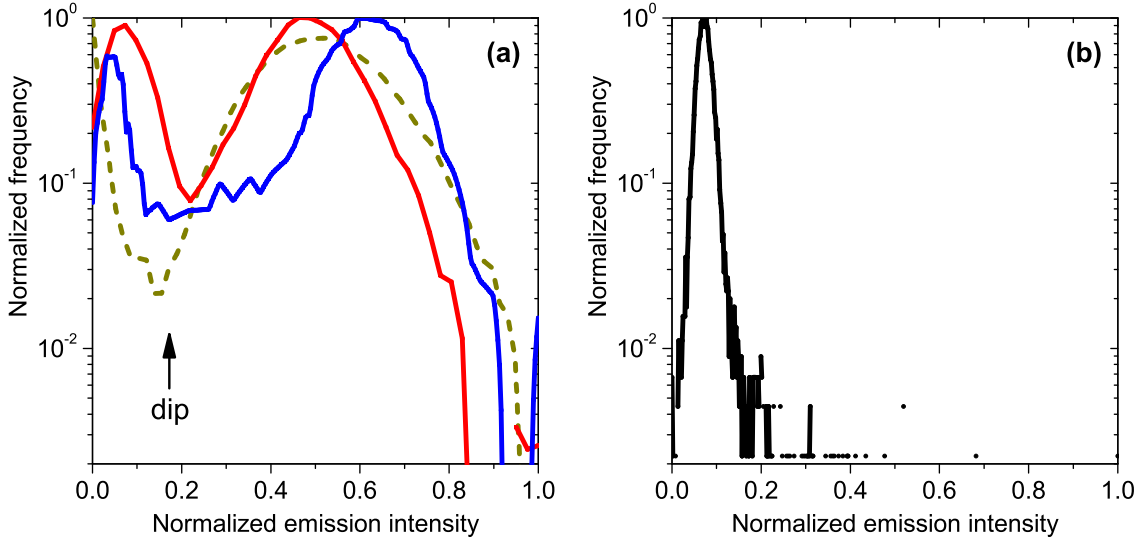


FIG. 12: (a) Intensity histograms of CdSe/ZnS QD emission as found in the literature. The intensity shown has been divided by the observed maximum intensity. (—) [ZhangK06] (—) [YuM06] (---) [Stefani05a] (digitized from the figures in the original publications). (b) Histogram of observed intensities for the fluorescence trace in Fig. 11.

variable n will be called the switching-event number in the remainder of this work. When the signal crosses the threshold twice, n increases by one.

3.7.4. Retrieve two-state data without thresholding

Two alternatives to intensity thresholding were tested: (i) The reliability of change-point estimation using an maximum likelihood estimator (MLE) [West97] was checked using simulated intensity traces with properties close to the experimental conditions. It proved to be less suitable in retrieving the state durations than thresholding, but is, in theory, able to provide sub-frame time resolution. (ii) For a dye, a threshold level for the numerically differentiated intensity time series was defined [Sharaabi05]. This works if all intensity change is sudden. For our experimental data, no reproducible and stable method for the threshold selection was found.

3.8. Power-law exponent estimation

It is crucial to assess the exponents of experimental power laws in order to identify the underlying process. That is not an easy task, because even if the power law is the correct model distribution for a wide range of values, deviations from this dependence may appear in experimental data for very short times due to the acquisition technique and the physics of the system. For very long times the setup may be unstable (for example partial loss of focus) or some intrinsic physical process may introduce an exponential cut-off in the probability distribution.

The following methods can be used for the exponent estimation and will be explained in what follows:

- (a) Fitting of histograms
- (b) Maximum likelihood estimator (MLE)
- (c) Analysis of the probability of the persistence of a state
- (d) Power spectra analysis
- (e) Autocorrelation curve analysis

Methods (a)-(c) depend on two-state telegraph data, whereas (d)-(e) can be calculated directly from the data.

3.8.1. Fit of histogramming-based estimate of $P(\tau)$

When plotted on the double-logarithmic scale, power laws appear as straight lines. Therefore they can be conveniently fitted as

$$\log P(\tau) = -m \log \tau + A, \quad \tau > \tau_{\min} > 0, \quad (3.5)$$

with m and A being free fit parameters. Another possibility is to fit the power law directly, without scaling the axes logarithmically, to the model

$$P(\tau) = A/\tau^m, \quad \tau > \tau_{\min} > 0. \quad (3.6)$$

In both models, A carries no physical meaning and is either defined by the number of events in the histogram, or by the normalization of the probability to 1.

The (non-linear) least squares fitting algorithm was originally developed for experimental data contaminated with Gaussian noise. In this case, the sum of squared residuals

$$R^2 = \sum_i (y_i - f(x_i, m, A))^2$$

will be influenced to the same extent by all data points. In the current context, y_i corresponds to either $\log P(\tau)$ or $P(\tau)$, depending on the model used. Accordingly, x_i can be either $\log \tau$ or τ ; and f is either the right side of Eq. (3.5) or of Eq. (3.6).

If experimental data contains data points with a greater uncertainty than others, the sum R^2 will be strongly influenced by the points with the wider distribution. As a result, the fitting algorithm will yield unstable and irrelevant parameter estimates. In this case, one has to divide each summand of R^2 by weights (proportional to the standard deviation of expected distribution of that data point), that control how much can contribute to R^2 . Since the value of a particular histogram bin is proportional to the number of events, then under the assumption that these events are independent, this number of events is Poisson-distributed. In this case, the estimate of the root-mean-square error of the histogram value $h(\tau)$ is proportional to $\sqrt{h(\tau)}$. The Gaussian distribution is the large-number limit of the Poisson-distribution, hence least-squares fitting is applicable.

It has been shown that exponents derived from non-weighted least-square fits of pure power laws are biased, which is not surprising in the context of the above discussions, and the bias is towards zero [Hoogenboom06]. Only for logarithmically spaced bin edges, the bias decreases for

longer measurements. Therefore, this bin arrangement has been used. In case of logarithmic spacing, histogram bins have different widths. To use the histogram as a density estimator, the value of each bin was divided by the bin width. The number of bins was calculated by applying the Freedman-Diaconis rule [Freedman81] to the logarithm of durations.

For fitting, the horizontal position of a bin cannot be an interval, but has to be pin-pointed. Of the two choices, (i) by taking the mean of the durations in the bin, or (ii) the center of the bin, the latter has been taken in the present work, because it is easier to calculate and proved to be as reliable as the former.

The histogram of durations was then fitted via least-squares with a power law model. This led to an exponent estimate for each simulated particle.

The first bin (corresponding to the shortest duration) was disregarded while fitting, because it proved to contain a large fraction of unresolved state switches (shorter than integration time or simulation time step). Also, in the experimental data, a certain amount of noise might be part of the content of the first bin (see Fig. 13(a)). Likewise, the last bin was disregarded, because it underestimates the probability density due to limited length of the experiment.

3.8.2. Maximum likelihood estimator

Whenever the distribution, from which random numbers X are drawn, is known exactly, a maximum likelihood estimator can be derived. This has been done for power laws [Hoogenboom06] (exponent $m > 1$), but one can also use the standard formulas implemented in statistical packages such as Matlab, by noticing that $1/X$ is distributed as $\beta(m - 1, 1)$, where β is the beta distribution on $[0; 1]$.

Problems appear if the measured distribution $P_{exp}(\tau)$ deviates from the model—the power law. A physical particle having a pure power law behavior for its on-state durations will give experimental durations with a slightly different distribution, as we show via simulations in Fig. 13. The reasons for this are as follows: (i) Experiments have finite total acquisition times T , and, therefore only a subset of the support of the distribution is used. It follows from the lost transitions percentage

$$L_{\%} = \frac{\int_T^{\infty} \tau^{-m}}{\int_{t_{min}}^{\infty} \tau^{-m}} \stackrel{m \geq 1}{=} \left(\frac{T}{t_{min}} \right)^{1-m}, \quad (3.7)$$

that for a fixed exponent $m = 1.5$ and $T/t_{min} = 10^3$ (t_{min} is the time between video frames), 3% of all durations are longer than T and therefore lost.

(ii) Missed short durations will also change the shape of $P_{exp}(\tau)$. For example, if a very short on-state has been missed, the off-histogram will contain two events less in a middle region and one event more in the tail region. Since the physical system will probably be able to change states faster the video frame rate, the thresholding will return one long duration for what might have been two or more shorter states, with a very short state in between. This effect will contribute significantly since, under the assumption of a power law, short durations will happen much more often than longer ones.

(iii) Spurious short-time events such as Poisson counting noise may generate artificial state changes when the threshold method is used.

Therefore, MLE fails to retrieve an unbiased value for m , and was not applied further in this work.

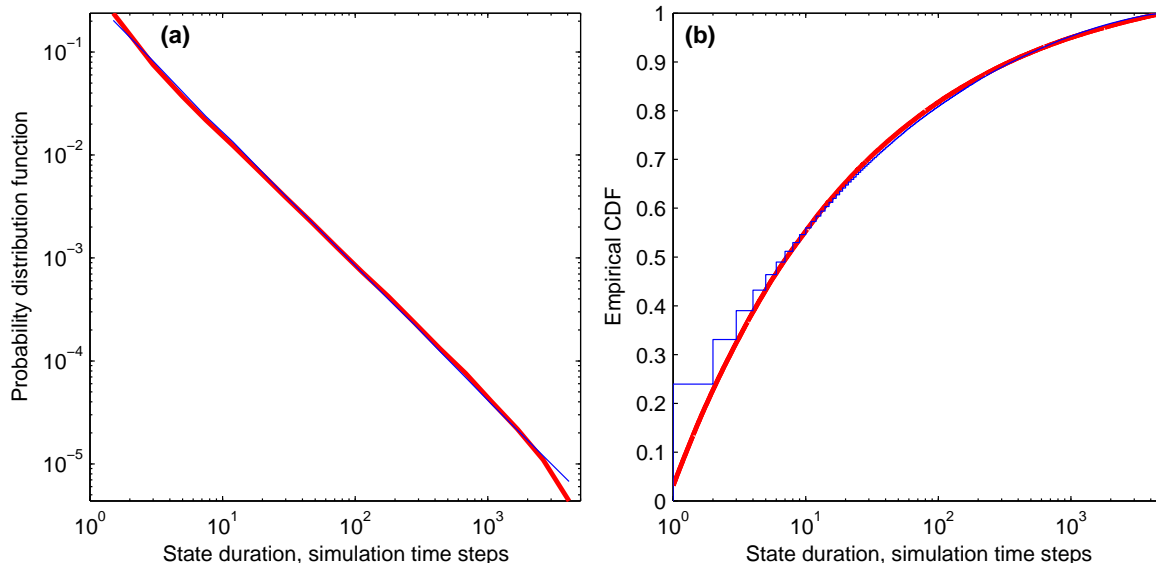


FIG. 13: Deviation from the power law due to intensity integration and thresholding. 80 000 telegraph processes have been simulated. The power law-distributed durations of the processes (—) were real numbers in the interval $(0.032, 5000)$, generated with exponent $m = 1.3$ as described on page 24. Thresholding the integrated “intensity” of the telegraph process, at its average intensity, resulted in a new set of state durations, now integer-valued (—). (a) Approximation of the probability distribution by histogramming. The bin width is logarithmically increasing. The small difference between the curves is enough to stop the maximum likelihood estimator from being meaningful at all. (b) Presentation of both distributions by their cumulative distribution function (CDF).

3.8.3. Persistence of state probability

One can compute the probability $\Pi_1(t, t + t')$, that no state switch event occurs between the experimental times t and $t + t'$, called the persistence probability. In [Bouchaud95], it is shown for power law systems with independent state durations (no memory, see page 67), that

$$\Pi_1(t, t + t') = \Pi_1\left(\frac{t}{t + t'}\right) = \frac{\sin(\pi x)}{\pi} \int_{\frac{t}{t+t'}}^1 du (1-u)^m u^{-m}. \quad (3.8)$$

This quantity can also be calculated for experimental data by dividing the number of particles that didn’t change their state by the total number of measured particles. By overlaying theory and experiment, the exponent estimation is feasible and has been done in [Brokmann03]. The disadvantage is the lack of an analytic expression for Π_1 , which results in the need for specialized dedicated software instead of standard fitting algorithms.

3.8.4. Fit of power spectra

The spectral power density $S(f) = |\mathcal{F}\{I(t)\}|^2$ of the recorded intensity $I(t)$ characterizes the frequency content of the stochastic process. It has also been claimed that the emission intensity of power-law distributed off-duration shows self-similarity [Verberk02]. If $I(t)$ is self-similar in a certain

range of time scales, $S(f)$ will decay as a power law $\sim f^{-\beta_S}$. If both the on- and the off-durations share a common power law exponent m , that is $P(\tau_{\text{off}}) \propto \tau_{\text{off}}^{-m}$ and $P(\tau_{\text{on}}) \propto \tau_{\text{on}}^{-m}$, the power density exponent follows [Pelton04]

$$\beta_S = 3 - m. \quad (3.9)$$

It has been shown for QD emission [Pelton04], that the spectrum can be fitted to a power law $S(f) = Af^{-\beta_S} + B$ for a certain range of frequencies.

We simulated telegraph processes with power law-distributed waiting times (with exponents m_{off} and m_{on}) and calculated their power spectrum. For equal exponents ($m_{\text{off}} = m_{\text{on}}$), the simulated exponent was recovered with an accuracy of about 5%. For unequal exponents $S(f)$ was found to follow a power law, but no expression for the exponent like Eq. (3.9) could be identified. Also, we are not aware of any theoretical treatment of power spectra for emission blinking characterized by different exponents m_{on} and m_{off} , though the following two cases have been considered in the literature: Equal exponents have been investigated in [Godreche01]. Unequal exponents $m_{\text{on}} \neq m_{\text{off}}$ with exponential cut-offs and, most importantly, measurements much longer than the cut-off time constant, were treated in [Verberk03]. There, the Laplace expression

$$g(s) = \frac{1}{s} - \frac{1}{s^2 \tau_{\text{on}}} \frac{1}{(\theta s)^{1-m_{\text{on}}} + (\theta s)^{1-m_{\text{off}}} - 1}$$

for the unnormalized autocorrelation is given, with θ corresponding to a short-time cutoff. Theoretically, the expression could be transformed to a spectral power density:

$$S(f) = \mathcal{F}\{\mathcal{L}^{-1}g(s)\}$$

3.8.5. Fit of autocorrelation curves

It is straightforward to calculate the intensity correlation function

$$G(t, t_{\text{lag}}) = \frac{\overline{I(t)I(t+t_{\text{lag}})}}{\overline{I(t)}\overline{I(t+t_{\text{lag}})}} - 1 \quad (3.10)$$

averaged over CCD pixels, which would approach the theoretical ensemble average for infinitely many particles. Then, $G(t_{\text{lag}})$ was fitted to the three parameter model $G(t) = A - Bt^\alpha$. Due to lack of a adequate theory, simulation is currently the only way to interpret the fit parameters, especially to relate α to m . Bachir *et al.* found an anti-correlation between the two: for $m=1.5$, α was around 0.4, decreasing to $\alpha=0.2$ for $m=1.9$. There are also Laplace space expressions [Verberk03, Margolin04], which might be used to prove the $\alpha = 2 - m_{\text{on}}$ statement from [Durisic07]. Unfortunately, with the calibration data presented by Bachir, the error of the method was always larger than 10%.

3.8.6. Conclusion

For practical purposes the following easy method to extract the exponent of experimental data under the assumption of a power law will be used in the remainder of this work:

1. Obtain durations via thresholding
2. Plot histogram with log-spaced bins

3. Ignore the first bin
4. Fit with model Eq. (3.5)

For short time series of a power law-driven telegraph process, this simple procedure will result in an exponent estimate biased towards zero.

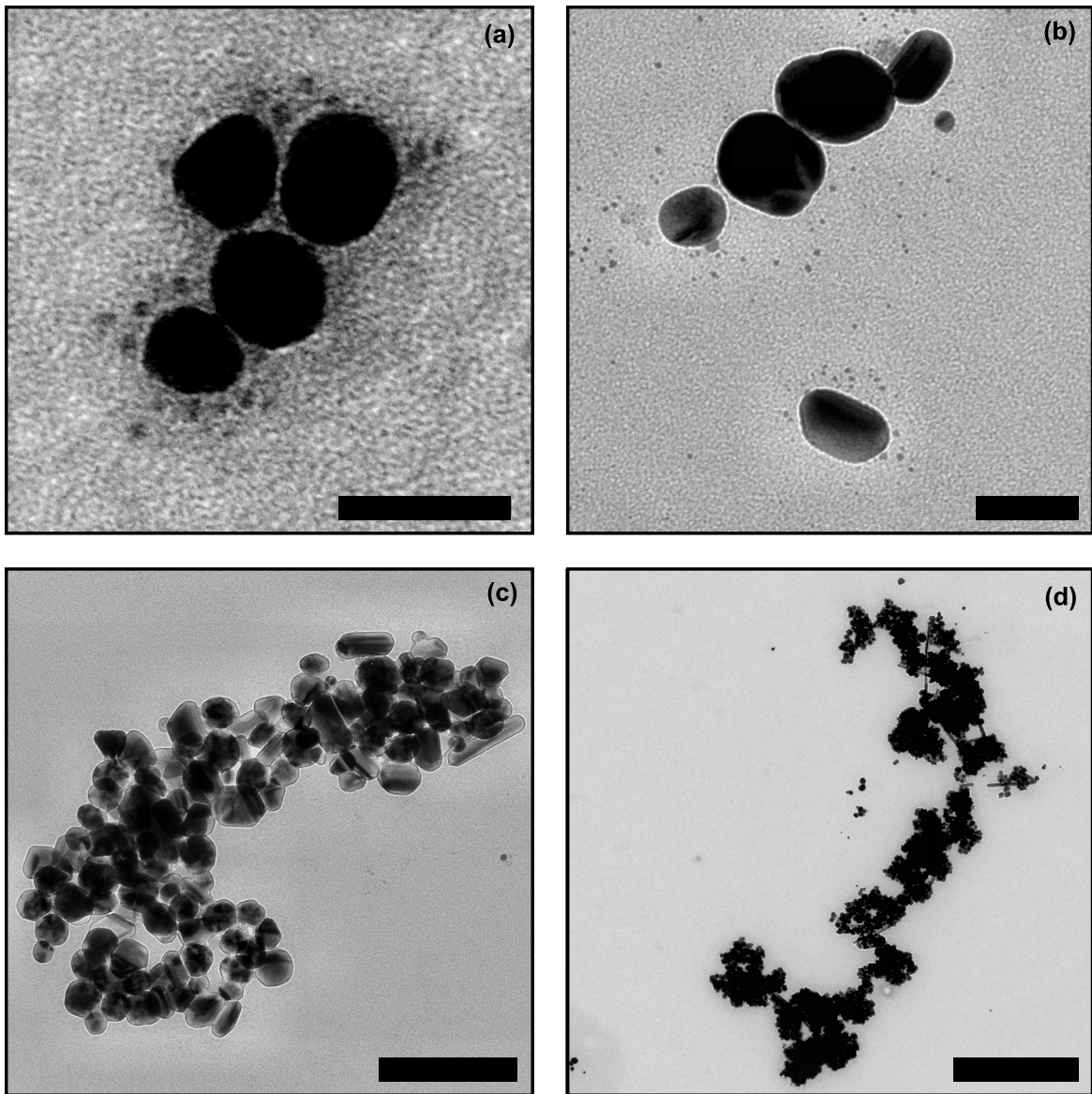


FIG. 14: Transmission electron micrographs of aggregates of nanoparticles. Bars correspond to 25 nm (a), 50 nm (b) 200 nm (c) and 800 nm (d).

4. Sample characterization

Within this work, the term nanoparticle (NP) is used to describe silver clusters of several tens of silver atoms, with diameters of 2 or more nanometers.

4.1. Transmission electron microscopy

Transmission electron microscopy (TEM) was carried out using a side-entry Tecnai 12 microscope (Philips, Amsterdam, The Netherlands) at the Max-Planck-Institute for Cell Biology and Genetics

(Dresden). Samples were prepared on standard carbon-coated films on copper grids (hexagonal mesh) by drying a 10 μl droplet of nanoparticle sol solution under atmosphere. The grids were imaged one hour later; one could observe mostly aggregates (see Fig. 14) of NPs, but also a few isolated particles. Larger aggregates clearly showed a fractal character.

The composition of all aggregates observed was highly heterogeneous in terms of size and shape. A fraction of the particles was round, but most had ellipsoid shapes. Additionally, a few rod-like particles were observed.

To get an estimate of the particle size, the long and short axes were measured for 30 particles. The mean diameter was (41 ± 3) nm, which is in line with the literature, as listed in Table I. Following the calculations in [Narayanan08], this corresponds to an average of about two million silver atoms per particle. However, particles of sizes in the order of 2 nm are also visible in the TEM images and it can be assumed that even smaller particles with only a few atoms were also present in the sample. The mean aspect ratio (long axis to short axis) was 1.5 ± 0.1 , which, too, is in agreement with previous observations [Emory98a].

It was reported in [Emory98b], that only particles with a diameter of 80 nm or bigger were optically active when excited with 514.5-nm laser light, whereas the majority of the active particles were smaller than 100 nm. In our study, only 10% of the particles had an axis longer than 80 nm.

4.2. Scanning electron microscopy

A droplet of nanoparticle sol solution was dried on a conductive carbon sheet, which was inserted into an electron microscope (DSM-962, Zeiss, Oberkochen, Germany) with a tungsten electron gun run at 30 keV. The microscope was situated at the Institut für Strukturphysik of the TU Dresden. It was observed that most of the particles assembled into patches of fractal-like appearance. The patches showed a wide size distribution, which was quantified by thresholding SEM images with their mean and counting the pixels that are part of connected patches. The average particle aggregate area was $(46 \pm 7) \cdot 10^{-3} \mu\text{m}^2$

Most of the smaller patches were 2-dimensional (monolayer or less) with diameters up to 400 nm, but the larger aggregates consisted of at least 3 layers of particles.

One can get a rough estimate of the concentrations involved by thresholding a SEM image and counting the pixels above the threshold level. At the center of a dried droplet, a surface fraction of $\approx 5\%$ was covered with particles. By assuming a volume V_{drop} of 10 μl and a dry area of 20 mm^2 , this leads to a sol solution concentration of $c \approx 0.03$ nM for 80 nm-sized particles or $c \approx 1$ nM for 40 nm diameter particles. These numbers underestimate the true volume concentration because (1) the edges of the dried droplet contain much more material than the center and (2) there were patches with more than one layer of silver particles.

4.3. Optical absorption

For non-magnetic sub-wavelength particles, theoretical cross sections σ can be calculated by an exact solution of the Maxwell equations, the Mie theory [Bohren83, Kreibig95], which describes collective dipole surface density resonances of electrons. The oscillation frequency of these resonances strongly

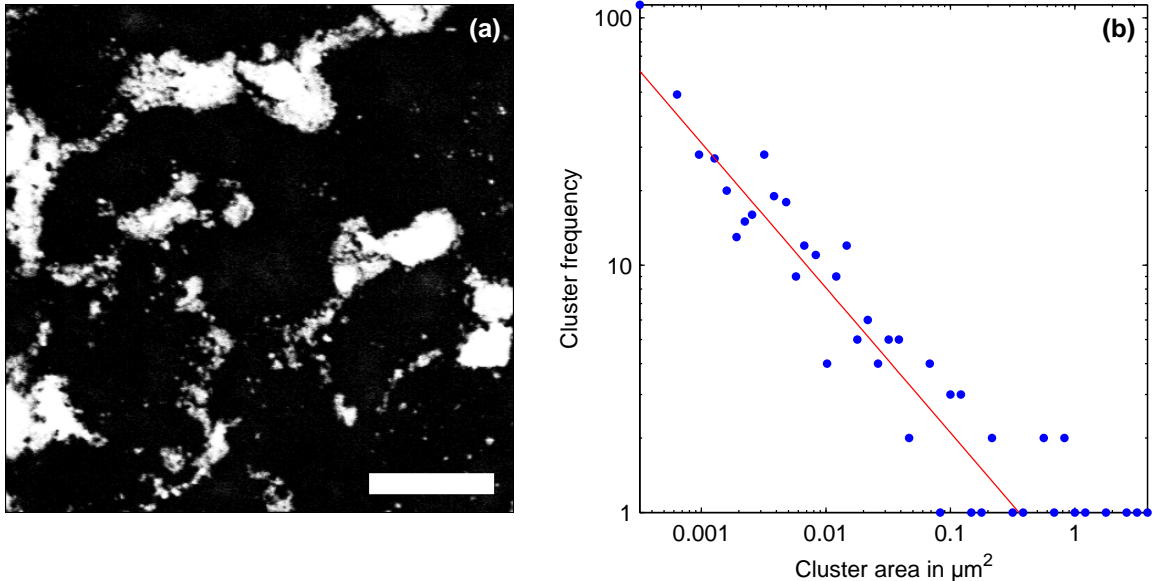


FIG. 15: (a) Scanning electron microscopy (SEM) image of silver (white) particles on carbon (black). The bar corresponds to $2 \mu\text{m}$ long. (b) Distribution of silver particle cluster sizes as determined from image (a). The line, a power law with the exponent -0.59 , is meant to guide the eye.

TABLE I: Electron microscopy-determined silver particle sizes reported in the literature. All particles were prepared by the method proposed by Lee and Meisel [LeeP82], which was also used for our experiments.

Typical Ag nanoparticle size, nm	Reference
30 (spheres), 60 (rod length)	[Hildebrand84]
35-50	[Emory98b]
50	[Weiss01]
50	[Sharaabi05]

depend on the shape and the size of the particle [Kooij06]. The exact solution for ellipsoids are known, but the spectral deviation is minor for curved particles with aspect ratios close to one. The software MiePlot [Laven08] was used to calculate the theoretical molar absorptivity $\epsilon = \sigma N_A / \ln(10)$ for a Ag sphere of a given radius r immersed in water. While for the smallest particles, the extinction is fully determined by absorption and scattering is negligible, for larger spheres the overall extinction increases and scattering becomes considerably more important. The exact shape of the particle will influence its absorbance, but only the spheres have been considered here, hence the result may be biased. For particles with aspect ratios larger than one, experiments show a red shift of the absorption maximum, due to the plasmon oscillation along the major axis [Link00].

Absorption spectra $A(\lambda)$ of a dilute nanoparticle sol solution were recorded using a Bioline Specord S100 spectrophotometer (Analytik Jena). The main feature observed was a peak centered at 418 nm, with a FWHM of 93 nm and a maximum absorbance of 0.155. This peak had a small knee at 350 nm. Since the sol solution most likely contains a distribution of particle sizes, each size gives a contribution to the spectrum, according to its relative concentration.

These data can then be fitted using a non-negative least-squares algorithm to find a solution to the following equation

$$\begin{aligned} c(r) &= \operatorname{argmin} \sum_{\lambda} \left(\sum_r \epsilon(r, \lambda) c(r) - A(\lambda) \right)^2 \quad \text{with } c(r) \geq 0. \\ &= \operatorname{argmin} \|\epsilon c - A\|_2 \end{aligned}$$

Unfortunately this approach yields an physically unlikely result: the sample allegedly only contains Ag particles of one size with no distribution at all. This behavior stems from the high condition number (a measure of the sensitivity of the solution of a system of linear equations to errors in the data) of the matrix, $\operatorname{cond} A \approx 10^{21}$, suggesting nearly linearly dependent vectors. In other words, the theoretical absorptivities ϵ for different radii r are so similar to each other, that any small perturbation in A can cause a large deviation in c .

This problem can be dealt with by using the regularization approach: Instead of only minimizing the norm of the residuals, one can additionally penalize solutions c with a great norm $\|c\|_2$. This constraint makes sense because a major difficulty with the ordinary least squares solution is that its norm $\|c\|_2$ is significantly greater than the norm of the exact solution [Hansen07]. For a fixed value of α_{reg} , a non-negative parameter determining the smoothness of the solution,

$$c(r) = \operatorname{argmin} \left(\|\epsilon c - A\|_2^2 + \alpha_{\text{reg}}^2 \|c\|_2^2 \right) \quad \text{with } c(r) \geq 0. \quad (4.1)$$

was solved. A common practice to find a reasonable value for α_{reg} is to analyze the so-called L-curve and select a value from the “knee”, a region of fair balance between minimizing $\|c\|_2$ and minimizing the residual norm $\|\epsilon c - A\|_2$.

The obtained values are the total particle volume concentration of roughly 1.2 nM in the stock silver sol solution and a mean diameter of (50 ± 18) nm. One needs to state that the absorbance of a given metal particle increases with the third power of its radius [Bohren83], therefore only the largest particles will dominate the absorption spectrum and the stated diameter should be seen as an upper limit. Smaller particles may be present in abundance without being detected via their absorption. Still, the obtained diameter is in good agreement with the TEM findings.

4.4. Optical microscopy

When one dried silver sol solution droplet was imaged on the wide-field setup, an approximately 200 μm thick rim of material was observed where the edge of the droplet was before. In the center of the circle, silver aggregates were rather sparse. It was observed that almost all visible structures had a fractal-like shape, with a circumference-to-area ratio much larger than simple geometric shapes like rectangles; see Fig. 17 for a typical example. When imaged with the transmitted light of a fluorescent lamp, three different intensities can be distinguished: (i) black material, that shows luminescence

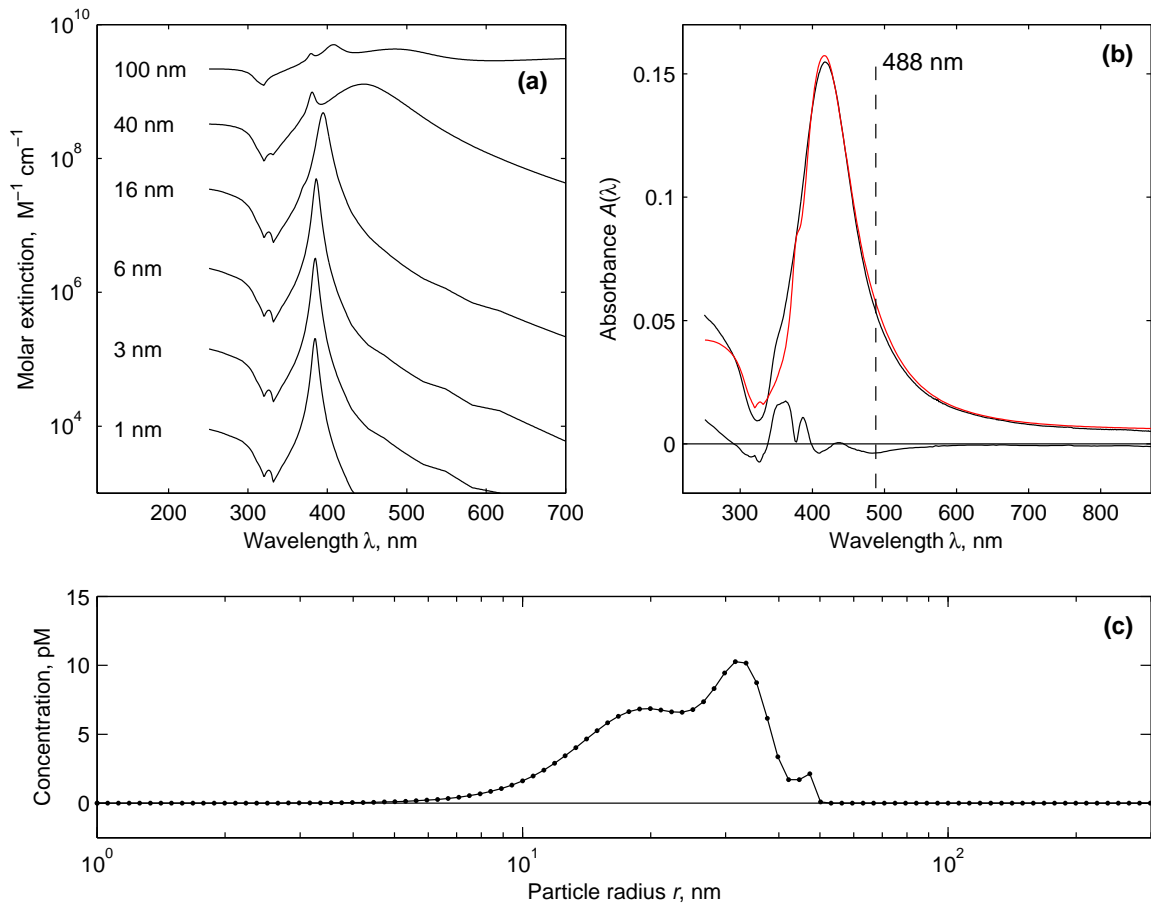


FIG. 16: Size and concentration estimation via absorption spectra. **(a)** Some examples for theoretical extinction curves for mono-disperse Ag spheres of different size in water. The radii are given next to the curves. **(b)** measured absorbance of diluted sol solution (black line). The fit is given as a dotted red line. **(c)** Partial concentrations as obtained from the fitting algorithm. The sum of all partial concentrations is 0.1 nM.

when excited with a laser, (ii) brighter material and (iii) a slightly darker background, that was of the same brightness on a clean, empty coverslide. When only laser light is used, most of the field of view remains dark, because of the epi-illumination setup used. Very bright spots appear, that are easily visible through the eyepiece as blinking spots with distinct colors. Most of the spots are emitting green, some yellow and a few red light. Additionally, most of the locations of the black material described before is dimly fluorescent. With the laser powers used, this time-independent emission bleached irreversibly within minutes to a even dimmer but still observable level, in contrast to the bright spot, which remained fluorescent and blinking even in experiments with durations of several hours.

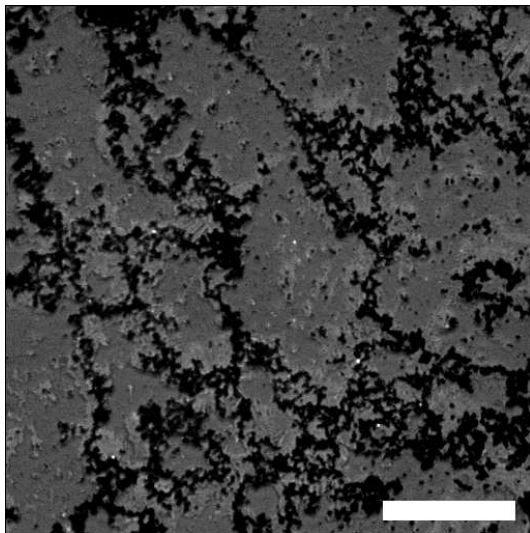


FIG. 17: Micrograph of a dry silver NP sample, simultaneously illuminated with both a standard mercury gas discharge fluorescent lamp and a 488 nm laser line, detected with a CCD. White spots are the result of very strong fluorescence; silver aggregates are visible as a black fractal-like structure. The bar corresponds to 20 μm .

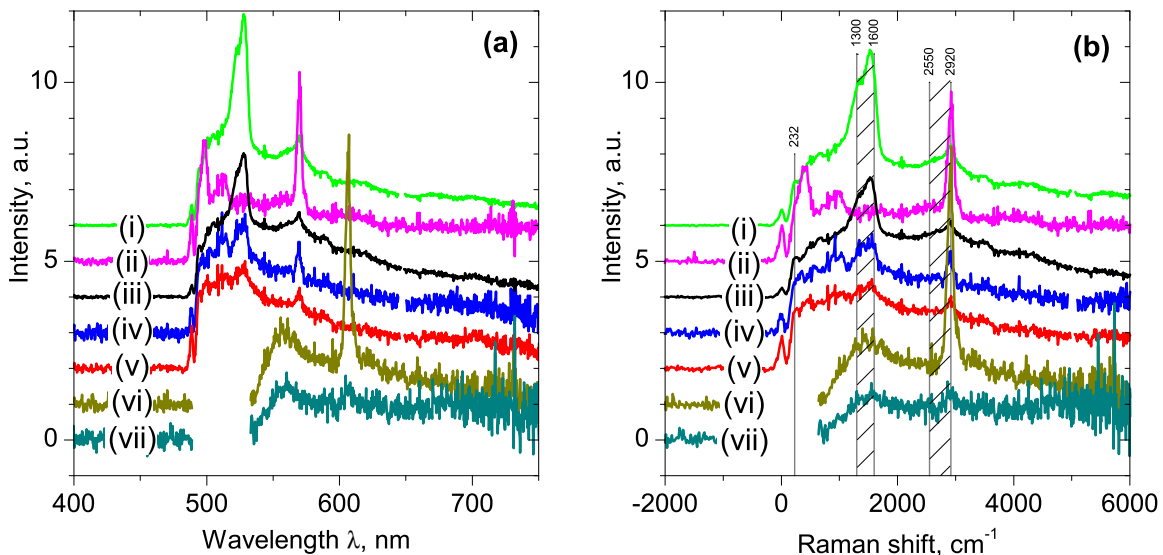


FIG. 18: (a) Spectra of approximately 20-60 emitters on different dry silver samples, individually normalized to their intensity around 630 nm. Curves (i-v) were obtained with excitation at 488 nm laser light, (vi) at 514 nm. The individual curves are vertically offset for clarity. (b) The same spectra transformed into the emission frequency scale and presented as a function of the Raman-frequency shift $\nu_{\text{laser}} - \nu_{\text{em}}$. Dashed vertical lines show Raman lines.

5. Emission spectra and excited-state lifetimes

5.1. Emission spectra of Ag samples

In analytic chemistry, silver nanoparticles are widely employed to enhance the extremely weak Raman signal of close-by molecules. There, these molecules are called analyte, whose concentration is attempted to be detected. In [Peyser02] it was noticed that silver particles emit light with very characteristic spectra, even without any analyte added. Therefore, intensive studies have to be performed to avoid confusing the source of specific Raman lines, as they may originate from the analyte or the silver NPs. In this section, experiments in different environments are described to add to the picture.

For silver particles it is suggested, that the emission light does not stem from the comparatively large nanoparticle, but from molecules or few-atom Ag clusters at its surface [Peyser01, Treguer05]. Additionally, it is known that both Raman scattering and fluorescence can be more intense in the presence of large silver clusters [Chowdhury07], but the exact enhancement of the molecule's signal depends very much on the distance to the NP, the relative orientation of emitter with local electric field shaped by the NP [Chowdhury07, Wang05], and, if present, the chemical bond with the NP [Hildebrand84, ItohT06b]. In the present work, the focus was set to the emission of silver particles without a deliberately added analyte.

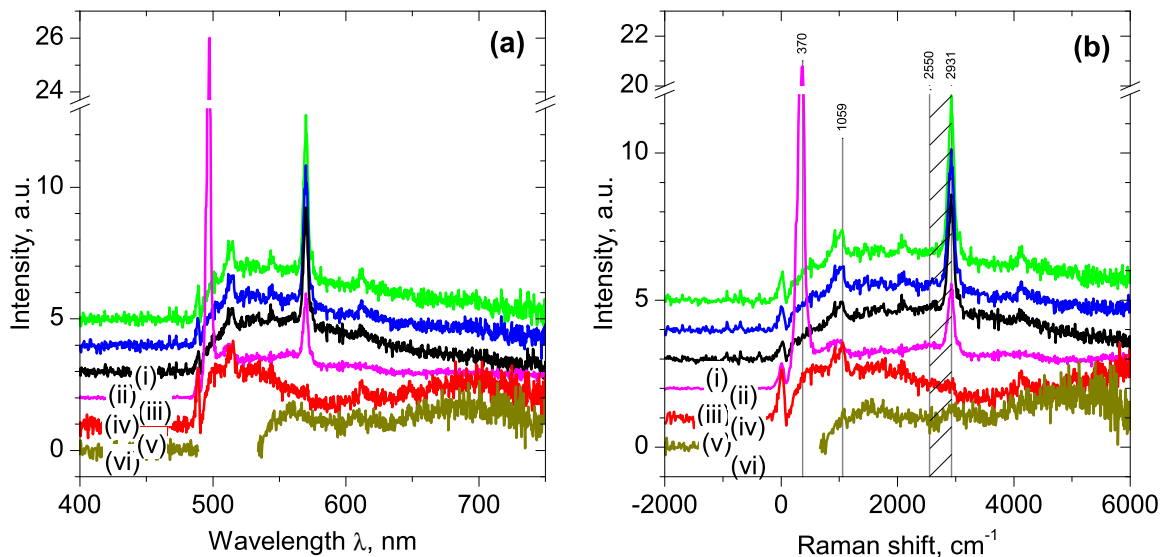


FIG. 19: **(a)** Spectra of point-like emitters on spin-coated PVP-Ag NP silver samples, individually normalized to their intensity around 630 nm. Curves (i, ii and v) were obtained from distinct single emitters, the curves (iii-iv) were obtained from larger aggregates. (i-v) were excited with 488-nm laser light, (vi) at 514 nm. The individual curves are vertically offset for clarity. **(b)** The same spectra transformed into the emission frequency scale and presented as a function of the Raman-frequency shift $\nu_{\text{laser}} - \nu_{\text{em}}$. Dashed vertical lines show Raman lines.

In Fig. 18, we present the spectra of dense silver NP samples. Care was taken not to detect emission from “clouds” - regions of comparably low, time-independent emission. Instead, the emission came predominantly from sub-resolution blinking spots. Ag sol solution was dried on a coverslide and both spectra and videos were taken. In order to observe potential effects of the local environment, emission of Ag NPs in oil (Immorsol 518 F, Zeiss) environment was measured (Fig. 20). To do so, a droplet of liquid was deposited on a coverslide with dried Ag sol. Twenty minutes after the deposition, emission spectra were measured from the coverslide-liquid-interface. For more information on the dynamic behavior of the samples, the reader is referred to page 57.

One more environment was checked for its influence: the polymer PVP was used to create a 3-dimensional structure with embedded Ag particles.

Using the microscope eyepiece, blinking particles of distinct colors (green, yellow, red) could clearly be identified. Changes of the color of bright emitters were not witnessed. Since the spectra were recorded of an ensemble, the individual color features are added to form one band stretching from green to the long-wavelength end of the spectrum. When changing the excitation wavelength, the broad band remains fixed, but the finer structures move; therefore they are clearly Raman peaks. It has been observed that the relative contribution of different spectral ranges to the fluorescence signal changes when different parts of the sample are analyzed. This is attributed to the above-mentioned

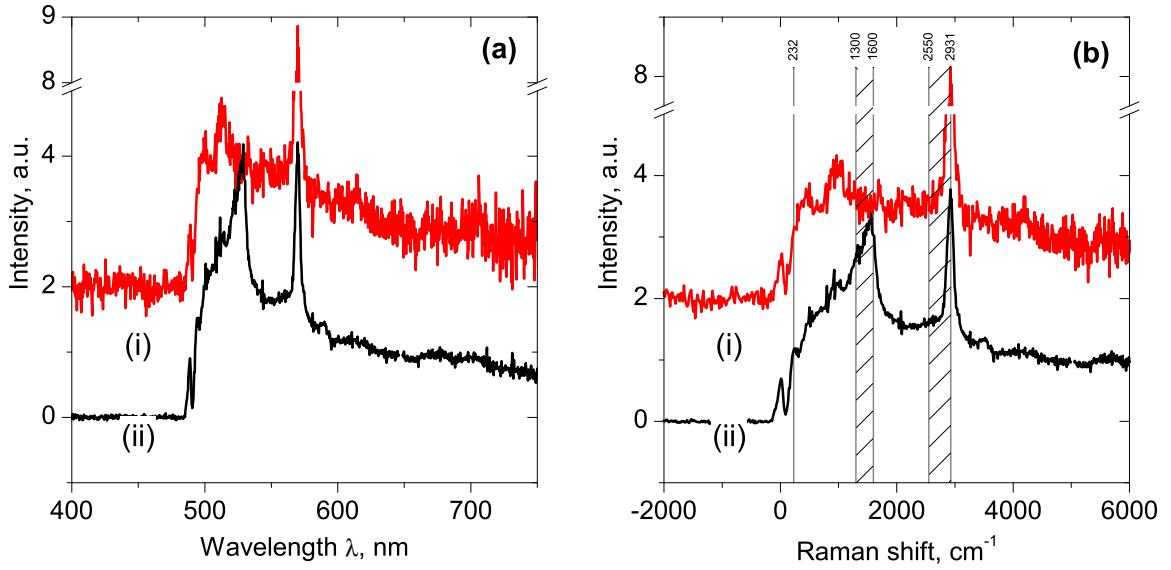


FIG. 20: (a) Spectra of point-like emitters on previously dry silver samples, freshly covered by a droplet of oil, individually normalized to their intensity around 630 nm. Excitation wavelength 488 nm. The individual curves are vertically offset for clarity. (b) The same spectra transformed into the emission frequency scale and presented as a function of the Raman-frequency shift $\nu_{\text{laser}} - \nu_{\text{em}}$. Dashed vertical lines show Raman lines.

narrow fluorescence bands of individual emitters. It may be that the emission of a Ag NP is governed by the exact energy of its plasmon resonance, that selectively enhances the fluorescence of close-by emitters in this specific spectral range.

TABLE II: Identified peaks in the spectra measured.

Frequency shift from literature	Fig. 18	Fig. 19	Fig. 20	Assignment
232 cm^{-1}	✓		✓	Ag-Cl [Fleischmann81], Ag-N [Hildebrand84]
370 cm^{-1}		✓		unknown
1059 cm^{-1}		✓		C-O [KneippJ06]
1300-1600 cm^{-1}	✓		✓	C=C [Mahoney80, Pettinger81, Moyer00]
1530 cm^{-1}	✓			C-H [Pettinger81]
1560 cm^{-1}			✓	C-H [Pettinger81]
2550-2888 cm^{-1}	✓	✓	✓	Carbon [Moyer00]
2840-2920 cm^{-1}	✓	✓	✓	Carbon [Mahoney80]
2931 cm^{-1}	✓	✓	✓	CH ₂ [Fleischmann81]
2900 cm^{-1}	✓	✓	✓	C-H [Pettinger81]
3520 cm^{-1}			✓	Water [Pettinger81, Fleischmann81]

The spectra found in experiments with vapor-deposited thin silver films [Jacobson05, Jacobson06], resemble those measured of dry samples in this work closely. This is remarkable since known contained chemicals and potential contaminants are different in the two systems; the only remaining commonality being the silver.

In many cases, the SERS signal intensity was measured to be not proportional to the concentration of the analyte [Murray84, Zeman87]. For example, spectral peaks of species such as water are not or hardly observed [Otto02]. It is noteworthy that in SERS experiments, scientists very often report the presence of amorphous carbon [Mahoney80, ItohK05, Vosgroene05, Emory06], even when it was not added consciously. It has been claimed that it is generated by photo-degradation of organic molecules and is adsorbed to the SERS-active sites. It is also known tiny concentrations of carbon already give an appreciable contribution to the spectrum. The affected lines 1335, 1518 and 2910 cm^{-1} , are measured for different Ag production methods [Mahoney80, Zhu97, Moyer00, Otto02], some of which do not require any chemicals other than bulk silver.

Whereas bulk silver only shows extremely low luminescence caused by optically excited plasma [Steinmann63], this radiation source becomes important for silver particles smaller than ≈ 5 nm. Spectral peaks at energies of surface and volume plasmon resonance frequencies have been reported [Boyd86], therefore very weak luminescence may be expected according to the absorbance spectrum (Fig. 16) which follows these resonances. Due to the increased electric field generated by plasmons, another source of luminescence is the greater rate of photoactivated chemical reactions, leading to either chemiluminescence or creation of fluorescent species [Ievlev00]. The reported peaks are listed in Table III and explain the broad spectral band observed.

TABLE III: Luminescence peaks of Ag nanoparticles, as reported in the literature.

Emitter	Wavelengths, nm	Publication
DNA + Ag	400-800 ^f	[Richards08]
DNA + Ag	420-740 ^f	[Sengupta08]
DNA + Ag	540-650 ^f	[Gwinn08]
PMAA-stabilized Ag NPs	550-800 ^f	[Shang08]
Ag ₂ clusters in noble gas	428-455 ^f , 444-536 ^c	[Rabin98]
Ag ₃ clusters in noble gas	595-610 ^f , 609-628 ^c	[Rabin98]
Ag ₃ clusters in noble gas	490-506 ^f , 512-528 ^c , 565-640 ^c	[Ievlev00]
Ag NPs	520-780 ^f	[Geddes03]
Ag NPs	546-636 ^f	[ItohT06a]
Ag sol	500-720 ^f	[ZhangA08]

Note: superscripts ^c and ^f mark chemiluminescence, and fluorescence, respectively.

In view of possible applications, such as fine-tuned secondary light sources in fluorescence lamps [Cremer08], it would certainly be fruitful to further investigate the spectra of silver NPs and their dependencies.

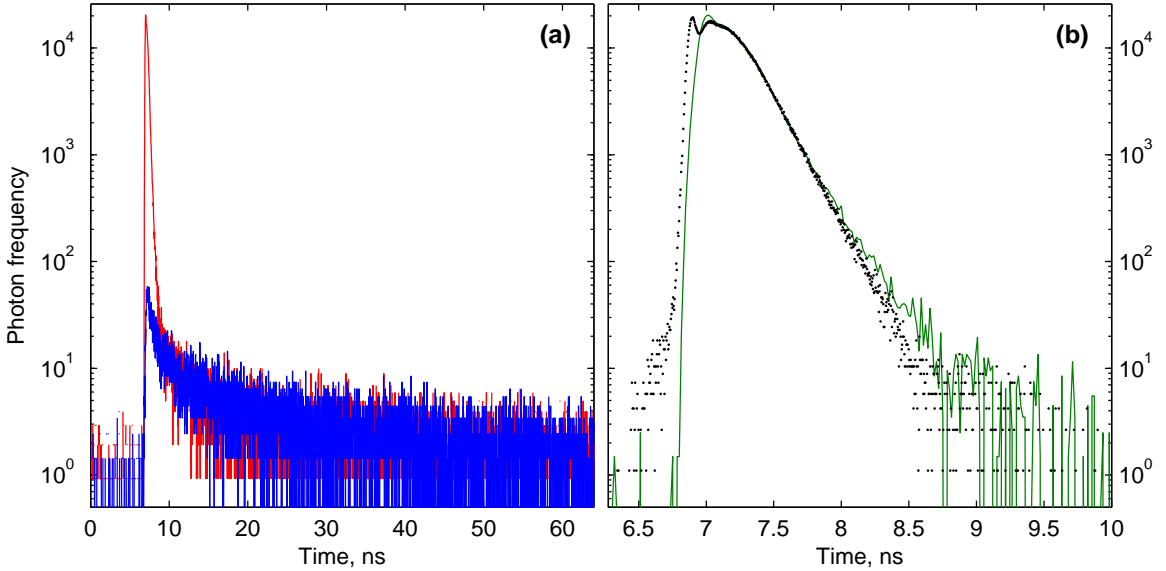


FIG. 21: Photon arrival times histograms to determine the lifetime of the emitting state. The dark counts, as estimated by the mean of the first 120 channels, have been subtracted. **(a)** Decay curve of emission of a silver particle (—), and of the emission of its surroundings (—). The channel width was 16 ps, the pulse repetition rate 500 kHz. **(b)** Difference of the curves in (a) (—) overlaid with the instrument response function (····), measured at a channel width of 4 ps.

5.2. Fluorescence decay kinetics

As is clearly visible in Fig. 21(a), the detected signal is a combination of a slow component, dominating the background signal, and a fast component which is only measured directly at the strongly emitting silver particle. The fast component shows almost the same rate of decay as the instrument response, and is most likely faster than the resolution of the setup. The instrument response $h_{\text{IRF}}(t)$ has been fitted with the function $f(t) \propto \exp(-t/\tau_{\text{IRF}})$, resulting in an approximate decay time τ_{IRF} of 180 ps. The silver particle radiative decay kinetics can be fit with the sum of three exponentials

$$f(t) = A_0 + A_1 e^{-\frac{t-t_0}{\tau_1}} + A_2 e^{-\frac{t-t_0}{\tau_2}} + A_3 e^{-\frac{t-t_0}{\tau_3}}, \quad (5.1)$$

revealing two further lifetimes, ≈ 2 ns and 16 ns, and was also present in regions of extremely low emission. It is possible that the latter component is a result of a contaminant for example of the glass, because it was measured even outside the dried droplet and unlike in cell or solution measurements, we focused the objective onto the upper glass-air interface.

The slow lifetime component was measured for both Menzel and Cornell coverslides, taken directly from their container. For further discussion, we will ignore the two slow components, because (i) luminescence of glass has been observed before for certain impurities [Trukhin04, Righini05] and (ii) the relative amplitude $(A_2 + A_3)/(A_1 + A_2 + A_3)$ accounts for less than 2%.

The prominent very short lifetime could lead one to think that it is caused by quenching. Fluorescence is quenched if a competing non-radiative mechanism is de-exciting electrons with a

TABLE IV: Fluorescence lifetimes observed for silver nanoparticles without dyes in the literature. Typical fluorescence lifetimes of isolated dyes fall in the range of 0.5 - 20 ns.

Publication	Preparation method	Excitation	Lifetime
[Treguer05]	Ag _n @Ag ⁺ (radiolytic prep.)	confocal at 476 nm	< 0.038 ns
[Wu08]	Lee & Meisel	confocal at 635 nm	< 0.1 ns
[Vosch07]	DNA-encapsulated Ag	laser at 647 nm	2.6 ns
[Konig96]	Ag _n in a Ne matrix	chemical	4.6-12.7 ns

high rate. But quenching is not plausible if one considers the high emission intensities observed. Instead, the short lifetime is believed to be an effect of the proximity of conducting metal to a fluorophore. The effects of metals on fluorescence have been treated theoretically [Chance74, Ford84] and observed experimentally [Maliwal03, Lakowicz05] before. Depending on the distance between metal and fluorophore, the de-excitation of the fluorophore can be faster than isolated fluorescence. With this effect, termed metal-enhanced fluorescence (MEF) [Lakowicz05], a fluorophore can absorb more photons per time than without the Ag NP, thus leading to higher emission intensities. In this case, the shape of the observed decay kinetics will reflect the rate of the energy transfer from the fluorophore to the metal plasmon and the subsequent emission of a photon from the metal.

All measured emission centers showed decay kinetics with a lifetime equal to the decay of the IRF ($\tau_{\text{IRF}} = 180$ ps).

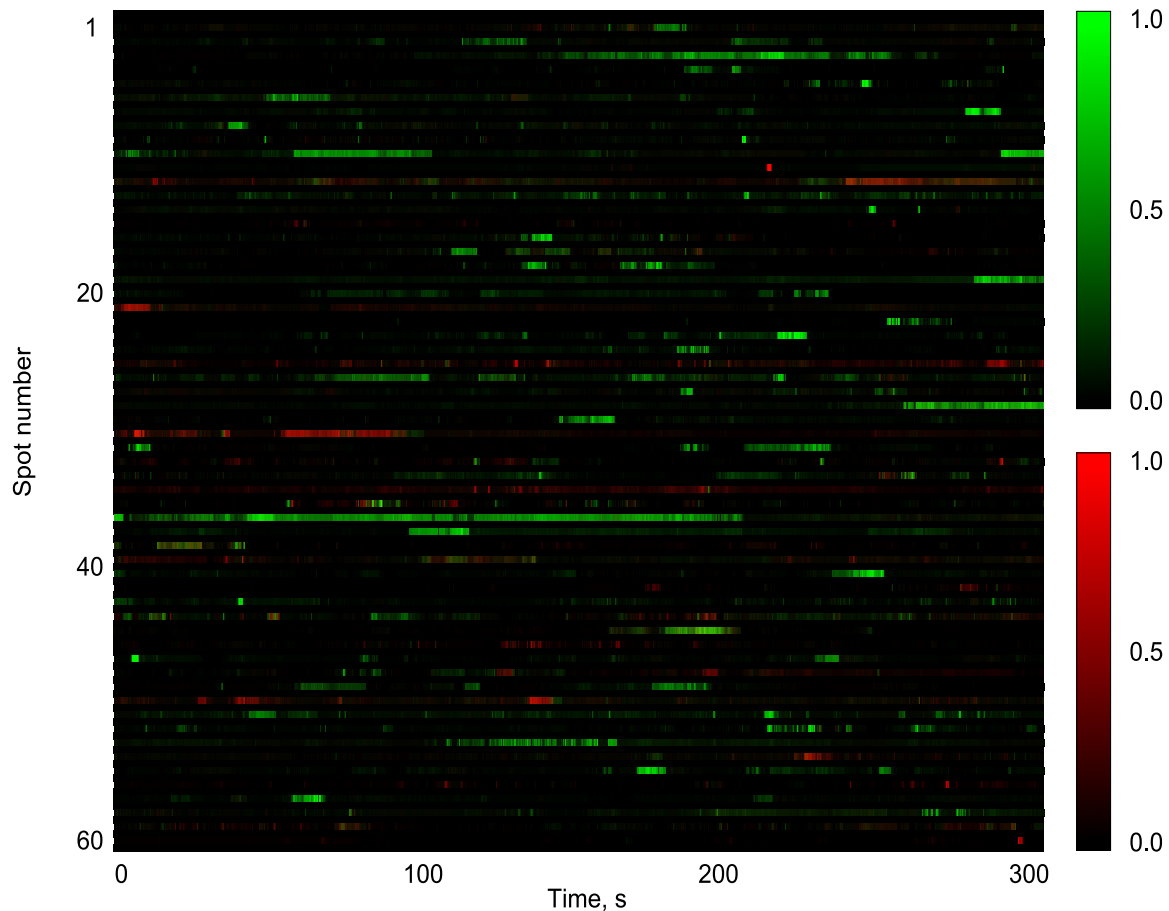


FIG. 22: Emission intensity of 60 different spots on a dried silver NP sample. Excitation wavelength 488.0 nm, power density 7.2 W/cm^2 , simultaneously imaged in two spectral channels. The emission of each particle was normalized by its maximum and then binned to 917-ms intervals. The color mapping is linear, as shown in the right.

6. Dynamic emission behavior

6.1. Power law blinking

Emission centers on a dried silver NP sample showed strong temporal intensity fluctuations, as can be seen in Fig. 22. To investigate the nature of the underlying process, the intensity data were analyzed as a simple two-state model, assuming that an emitter can be present in the fluorescent on-state and the dark off-state. In this and the following section, the laws governing the duration of each on- or off-state will be analyzed. First, the probability distribution P of $\tau_{\text{on/off}}$ was estimated, by creating a histogram according to the following algorithm.

1. Convert the measured intensity trace into a list of, on- and off-durations using thresholding. It is quite likely that the power-law distributions stretch to timescales shorter than accessible with

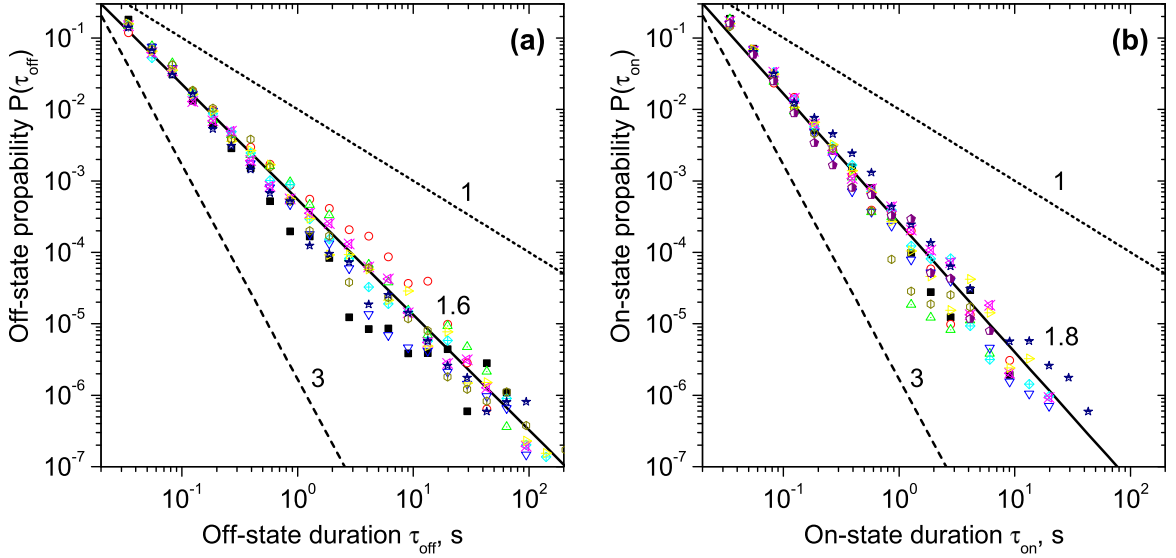


FIG. 23: On- and off-time distributions of ten distinct single emitting centers randomly chosen on a dry silver sample, shown by colored dots. The data was acquired at the wide-field setup using an excitation power density of 6.6 W/cm^2 . The solid lines are power law fits Eq. (3.5) to all data points, yielding the exponents $m_{\text{off}} = 1.6$ and $m_{\text{on}} = 1.8$. The other lines are power laws with exponent $m = 1$ (dotted) and $m = 3$ (dashed).

the setups employed in the present work. In that case, short on-states might generate short pulses of high intensity, which are, due to the comparably longer frame-to-frame time, still below the threshold level and, therefore, wrongly assigned. However, it was shown for single molecule emission [Yip98], that the probability distributions are robust against the exact positioning the threshold.

2. Create a histogram of durations, with a set of bin edges e_{PDF} .
3. Divide the histogram bin contents by the mean number of durations.

We found that the distribution of durations shows a dependency which can be well described by a linear law on a double-logarithmic scale (see Fig. 23), and can therefore be approximated by a power law $P(\tau) \sim 1/\tau^m$, $m > 0$. Such a dependency has been reported before for the emission of Ag NPs [Wu08] and other nanoscale emitters, including quantum dots [Kuno00, Shimizu01, Verberk02, Cichos07] and organic dyes [Haase04, Yeow06, Hoogenboom07]. The shape for both on- and off-probability density of several individual particles is shown in Fig. 23 (wide-field) and Fig. 24 (confocal).

6.1.1. Estimation of the power law exponent from single emitter data

The exponent of the distributions of on/off-durations was estimated for a set of $N = 453$ intensity traces of emitting spots. The set members were chosen so that the threshold was crossed at least 400 times, in order to create a meaningful probability distribution. Bins of the duration histogram were distributed on the log scale to avoid bias [Hoogenboom06]. Only fits with at least nine points

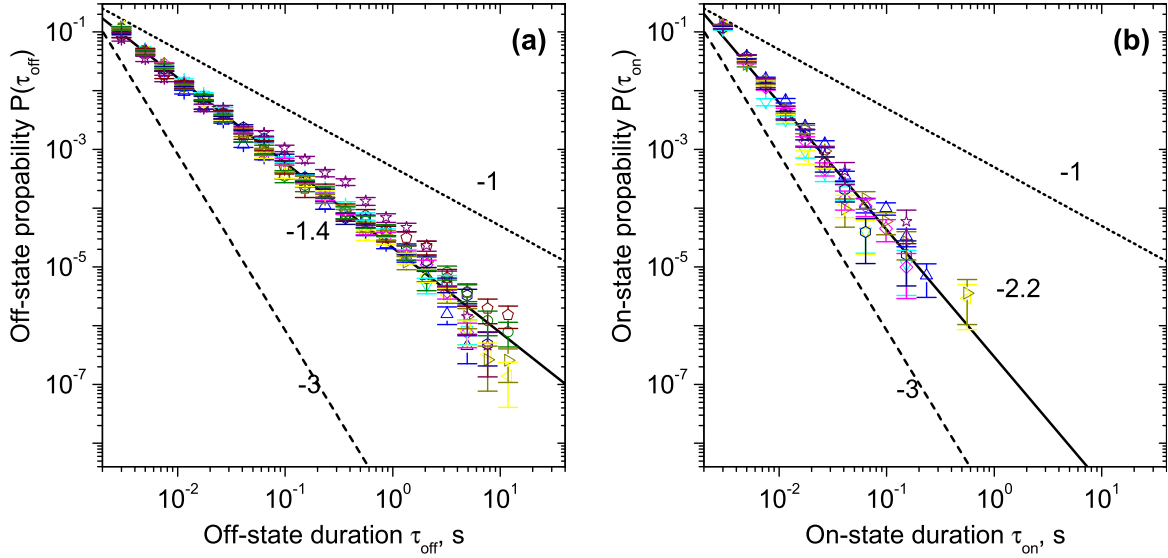


FIG. 24: On- and off-time distributions of three single emitting centers on a dry silver sample, shown by colored dots. The data was acquired at the confocal setup using an excitation power $1.82 \mu\text{W}$, corresponding to a laser power density of about $200\text{-}400 \text{ W/cm}^2$ (see page 23). The solid lines are power law fits Eq. (3.5) to all data points, yielding the exponents $m_{\text{off}} = 1.4$ and $m_{\text{on}} = 2.2$. The other lines are power laws with exponent $m = 1$ (dotted) and $m = 3$ (dashed).

were considered valid. Histograms of the retrieved exponents are shown in Fig. 25(a). The mean of the exponents was $m_{\text{off}} = 1.35 \pm 0.01$ and $m_{\text{on}} = 1.54 \pm 0.01$. The indicated error is $\sqrt{\text{variance}/N}$. These exponents coincide with the peak position of a Gaussian fit ($m_{\text{off}} = 1.40$, $m_{\text{on}} = 1.54$). The power law exponents reported previously are listed in Table V.

The dependency of the power law exponent on the laser power density is shown in Fig. 26. The off-exponent increases with stronger excitation. Wide-field data alone suggests an on-exponent independent of the excitation, coinciding with the data reported in [Wu08], whereas adding the data from the confocal setup clearly shows a power dependence.

It was found that 93% of the particles analyzed on the wide-field setup show an off-exponent smaller than the on-exponent, as can be seen in Fig. 25(b). For this situation, the ensemble intensity was found to decrease both in theory [Margolin04] and for simulated telegraph processes.

In QD experiments deviations from the power law for the limit of long times are sometimes encountered [Shimizu01, ChungI04], that can be modeled as an exponential cut-off:

$$P_{m,t}(\tau) = \frac{\exp(-\tau/\theta_{\text{cut}})}{A(m)\tau^m} \quad (6.1)$$

For single emitters, the limited number of threshold crossings results in a relatively large error for the histogram values for longer durations, making statements on a possible cut-off less convincing. To overcome this limitation, combined probability densities for several particles have been calculated. As can be seen in Fig. 27, the power law remains the best model to describe the on-durations, whereas the off-durations show a clear cut-off, Eq. (6.1), implying the presence of two processes. The obtained

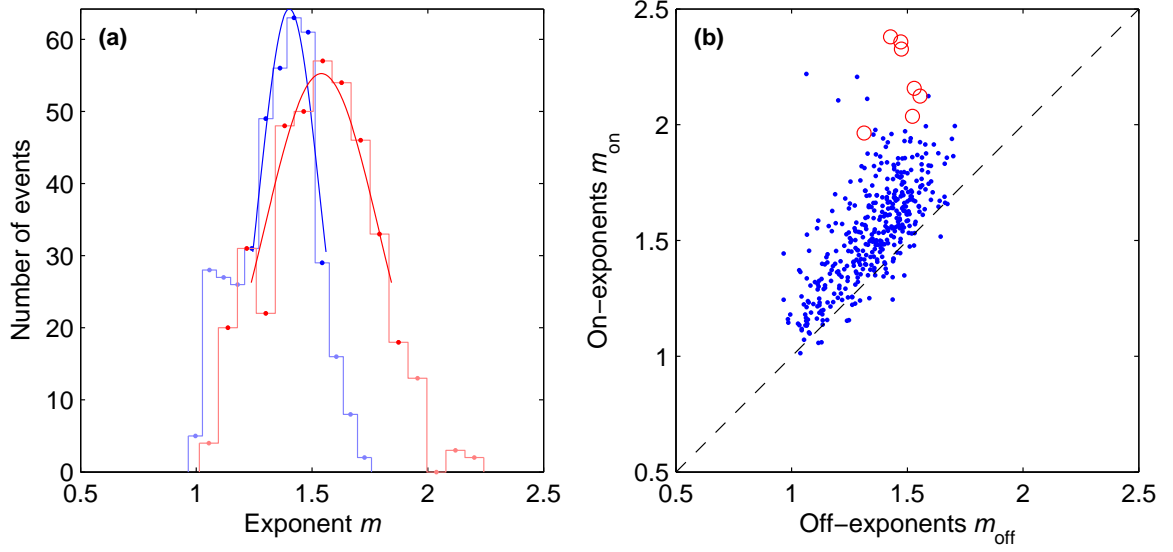


FIG. 25: (a) Histograms of exponents derived from fitting individual probability densities of 453 single emitters observed with the wide-field setup. Off-exponents are shown in blue, on-exponents in red. A Gaussian was fitted to each histogram to obtain the average exponent $m_{\text{off}} = 1.40$ ($\sigma = 0.13$) and $m_{\text{on}} = 1.54$ ($\sigma = 0.13$). (b) Off-exponents plotted against on-exponents, found in wide-field experiments (\bullet) and confocal experiments (\circ).

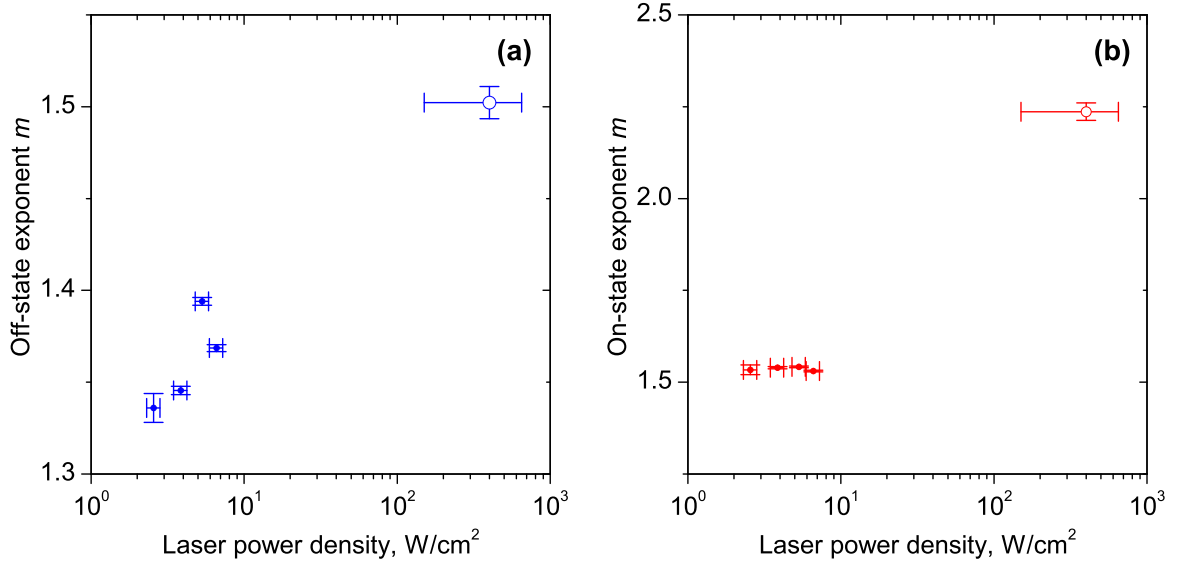


FIG. 26: (a) Laser power-dependency of the exponent of the off-duration probability distribution. Small dots stem from measurements on the wide-field setup, whereas the open circle is from measurements on the confocal setup. (b) On-exponents.

TABLE V: Parameters of power law-distributed durations $\sim 1/\tau_x^{m_x}$ of on- and off-times found in the emission of single molecules, semiconductor nanocrystals, and metal nanoparticles.

System	m_{off}	m_{on}	Excitation condition	Reference
Ag NPs with FePP	1.46 to 1.56	-	< 100 kW/cm ² at 515 nm	[Bizzarri05]
Ag NPs	1.4 \pm 0.1	2.1 \pm 0.1	at 633 nm	[Wu08]
Coated CdSe QDs	1.58 \pm 0.13	-	2.4 kW/cm ² at 488 nm	[Kuno00]
Coated CdSe QDs	1.44 \pm 0.1	1.44 \pm 0.1	0.1-3.0 kW/cm ² at 514 nm	[Shimizu01]
Coated InP QDs	2.0 \pm 0.2	1.5 \pm 0.1	0.24 kW/cm ² at 488 nm	[Kuno01a]
Uncoated CdS QDs	1.65 \pm 0.2	-	at 458 nm	[Verberk02]
Coated CdSe QDs	1.73 \pm 0.01	1.73 \pm 0.01	2.0 kW/cm ² at 514 nm	[Stefani05b]
Coated Si QDs	1.30 \pm 0.05	2.2 \pm 0.1	6.5 kW/cm ² at 514 nm	[Cichos04]
Organic molecules				
TPD	1.9	1.3	2.5-10 kW/cm ² at 568 nm	[Hoogenboom07]
PD	1.4	1.3	2.5-10 kW/cm ² at 568 nm	[Hoogenboom07]
“g0” molecules	1.5	1.75	2.5-10 kW/cm ² at 488 nm	[Haase04]
Atto565 molecules	1.9	2.6	0.3 kW/cm ² at 543 nm	[Yeow06]
KAP/VR (thresh.)	1.8	2.0	< 40 mW/cm ² at 532 nm	[Wustholz08]
KAP/VR (CPD.)	1.0	1.1	< 40 mW/cm ² at 532 nm	[Wustholz08]

fit parameters for the ensemble probability distributions are listed in Table VI. All parameters show a clear excitation power dependence. At higher power, the mean state duration decreases due to an exponent m_{on} further away from zero and a decreasing cut-off θ_{cut} for the off-durations.

TABLE VI: Fit parameters for ensemble probability density of on- and off-durations.

Experiment	m	θ_{cut} , s
wide-field, off-durations	1.538 \pm 0.001	102 \pm 3
wide-field, on-durations	1.886 \pm 0.002	
confocal, off-durations	1.382 \pm 0.005	6.9 \pm 0.5
confocal, on-durations	2.22 \pm 0.01	

6.2. Non-constant average state durations

If one assumes the on- and off-state duration drawn from a probability distribution that is proportional to a power law, the following can be concluded: For a known experimental acquisition time T , a state

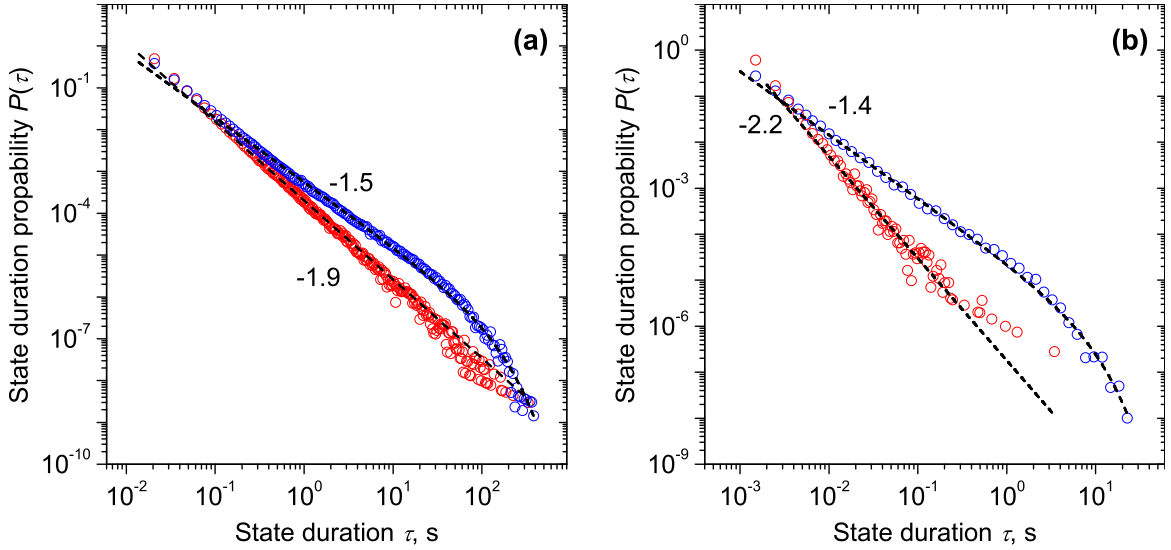


FIG. 27: (a) Probability densities calculated from on- and off-durations of 453 emitters observed with the wide-field setup. A joint histogram was calculated for all valid on-durations of all emitters and used for fitting; likewise for the off-durations. Whereas the short durations follow a power law for both on- and off-durations, a cut-off exists for longer off-durations. The numbers correspond to the short-time power-law exponents. The error of the data points (not shown for clarity) is smaller than the symbol size for short durations and increases towards longer durations. Fits were weighted according to these errors. (b) Probability densities calculated from data acquired at the confocal setup.

x starting at time t has an ensemble-averaged mean duration of

$$\bar{\tau}_x(t) = \sum_{\tau=1}^{T-t} p_t(\tau)\tau, \quad (6.2)$$

$$p_t(\tau) = A_t \left(\frac{\tau}{b}\right)^{-m_x} \quad \text{with } A_t \text{ being defined by } \sum_{\tau=1}^{T-t} p_t(\tau) \stackrel{!}{=} 1$$

The experimental setup used has a fixed integration time (a frame), during which photons are detected. Here, τ_x is normalized by that time, so it can only take integer values: 1, 2, 3, ... $\bar{\tau}_x(t)$ is a decaying function that reaches zero for $t = T$, because only on- or off-durations shorter than the remaining time of the experimental acquisition were recorded (Fig. 28)

Those states which extend over the end of the measurement interval need special attention. If they are truncated to the remaining length, the duration histogram will not follow the correct (but unknown) histogram. Instead, longer durations will be missing and shorter ones will accumulate. Alternatively, if these states are completely disregarded, the duration histogram will still be distorted, but only because longer states are missing. Therefore, the deviations in the histogram will only play a significant role for long durations. Thus the latter treatment has been used throughout this thesis.

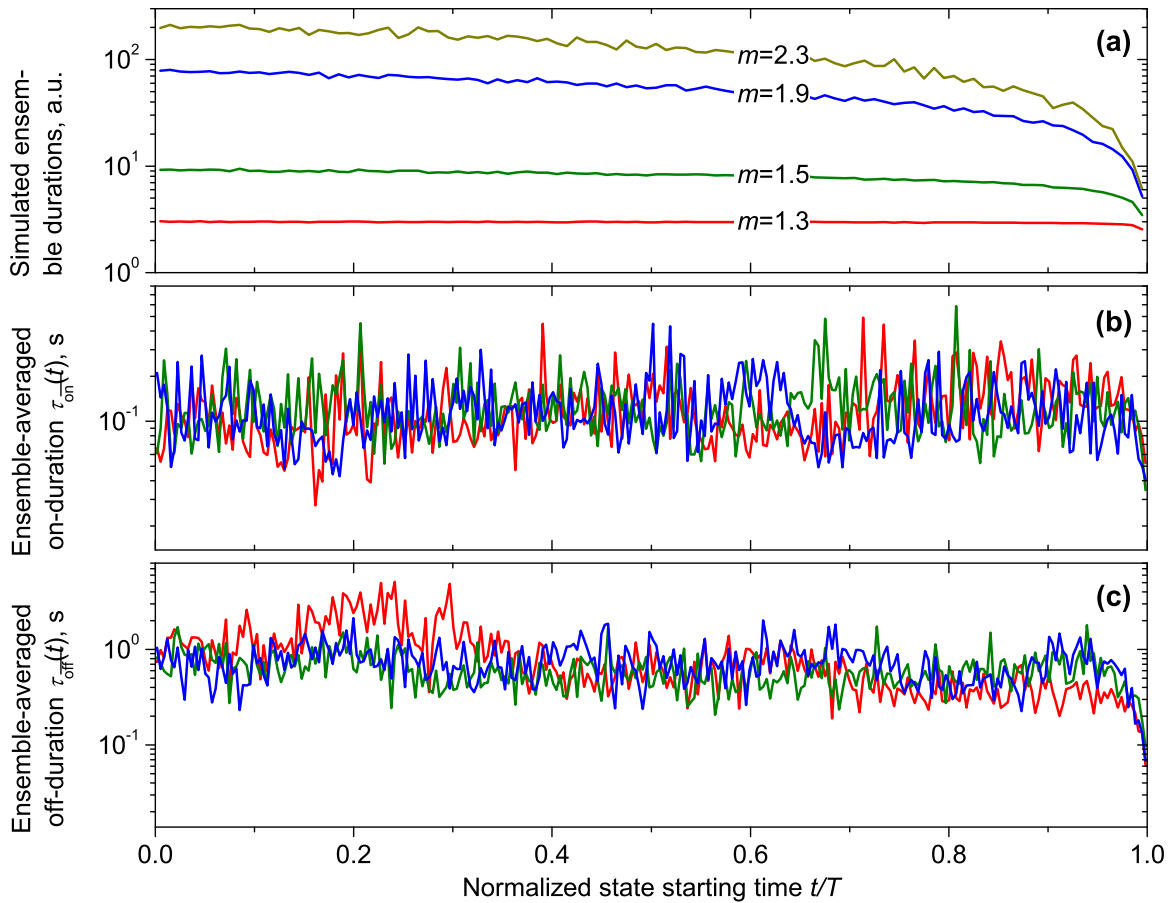


FIG. 28: Ensemble-averaged state durations as a function of the starting time. (a) Results from the simulation of 80 000 particles. The calculations have been performed for the exponents given on each curve. The shortest possible duration was 1 unit. (b) Experimental on-durations of 100 emitters; different colors denote different measurements of the same sample under equal conditions. The frame-to-frame time and therefore the shortest duration was 13.8 ms. The total length T of each experiment was 20 minutes. In order to reduce noise, the starting times have been grouped to four-second intervals. (c) On-durations from the same experiments as (b).

The observed experimental durations show the expected decay to short durations at the end of the experiment. Uncorrelated noise with a standard deviation σ of about 50% of the mean duration contributes to $\bar{\tau}(t)$.

6.3. Reversible intensity decay upon CW excitation

To study whether emitters in Ag NP samples can be reversibly or irreversibly photobleached, the ensemble fluorescence intensity of dry silver samples was measured using wide-field illumination and detected by a CCD camera as a function of time over periods of several hours, during which the

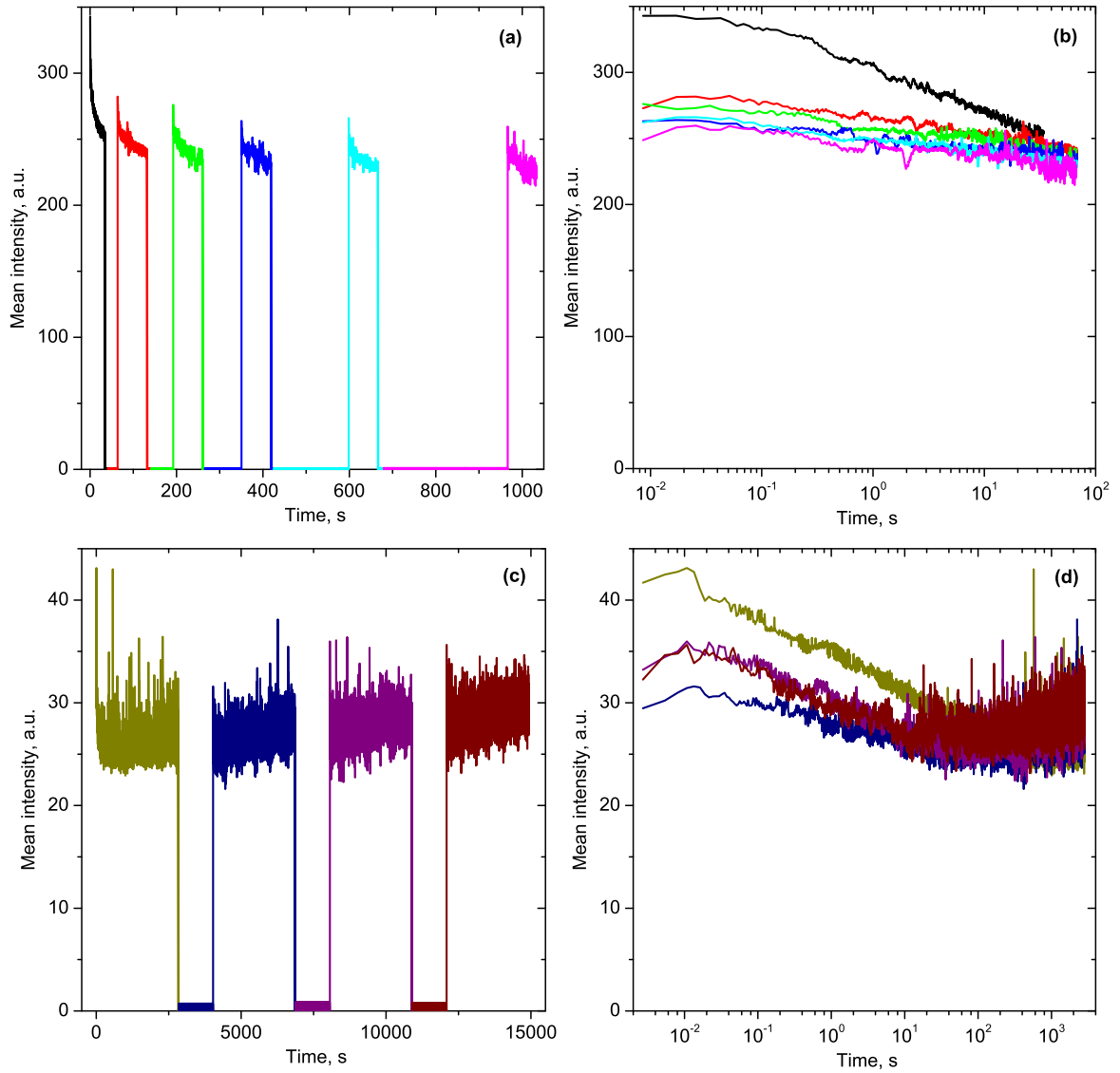


FIG. 29: **(a)** Mean intensity of dried silver NP sol: (—) was measured without any prior excitation. During the 5 periods with zero intensity (after dark count subtraction), the sample was not excited. The time intervals without excitation were 35...65, 132...192, 260...350, 420...600 and 665...965 seconds. The integration time was 8.5 ms. **(b)** Same data as (a), but aligned so that the time zero corresponds to the time when the laser was switched on via the AOTF. **(c)** Results of a similar measurement with \approx one hour periods of excitation, interrupted with periods of 20 minutes of no excitation. The first measurement (—) was recorded without any prior illumination. **(d)** Data shown in (c), aligned to beginning of laser excitation.

excitation was occasionally switched off and on, as will be described below. Samples were stored in darkness at 4°C for two days prior to the experiment and placed on the microscope stage with minimal illumination.

The emission of a previously un-illuminated area was recorded while exciting with continuous laser light at 488 nm and a power density of 7.7 W/cm². The fluorescence intensity decreased over

time from a high initial value. When the sample was excited long enough, a minimum was reached after several minutes. From that minimum on, the mean intensity was observed to slowly increase again (see Fig. 29). During all measurements, individual particles continued blinking. Then, the excitation was disabled for periods between 30-1200 seconds. During that period, no fluorescence signal was recorded (the fluorescence stopped instantaneously, considering the available temporal resolution of a few ms). Finally, the excitation was switched on again and the fluorescence trace was recorded. In most traces, an interval of increasing fluorescence with a duration of up to 20 ms was detected. The maximum intensity was a fraction r_{ampl} of the initial fluorescence maximum, followed by a decrease. The ratio r_{ampl} of the initial maximum amplitude of the consecutive run to the first was 0.5 ± 0.3 . The minimum level depended on the sample location and a very similar fluorescence level was reached again after about some minutes of excitation, independent of the duration of the dark period. The quantity r_{ampl} appeared to be rather uniform (standard deviation ≤ 0.08) between cycles for a certain location.

In [Peyser02, Peyser01] the behavior of AgO films upon excitation in various environments was studied. A fluorescence intensity rise to a static level was observed within a few minutes. The static intensity level was reported to reflect the dynamic light-dependent equilibrium underlying the creation and destruction of emissive few-atom Ag_n clusters.

For vapor-deposited thin silver films, a similar behavior to the above-mentioned has been found [Jacobson05, Jacobson06]. There, fluorescence intensity was observed to (i) decay for high laser powers and to (ii) initially rise for 1-2 minutes and then decay for low laser powers. In both cases, the decay reached a static level after approximately 1000 seconds. This behavior was also explained by photoinduced creation and destruction of fluorescent chemical species. The chemical reaction responsible for the intensity decay was observed to require oxygen, as the fluorescence intensity of the silver film only increased when kept in a nitrogen atmosphere. Chemical reactions approach the equilibrium concentration as an exponential function of time. Likewise, the intensity $I(t)$ can be expected to follow

$$I(t) = y_0 + \sum_i A_i \exp(-t/t_i), \quad (6.3)$$

with an amplitude A_i for each reaction i ; A_i will be positive if, at time zero (the begin of excitation, disturbance of the equilibrium), the concentration of the fluorescent species is higher than that of the non-fluorescent species. The times t_i are a measure of how fast the chemical reactions approach equilibrium.

Another system where recoverable intensity decays have been found are QDs [ChungI04, Cichos04]. There, two competing theoretical explanations exist: photophysics (for example diffusion-controlled electron transfer [Tang05]) and statistics [Brokmann03]. In the statistical explanation, both on- and off-durations are assumed to be governed by pure power laws with differing exponents. The mean intensity is then changing over time as a power law with an exponent equal to the difference of the on- and off-exponents, as was confirmed by numerical simulation (page 24). Both explanations only allow for a monotonous intensity behavior, whereas in the present work, both a rise and decay was observed. We therefore prefer the photochemistry-based explanation.

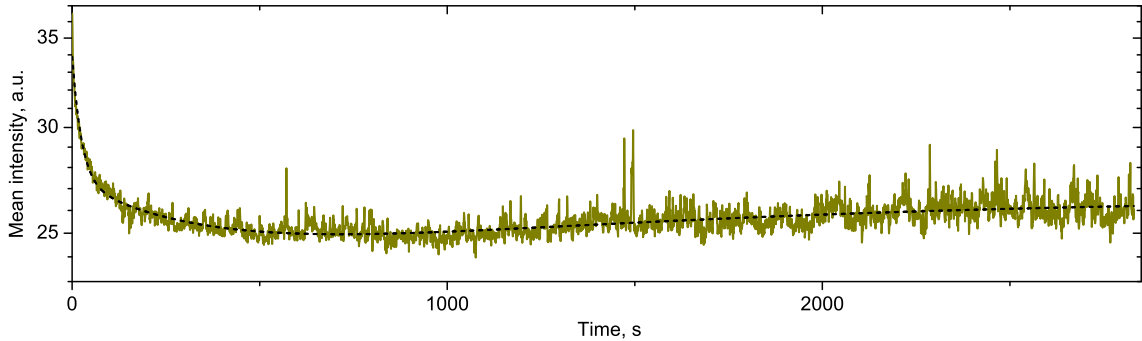


FIG. 30: The intensity shown in Fig. 29(c) was binned to 760 ms-intervals and fitted with a sum of three exponential functions (Eq. (6.3)).

When Eq. (6.3) is used as a fit model, the minimum number of exponentials necessary to successfully fit the ensemble-averaged intensity was three, as is shown in Fig. 30. The obtained intensities were $y_0 = 26.6 \pm 0.2$ units, $A_1 = 6.6 \pm 0.2$ units, $A_2 = 5 \pm 1$ units and $A_3 = -4 \pm 1$ units; The time constants were $t_1 = 23 \pm 1$ s, $t_2 = 367 \pm 60$ s and $t_3 = 1179 \pm 329$.

6.4. Fluorescence behavior in different environments

As was presented in the previous sections, dried silver samples showed strong luminescence when excited with continuous-wave green laser light. It is therefore interesting to check the dependence of the emission on different environments. To do so, we chose to surround silver NPs with the polymer PVP, water and oil.

6.4.1. PVP

Cover slides spin-coated with a PVP-Ag mixture showed few emitters. Typically, the field of view (80 by 80 μm^2) contained only 1-3 emitters. Bright fluorescence without bleaching or blinking was observed. Whereas most emitters stayed at a fixed position, some showed diffusion in three dimensions.

6.4.2. Water

No emission was detected while illuminating the silver sol aqueous solution in a Fluorolog-3 spectrofluorometer model FL3-22 (Horiba Jobin Yvon). It is therefore interesting to follow the behavior of a dry silver sample when brought into aqueous environment. A droplet of deionized water was placed on the sample coverslide while fluctuating emission (blinking) was observed. The sample was imaged for 20 minutes during which the blinking continued at the surface. Individual fluorescent NPs started moving within and out of the focal plane, diffusing into the aqueous environment. While diffusing, they showed constant bright emission in the range of seconds. No blinking was observed. Due to their relatively fast diffusion, no statement on the temporal stability of the emission can be

made. When the glass-water interface was kept in focus, individual particles were seen to come into focus, and at times, immobilized in the focal plane.

It has been reported, that Ag clusters show fluorescence in water, if their concentration is kept below of 0.35 mM [JiangZ05, Siwach08]. Above this threshold, fluorescence is self-quenched by multiple scattering processes. The reported threshold concentration is much higher than the concentrations used in the present work. Contrary to this, Treguer and coworkers [Treguer05] only observed luminescence of colloidal silver NP in Milli-Q grade water, if Ag^+ ions were added.

6.4.3. Oil

In measurements using a pulsed Ti-sapphire laser emitting at 820 nm, coupled to a confocal setup, very strong intermittent fluorescence, which can be attributed to two-photon excitation, was detected from a dried silver sol solution sample. To record intensities comparable to organic dyes, only about a thousandth of the excitation power was required. When the sample was covered with a droplet of oil (Immersion 518 F, Zeiss) the detected intensity of individual particles remained intermittent but the brightness of the on-states decreased continuously until each reached a dark state. No diffusion was witnessed. It needs to be noted that not only the laser was pulsed, but the sample was also scanned to collect the intensity of different emitters simultaneously.

In a similar experiment, a sample of dried silver sol solution was covered with oil while being excited with a CW laser at a power density of a few W/cm^2 at 488 nm. In the remainder of this section, the discussion will focus on this green excitation. Particles also continued blinking and remained fixed to the glass substrate. No fluorescence was detected with the CCD from within the oil. The ensemble emission intensity decreased, and after approximately 14 minutes reached a static level of about 80% of the intensity right after the addition of oil.

6.4.4. Quantitative discussion

The most intense emission was detected from a dried sol solution droplet in atmospheric environment. After coverage with oil, 3% of the 1376 spots disappeared while most stayed at their position and continued blinking. Their mean emission intensity just after coverage was 40% less than before. On the water-treated coverslide, number of spots lowered to 50% of the atmospheric value. The mean emission intensity of an emission center was not influenced by the changed environment; in the focal plane the spots were blinking.

6.5. Experiments with spectrally resolved detection

To determine the relative color of a particle, two intensity traces of each particle recorded in two separate color channels were thresholded individually (see page 26)., Frames with intensities above the threshold levels were counted (n_{red} and n_{green}). Then, the following function was used to map each particle to a number in the range $[0, 1]$:

$$\mathcal{C}(n_{\text{red}}, n_{\text{green}}) := \begin{cases} \frac{1}{2}n_{\text{green}}/n_{\text{red}} & : n_{\text{red}} > n_{\text{green}} \\ 1 - \frac{1}{2}n_{\text{red}}/n_{\text{green}} & : n_{\text{red}} \leq n_{\text{green}} \end{cases} \quad (6.4)$$

While the exact spectral ranges of the two channels depend on the filters used, $\mathcal{C} \approx 0$ corresponds to a green-emitting particle, whereas $\mathcal{C} \approx 1$ corresponds to a red-emitting one. Since there was no

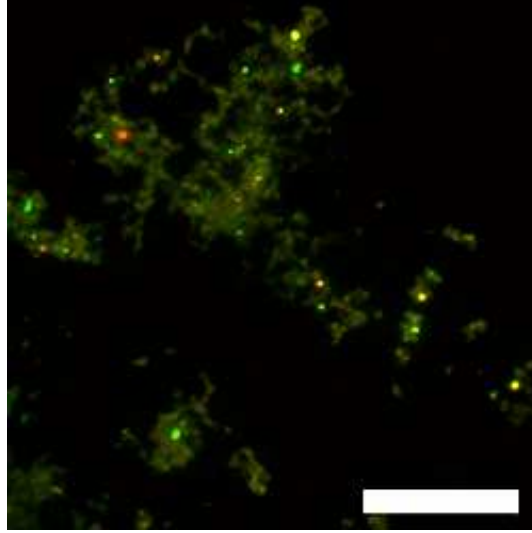


FIG. 31: Color image of silver nanoparticles, integrated over 20 minutes. The image was constructed by superimposing two images recorded simultaneously in two spectral ranges: green (500-550) and red (630-730). The bar represents 10 μm . A video is available at www.biotec.tu-dresden.de/cms/index.php?id=185

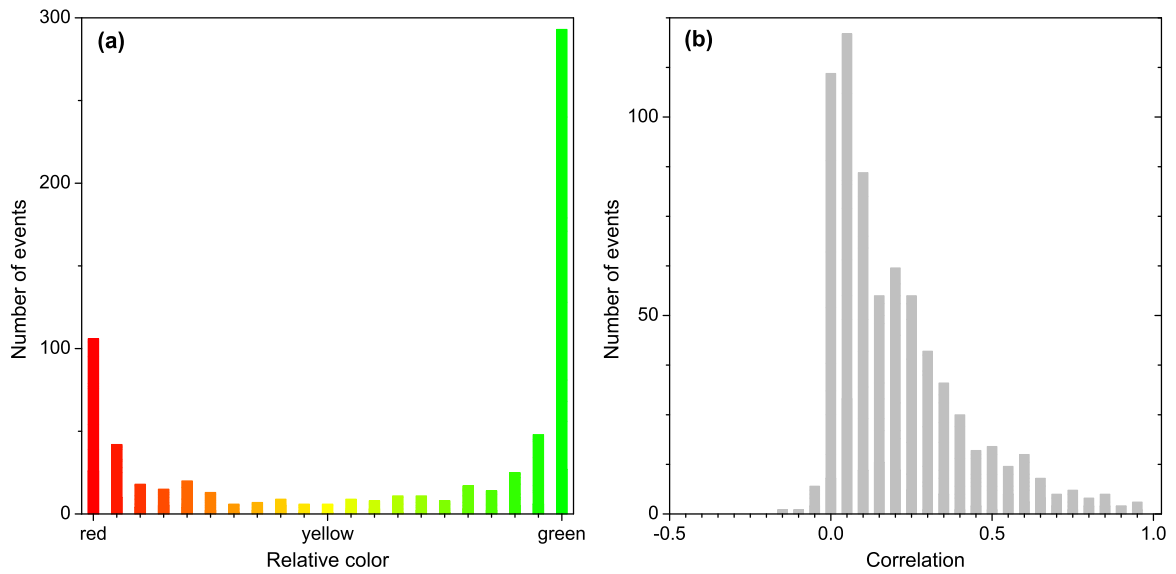


FIG. 32: Histogrammed properties of the intensities of the brightest particles in nine experiments. **(a)** Histogram of the ratio of the intensity detected in the two channels (Eq. (6.4)) for 692 distinct emitters observed for 18.5 minutes. **(b)** Zero-timelag Pearson correlation (Eq. (6.5)) of the intensity in the green channel vs. the red channel.

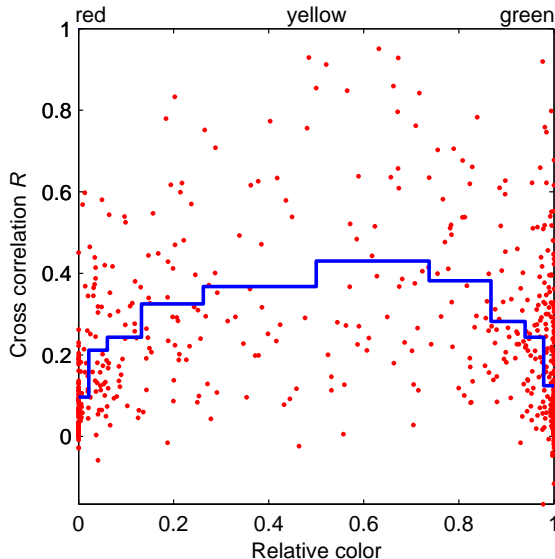


FIG. 33: Zero-timelag cross-correlation vs. the relative color for 692 emission centers (\bullet). To visualize the general trend, a mean R_{cc} has been calculated for several color intervals (—).

spectral overlap between the filters used, a particle emitting in the yellow range would contribute approximately equally to both channels. It was observed that $\sim 42\%$ of the particles emit only in the green band and $\sim 15\%$ emit only in the red band, as is shown in Fig. 32(a).

To find out whether the light detected in the spectral channels was coming from the same particle, one has to cross-correlate the corresponding time-dependent intensity of each channel. If there is no correlation, light in different channels is likely coming from different, independent particles. If there is positive or negative correlation, the source is most likely a single emitter. Another possibility, of course, is correlated emission of a spatially unresolved group of emitters.

To account for the range of $\text{var}\{I(t)\}$, stretching over 3 orders of magnitude, the Pearson correlation was chosen:

$$R_{cc} = \frac{\sum_t (I_{\text{red}}(t) - \langle I_{\text{red}} \rangle)(I_{\text{green}}(t) - \langle I_{\text{green}} \rangle)}{\sqrt{\sum_t (I_{\text{red}}(t) - \langle I_{\text{red}} \rangle)^2} \sqrt{\sum_t (I_{\text{green}}(t) - \langle I_{\text{green}} \rangle)^2}} \quad (6.5)$$

Mathematically, R_{cc} has to be in the range of $[-1, 1]$; in the present application however, anti-correlation appeared rarely. In other words, particles excited with 488 nm-laser light typically do not change their color. This is an important finding, because it rules out spectral diffusion between the two filter bands, on the accessible time scales. The minimum integration time used for the experiments described here was 3 ms, the length of each experiment was 18.5 minutes.

In experiments with single quantum dots [Empedocles97, Mueller05] or single fluorescent dyes [Yip98, Wustholz08], a phenomenon known as spectral diffusion (sometimes also called photoluminescence wandering) is observed. This is the random shift in emission frequencies of single emitters with time, caused by a corresponding change in the distance of energy levels.

For Ag NP samples, it was reported that the temporal evolution of the emission is a combination of at least five distinct spectral peaks (548, 594, 641, 673, and 725 nm) [Peysers01], that dynamically change their relative contribution to the observed emission. These five peaks are thought to correspond to few-atom Ag clusters, whose emission has been studied in noble gas matrixes [Rabin98]. While the 548-nm peak should be visible in green channel, the last three should be clearly observable in the red channel. Yet, it was also observed [Peysers01], that spectra did not show dynamic behavior when the sample was excited with a wavelength of 514.5 nm. In [Andersen04], the maximum of a peak was reported to drift within the interval of 630...640 nm, which would not be resolvable with the filters used.

7. Patterns in silver nanoparticle blinking

7.1. Fluorescence correlation spectroscopy of Ag nanoparticles

A typically way to study fluctuating emission is FCS. The autocorrelation function (ACF) is a tool to grasp the timescales of the dynamics of a process. The normalized function,

$$g(t_{\text{lag}}) = \frac{\mathcal{F}_{t_{\text{lag}}}^{-1}\{|\mathcal{F}_\nu\{I(t) - \langle I \rangle\}|^2\}}{\langle I \rangle^2}, \quad (7.1)$$

where $\mathcal{F}\{\dots\}$ denotes the Fourier transform, is insensitive to detection efficiency, and its shape is independent of a constant background [Verberk02] as introduced by the CCD. Additionally, computing a correlation function does not require thresholding, which involves estimating the threshold level from the experimental data; an error in this parameter can obviously affect the results of the data analysis. Experimental correlation functions can therefore be useful in comparing blinking data to theoretical models.

Similar calculations have been performed for emission data acquired on the wide-field setup and on the confocal setup. On the wide-field setup, the intensity of five distinct emission centers Fig. 34(a-e) was correlated according to Eq. (7.1). As can be seen in Fig. 34(f), the tail of the correlation did not smoothly approach the zero level, but oscillated randomly instead. This behavior is typical if the acquisition time is not enough comparable to the characteristic time scales in the dynamics of the sample. To check the influence of the background on the correlation curve, it was subtracted for the calculations shown in Fig. 35. It can be seen that the correlation functions decay faster. Before subtraction, half of the amplitude of the ACF was reached at a lag time of $t_{1/2} = 2.4 \pm 1.2$ s, whereas after subtraction, $t_{1/2} = 1.5 \pm 0.6$ s. On the confocal setup, $t_{1/2}$ was reduced from 3.1 ± 2.0 s to 0.34 ± 0.18 s by subtracting the background.

For other experimental systems like QDs [Messin01, ZhangK06], it has been observed that the shape of the time-averaged correlation function strongly depend on the length of the experimental observation. Also for the intensity ACF of SERS of Ag nanoparticles a random spread without any characteristic shape was reported [Emory06]. It is believed that the observed probability distributions for the on- and off-states are responsible for this behavior. As mentioned earlier, the off-times show a power law exponent between 1 and 2. In this range, the theoretical mean off-time diverges. Since an experiment with a finite length cannot sample the whole probability distribution, the time-averaged ACF will not be a meaningful tool to study the properties of the system. Alternatively, one can calculate the ensemble-averaged ACF (Eq. (3.10)), which for our experimental data indeed shows a much slower decay, as can be seen in Fig. 38. After 1000 s, the ensemble-averaged ACF decayed to $\approx 1/4$ of its short-lag value, whereas the time-averaged ACF decayed to negative values close to zero. This ergodicity-breaking behavior has been described and observed for QDs [Brokmann03].

In this work, the blinking behavior of silver nanoparticles is modeled by time series drawn from a power law-driven telegraph process. Whereas usually the variance of the correlation function at a specific lag tends to zero as the measurement time increases, the time-averaged autocorrelation of a will approach a constant, non-zero variance. In this model, even for a time series of infinite length T ,

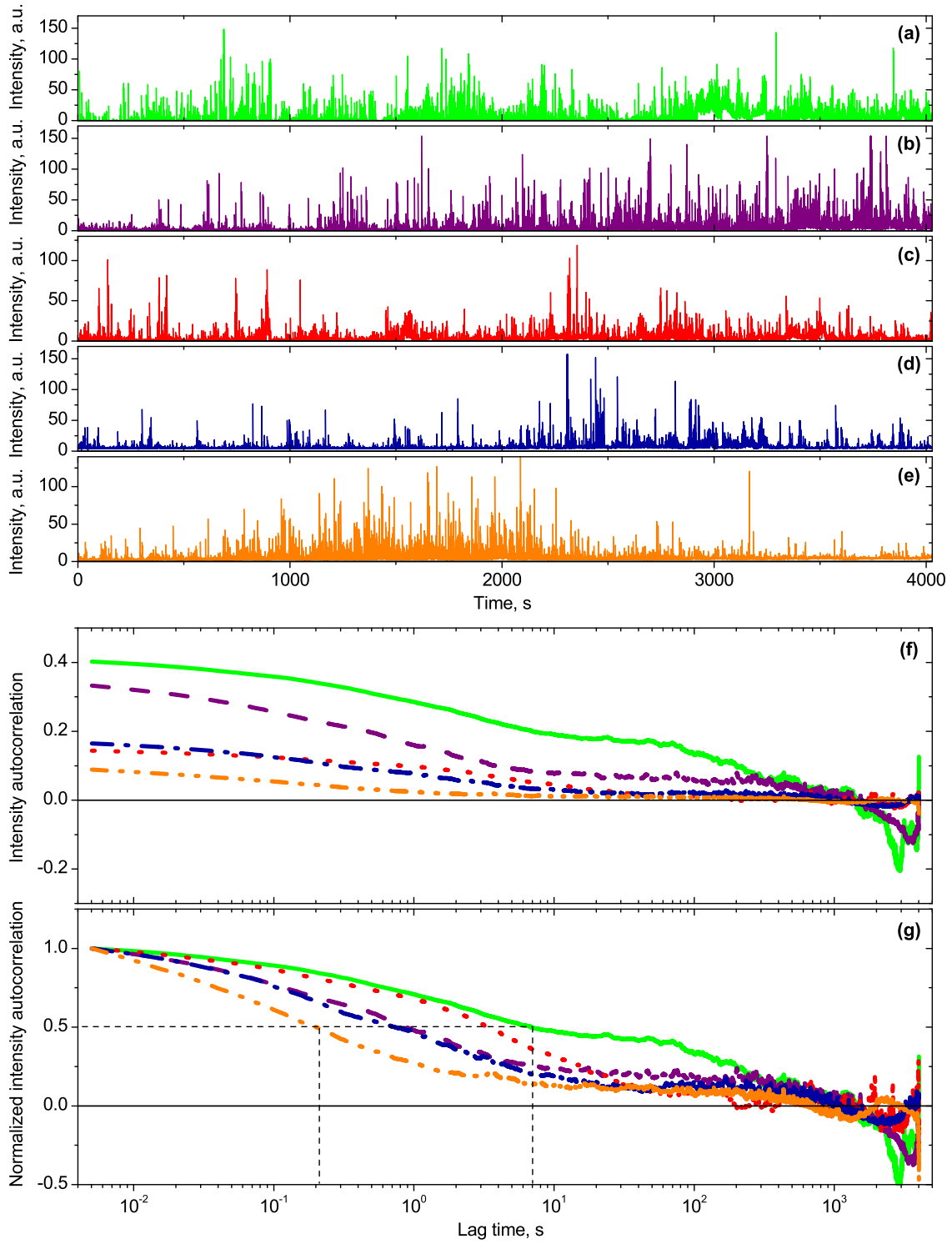


FIG. 34: (a-e) Emission intensity of five emission centers in a dry Ag nanoparticle sample excited with 488 nm light. The data was acquired on the CCD-based wide-field setup with an integration time of 5 ms, the laser power density was $P = 6.6 \text{ W/cm}^2$ (f) Time-averaged autocorrelation (Eq. (7.1)) of (a-e). (g) ACF normalized by the maximum amplitude.

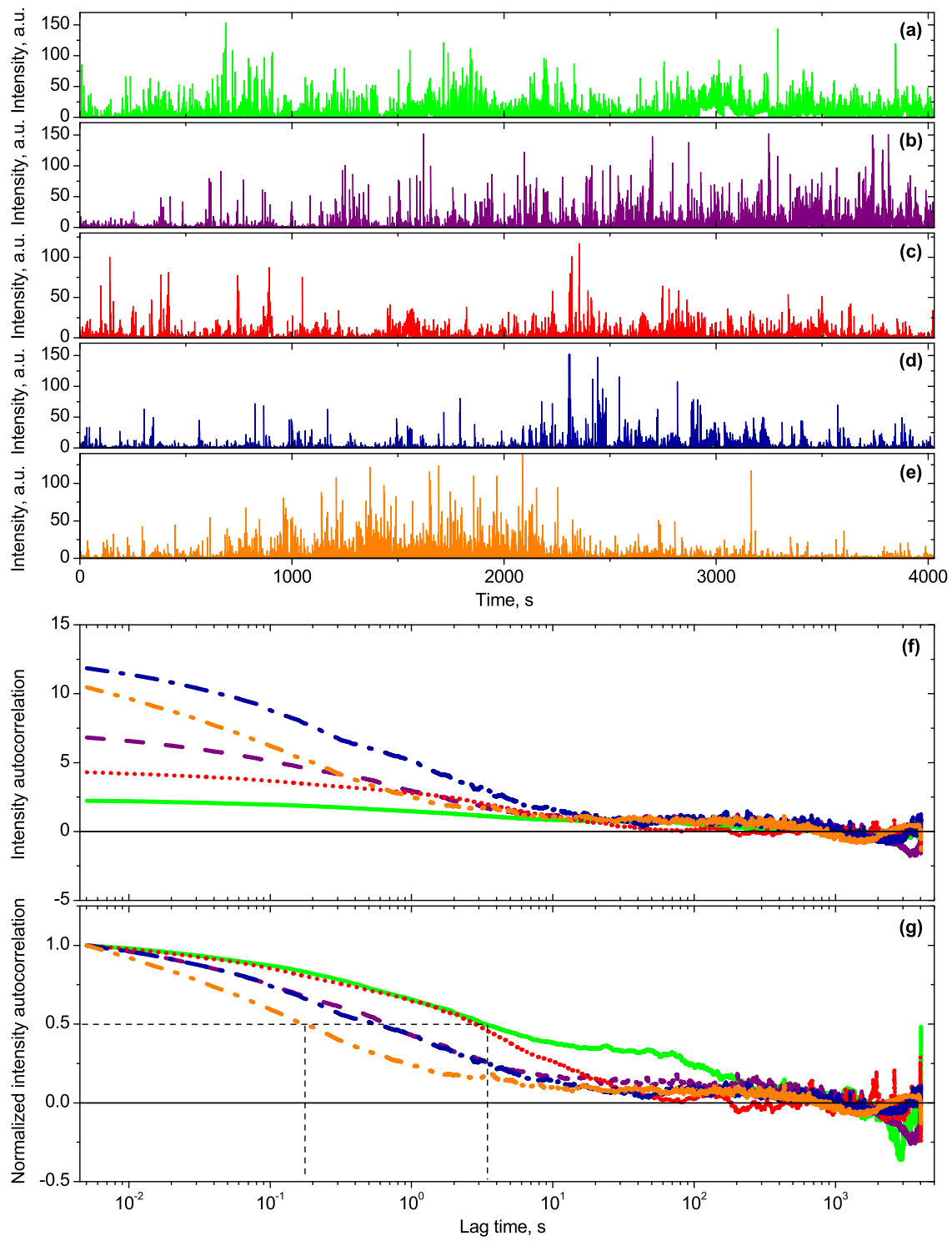


FIG. 35: Same emitters as Fig. 34, with the background subtracted from the intensity traces. The correlation curves were calculated from the data shown in (a-e).

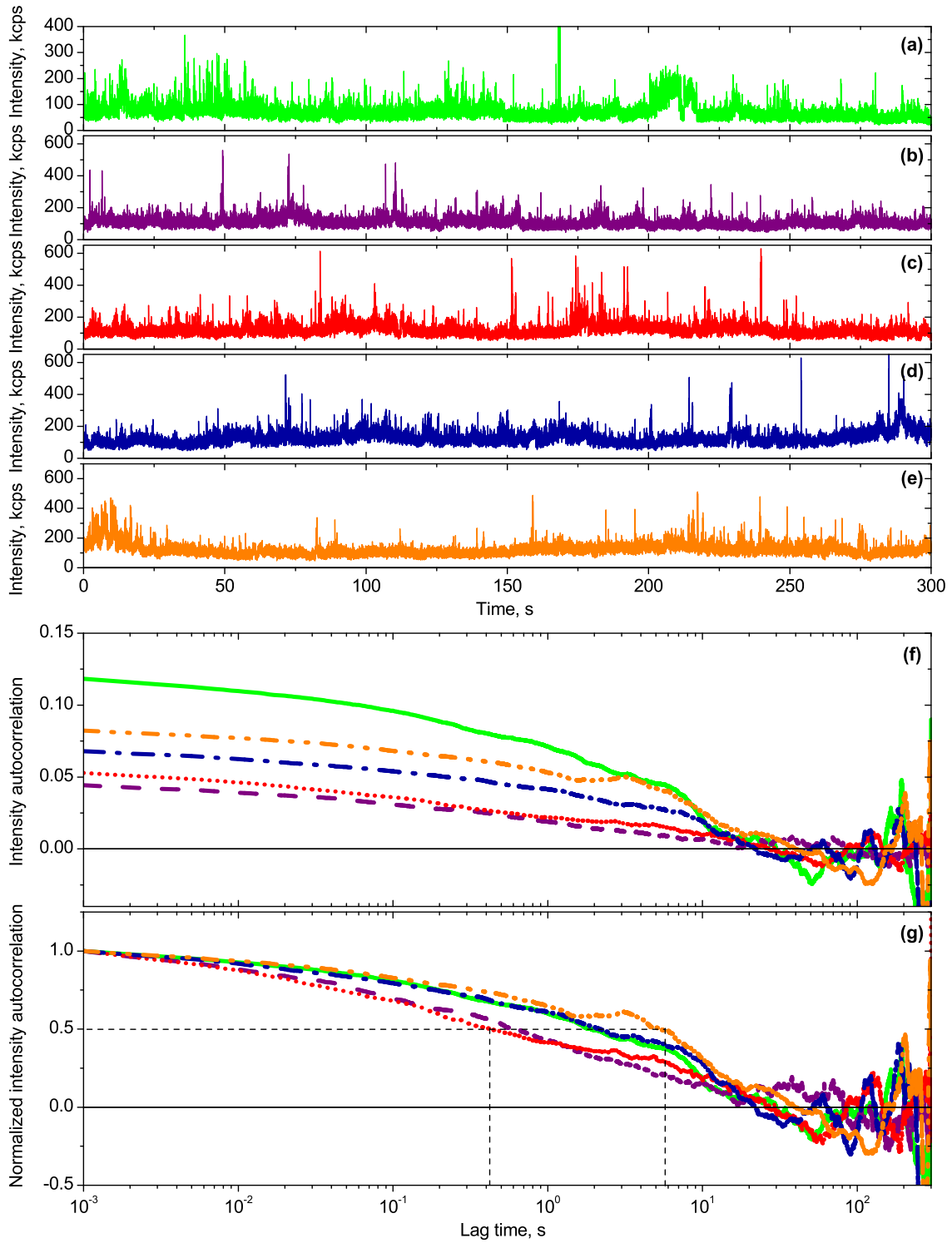


FIG. 36: **(a-e)** Emission intensity of five emission centers in a dry Ag nanoparticle sample excited with 488 nm light. Data measured at the confocal setup with a laser power of $1.82 \mu\text{W}$. The count rate has been binned to 1 ms-intervals. **(f)** Time-averaged autocorrelation (Eq. (7.1)) of (a-e). **(g)** ACF normalized by the maximum amplitude.

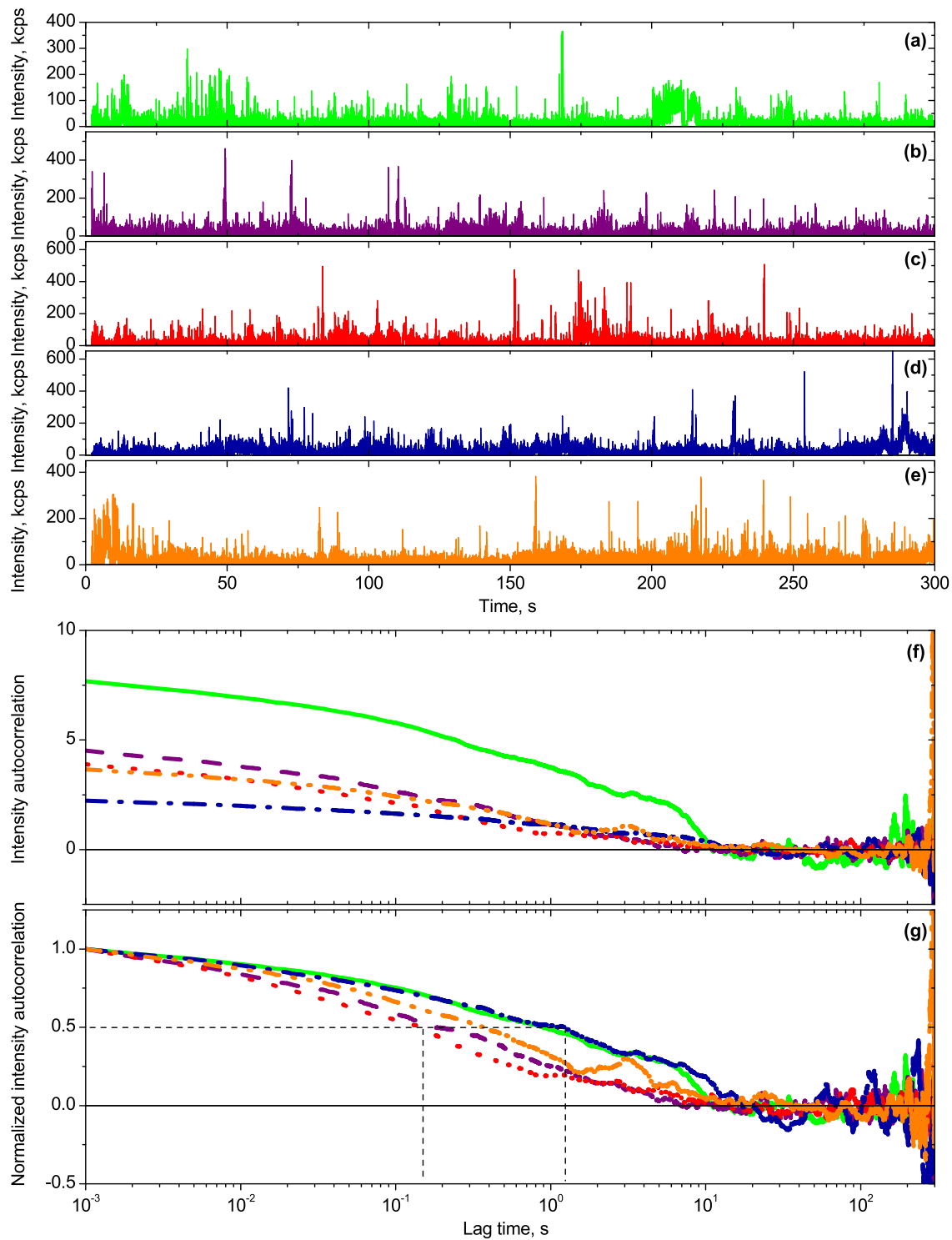


FIG. 37: Same emitters as Fig. 36, with the background subtracted from the intensity traces. The correlation curves were calculated from the data shown in (a-e).

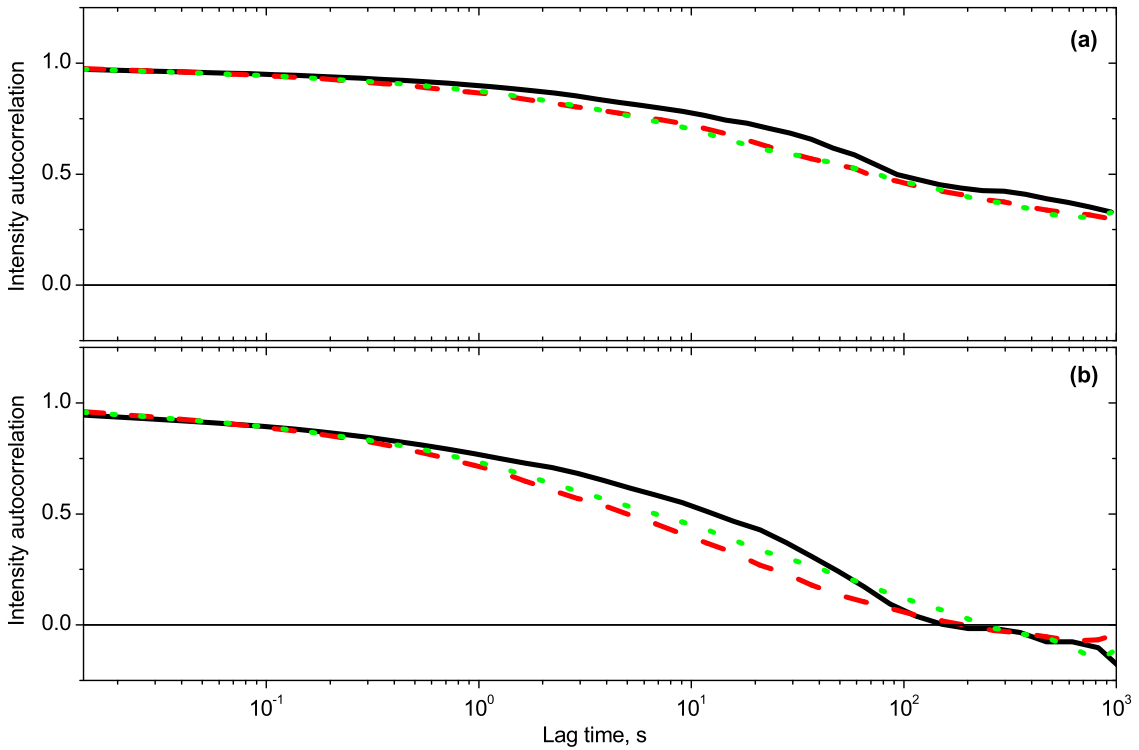


FIG. 38: **(a)** Ensemble averaged (Eq. (3.10), normalized intensity autocorrelation of 226 (— —), 355 (—) and 175 (· · ·) particles of three different samples, acquired on the CCD-based wide-field setup with an integration time of 13.8 ms. The laser power density was 5.3, 3.8 and 6.6 W/cm², respectively. **(b)** Time averaged (Eq. (7.1) ACF, normalized to the zero-lag value of each curve.

the ACF does not converge to a limit function. Instead, the autocorrelation continues to be a random function with a broad distribution having two maxima [Margolin04].

It is concluded that FCS is not an appropriate tool to study the blinking of silver nanoparticles.

7.2. On- and off-duration correlations (memory)

In 2000, a study on the emission of quantum dots [Kuno01b] reported on the correlation of successive on- and off-durations. No correlation was found, and it was concluded that the reported power law-distributed durations are not the consequence of a single exponential distribution with a rate constant changing with time. Later, a careful study [Stefani05b] revealed that there is a correlation between successive on-durations. Successive off-durations were also found to be correlated, and the log of on-versus the log of off-durations showed a weak anti-correlation. It was concluded that memory is a genuine characteristic of the blinking of QDs, lasting 3-4 seconds. Such a memory effect was also found for the emission of single fluorescent dyes [Hoogenboom08, Wustholz08], lasting for at least 200 ms. In all three references, it was concluded that nanoscale environmental dynamics can lead to the

power-law distribution of on-times and the observed memory. To our knowledge, the correlation of durations in the emission of silver NPs has not been studied before, but may offer an insight in the underlying mechanism. It may be, that not only the phenomenology of the different emitters listed above is similar, but also its underlying physics.

To explore the dynamics of the emission patterns observed for silver NPs, the duration of a given on- or off-state can be correlated with the next (or another) duration. This can be expressed by the Pearson correlation function defined as

$$g_{x,y}(\Delta n) = \frac{\langle (\tau_x(n) - \langle \tau_x \rangle)(\tau_y(n + \Delta n) - \langle \tau_y \rangle) \rangle}{\sqrt{\text{var}(\tau_x) \text{var}(\tau_y)}} \quad (7.2)$$

$$\text{var}(\tau) = \frac{1}{N-1} \sum_{n=1}^N (\tau(n) - \langle \tau \rangle)^2 \quad (7.3)$$

with Δn being an integer, $x, y \in \{\text{“on”}, \text{“off”}\}$, $\text{var}(\dots)$ being the variance averaged over switching events n , and $\langle \dots \rangle$ denoting averaging over switching event numbers n , which are defined in Fig. 11. For an infinite set of uncorrelated τ_x and τ_y , $g_{x,y}(\Delta n) \propto \delta_{xy} \cdot \delta(\Delta n)$, where $\delta(\Delta n)$ represents the Dirac delta function and δ_{xy} the Kronecker symbol. Any systematic deviation from the delta shape is a clue for a memory of the previous state duration, as it means that a given state duration tends to be followed by a time interval of approximately the same length.

Measurements were performed at two distinctively different setups, wide-field and confocal. Two sources of artifacts had to be avoided: (i) the ensemble emission intensity $\bar{I}(t)$ is not constant (see Fig. 29). The background of each emitter intensity was subtracted before thresholding, but it is not clear whether $\bar{I}(t)$ changes due to a fluctuating on-intensity level or whether the on-/off-duration statistics change. Since the time-scale of change in $\bar{I}(t)$ is slower (≥ 23 s) than of the correlation, as reported below. (ii) On- and off-durations extending over the beginning or the end of the acquisition were disregarded. Since only the “middle” of the data was reliable, on- or off-states closer to the beginning or end, than 100 times the mean duration, were disregarded.

As shown in Fig. 39, we observed a significant correlation for on- and off-state duration, indicating that the underlying physical process has a memory. In the confocal measurements, the correlation was kept over tens of on/off cycles. In order to get a rough idea of the time scale of the phenomenon, we calculated the mean state duration

$$\langle \tau_x \rangle = \frac{1}{N} \sum_{n=1}^N \tau_x(n).$$

The mean off-duration was 230 ms, whereas the mean on-duration was 2.6 ms. Taken together, $\frac{1}{2}(\langle \tau_{\text{off}} \rangle \langle \tau_{\text{on}} \rangle) = 83$ ms. When taking the last number to map Δn to seconds, the memory persisted over a few seconds.

Eq. (7.2) is mostly sensitive to the correlation between long durations. One can also calculate

$$g_{x,y}^{\log}(\Delta n) = \frac{\langle (\log \tau_x(n) - \langle \log \tau_x \rangle)(\log \tau_y(n + \Delta n) - \langle \log \tau_y \rangle) \rangle}{\sqrt{\text{var}(\log \tau_x) \text{var}(\log \tau_y)}} \quad (7.4)$$

to put more focus on short durations. This function showed an even more pronounced correlation of on-on, and off-off durations. Also, an anti-correlation between on- and off-durations was found. Here,

two variants exist: one can either (i) calculate the correlation of a given on-duration with next off-durations. This is equivalent to calculating the correlation between off-durations and the preceding on-durations. Or (ii) one calculates the off-durations with the following on-durations, which, in turn, is numerically equivalent to calculating the correlation between an on-duration and the preceding off-durations. Calculations showed that the shape of both (i) and (ii) are the same, differing only in noise. Therefore, only variant (i) is shown in the figures.

Data acquired on the wide-field setup were also correlated (Fig. 40). There, the general picture is the same: The memory persisted for several seconds (mean state duration 0.39 s). In contrast to the anti-correlation seen in the confocal data, virtually no correlation was found when Eq. (7.2) was used to calculate the cross-correlation between on- and off-durations.

To be certain that the observed memory is not an artifact, extensive checks have been performed: (i) Randomizing the order of the experimental on- and off-durations removed the observed memory entirely. (ii) Higher and lower threshold levels than the $4\sigma_b$ used (see page 28) introduced more noise in the correlation function, but above $2\sigma_b$, the shape remained the same. Below $2\sigma_b$, the correlation gradually disappeared. (iii) Monte Carlo simulations with different exponents m in the interval [1, 2.5], treated just as the experimental data, did not show any correlation. Adding Gaussian-distributed (white) noise did not introduce any correlation, independent of the relative amplitudes. (iv) It was shown on page 52, that the average length of a state $\bar{\tau}(t)$ as a function of the time it starts, drops just before the end of the experiment. To remove the possibility of an apparent correlation due to this drop, only the first 80% of the data were used.

7.2.1. Dependence of correlation $g_{x,y}(\Delta n)$ on mean pixel intensity $\langle I \rangle(p)$

To make sure that the observed memory effect is not created by excitation power fluctuations, which might cause deviations in the background level, and therefore cause threshold crossings unrelated to the Ag particle emission intensity, the laser power was checked with an 841-PE (Newport, Irvine, USA) during the course of the experiments. The observed fluctuations were in the range of 4% of the mean power, and, assuming a linear relationship, cannot be held responsible for the strong correlation observed.

We grouped individual emitters according to their temporal mean intensity and calculated $g_{x,y}(t)$, $x, y \in \{\text{“on”}, \text{“off”}\}$ for each group. The shape of the curves, and the range of the correlation, was the same in each group, indicating that the source of the correlations was independent of the detected intensity.

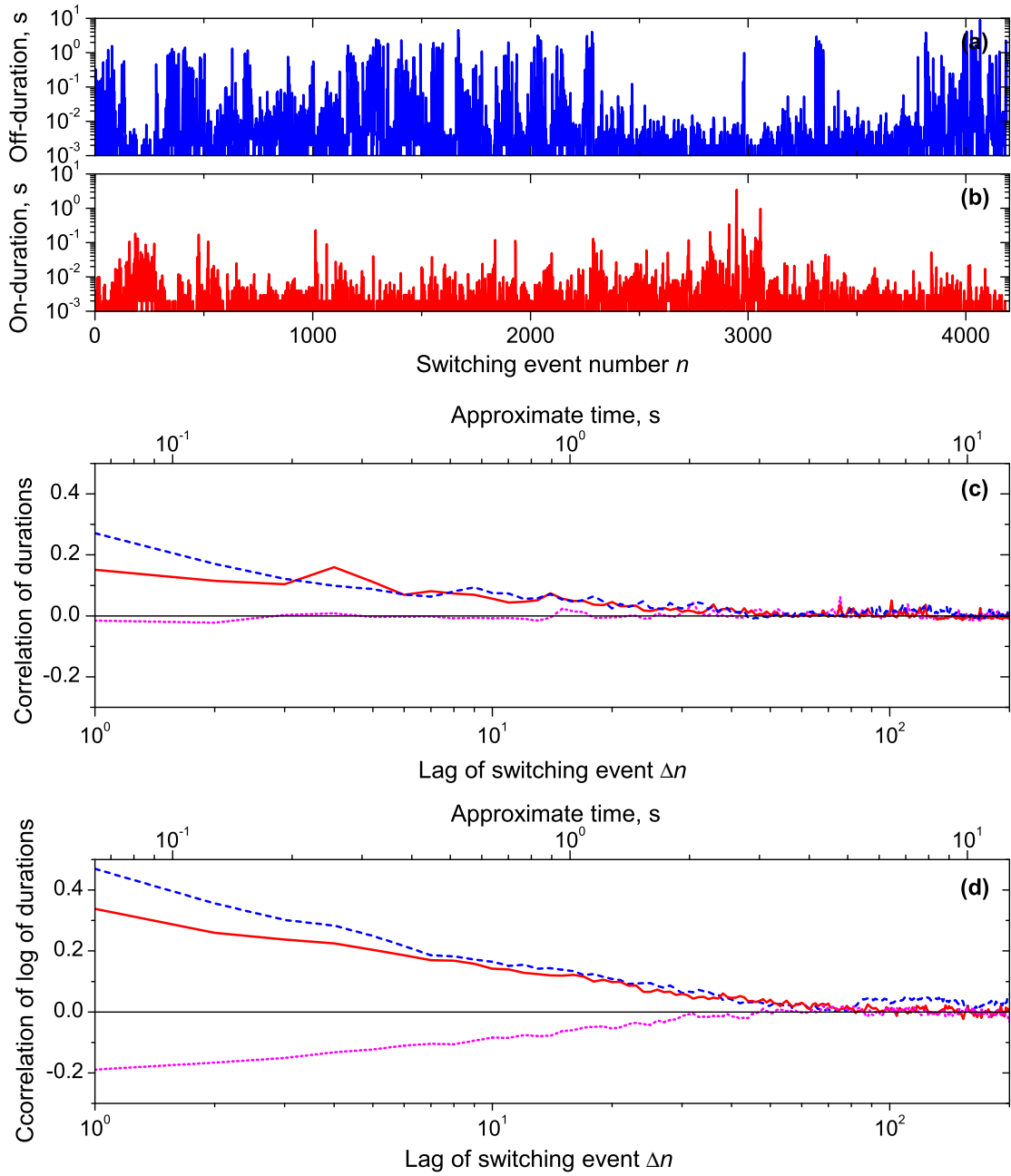


FIG. 39: **(a)** Off-state durations τ_{off} of one isolated emitter, calculated from the photon count rate measured with the confocal setup. The shortest possible duration was 1 ms, since the count rate was binned to 1 ms. **(b)** On-state durations for the same emitter. **(c)** Autocorrelation (Eq. (7.2)) between on-durations (—), off-state durations (---) and cross-correlation (.....) between on- and off-durations. **(d)** Correlations of the log of durations, according to Eq. (7.4).

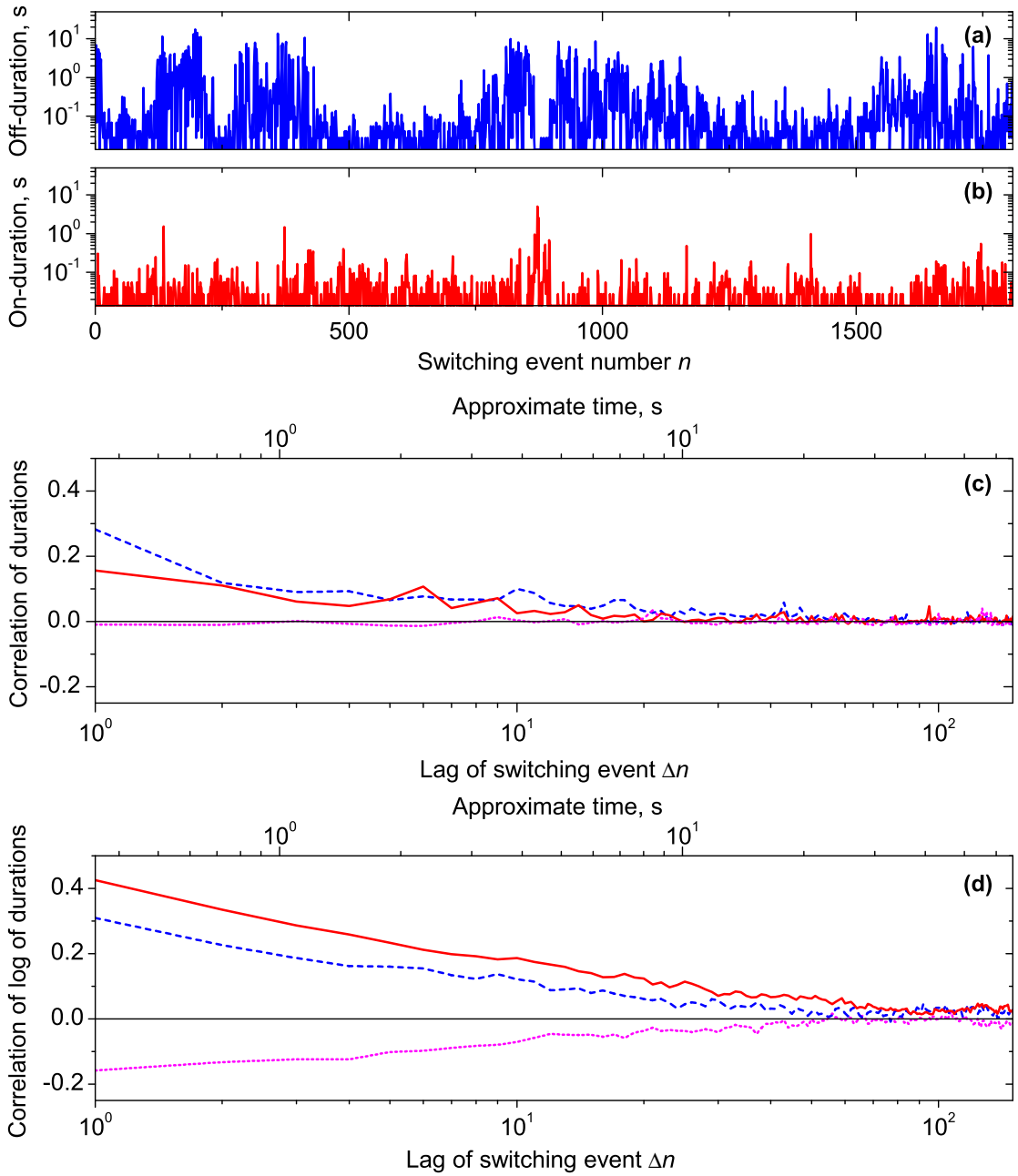


FIG. 40: Same calculation as Fig. 39, but for the CCD-based wide-field setup. **(a)** Off-state durations τ_{off} of one isolated emitter. The shortest possible duration was 13.8 ms, corresponding to the frame-to-frame time of the CCD acquisition. **(b)** On-state durations for the same emitter. **(c)** Autocorrelation (Eq. (7.2)) between on-durations (—), off-state durations (---) and cross-correlation (⋯) between on- and off-durations. **(d)** Correlations of the log of durations, according to Eq. (7.4).

8. Conclusions

In this study, emission properties of silver nanoparticles with sizes below 100 nm have been investigated. These nanoparticles were deposited on glass substrates in air as well in other environments such as polymer film and oil. They showed bright emission upon optical excitation in the visible spectral range. The measured emission spectra showed broad fluorescence bands that were independent of the specific environment, superimposed with distinct peaks whose amplitude and position depended on the particular chemical composition of the local environment. Experiments with different excitation wavelengths allowed to ascribe these peaks as surface enhanced Raman scattering (SERS) of molecules located in the vicinity of Ag nanoparticles.

Emission intensity decay traces of silver nanoparticles upon pulsed optical excitation were investigated in picosecond and nanosecond time scales. The time resolution of the setup set the upper estimate of the fluorescence decay time $\tau_f \approx 100$ ps. While the exact reason for the surprisingly fast fluorescence decay is unclear, it can be assumed that it is due to proximity of the emitter to metal surfaces (metal enhanced fluorescence).

The long-term behavior of the ensemble-integrated emission intensity of silver nanoparticles upon CW laser excitation was studied. In the first few minutes after turning the excitation on, the intensity was observed to decay to about 50% of the initial value. This decay can be characterized by a sum of two exponential functions, with time constants of about 20 and 400 s. After the initial decay, no further bleaching or photodegradation was observed. Instead, the intensity showed a gradual partial recovery to about 60% of the initial value. The time constant of this process was found to be ~ 1200 s. The sample continued to emit at this intensity in experiments lasting for several hours, which allowed us to study the properties of the emission of individual nanoemitters in detail using video microscopy and confocal microscopy.

It was found that emission of individual nanoparticles is intermittent: periods of random duration of high emission (on-state) and dim or no emission (off-state) were observed. The duration of intensity bursts (on-duration) and the interval between two bursts (off-duration) were studied. It was found, that the probability distribution of on-durations τ_{on} closely followed a power law $P(\tau_{\text{on}}) = \tau_{\text{on}}^{-m_{\text{on}}}$, whereas the off-durations τ_{off} showed a power law with an exponential cut-off, $P(\tau_{\text{off}}) = \tau_{\text{off}}^{-m_{\text{off}}} \exp(-\tau_{\text{off}}/\theta_{\text{cut}})$. The power law exponents of on-durations and the off-durations m_{off} as well as the cut-off time θ_{cut} showed a dependence on the excitation power density at the sample. The parameters of the on-duration probability distribution were found to be $m_{\text{on}} = 1.9$ for 6 W/cm^2 and $m_{\text{on}} = 2.2$ for $\approx 200 \text{ W/cm}^2$; those of the off-duration distribution were $m_{\text{off}} = 1.5$, $\theta_{\text{cut}} = 102 \text{ s}$ for 6 W/cm^2 and $m_{\text{off}} = 1.4$, $\theta_{\text{cut}} = 6.9 \text{ s}$, for $\approx 200 \text{ W/cm}^2$. The absence of an observable cut-off for the on-durations at the accessible experimental times indicates that the mean on-duration may be considered to be infinite on the experimentally accessible time scale, and therefore one can expect that the system will show signs of non-ergodic behavior.

Intermittent emission was also studied by means of fluorescence correlation spectroscopy (FCS). Autocorrelation curves of emission of individual particles showed no convergence to a common dependence, even for experiments with durations of the order of an hour. In agreement with the theory predicting this behavior for autocorrelation functions of a telegraph processes with power law-distributed waiting times (and thus showing ergodicity breaking), FCS proved not to be the right

method to study the dynamics of blinking Ag nanoparticles. The non-ergodic behavior was further confirmed by finding that ensemble-averaged intensity correlation curves showed a shape different from that of time-averaged correlation curves.

To further study the dynamics of intermittent emission of Ag nanoparticles, we investigated the on- and off-durations τ_{off} and τ_{on} as a function of the on-off switching event number n . Interestingly, both $\tau_{\text{off}}(n)$ and $\tau_{\text{on}}(n)$ did not behave completely randomly, but were found to show non-zero autocorrelation. Additionally, $\tau_{\text{off}}(n)$ and $\tau_{\text{on}}(n)$ were found to be anti-correlated. These auto- and cross-correlations extend up to several tens of switching events, which indicates the presence of memory in the blinking dynamics of silver nanoparticles.

It should be pointed out, that a similar effect was previously observed for semiconductor nanocrystals and, very recently, for organic dye molecules. The fact that we observe this phenomenon for the first time for yet another different system, namely Ag nanoparticles, points to its universal character. The exact physical origin of the process leading to this memory remains to be elucidated.

References

- [Andersen04] P. C. Andersen, M. L. Jacobson and K. L. Rowlen (2004). Flashy silver nanoparticles. *J. Phys. Chem. B*, **108**: 2148.
- [AshaRani09] P. V. AshaRani, G. L. K. Mun, M. P. Hande and S. Valiyaveetil (2009). Cytotoxicity and genotoxicity of silver nanoparticles in human cells. *ACS Nano*, **3**: 279.
- [Biju08] V. Biju, T. Itoh, A. Anas, A. Sujith and M. Ishikawa (2008). Semiconductor quantum dots and metal nanoparticles: syntheses, optical properties, and biological applications. *Anal. Bioanal. Chem.*, **391**: 2469.
- [Bizzarri05] A. R. Bizzarri and S. Cannistraro (2005). Lévy statistics of vibrational mode fluctuations of single molecules from surface-enhanced Raman scattering. *Phys. Rev. Lett.*, **94**: 068303.
- [Bjorneld00] E. J. Bjorneld, P. Johansson and M. Käll (2000). Single molecule vibrational fine-structure of tyrosine adsorbed on Ag nano-crystals. *Single Molecules*, **1**: 239.
- [Bohren83] C. F. Bohren and D. R. Huffman (1983). *Absorption and Scattering of Light by Small Particles*. Wiley, New York.
- [Bouchaud95] J. P. Bouchaud and D. Dean (1995). Aging on Parisi's tree. *J. Phys. I France*, **5**: 265.
- [Boyd86] G. T. Boyd, Z. H. Yu and Y. R. Shen (1986). Photoinduced luminescence from the noble metals and its enhancement on roughened surfaces. *Phys. Rev. B*, **33**: 7923.
- [Brokmann03] X. Brokmann, J.-P. Hermier, G. Messin, P. Desbiolles, J.-P. Bouchaud and M. Dahan (2003). Statistical aging and nonergodicity in the fluorescence of single nanocrystals. *Phys. Rev. Lett.*, **90**: 120601.
- [Chance74] R. R. Chance, A. Prock and R. Silbey (1974). Lifetime of an excited molecule near a metal mirror: Energy transfer in the Eu^{3+} /silver system. *J. Chem. Phys.*, **60**: 2184.
- [Chia09] Z. Chia, R. Liua, L. Zhaoa, P. Qina, X. Pana, F. Suna and X. Hao (2009). A new strategy to probe the genotoxicity of silver nanoparticles combined with cetylpyridine bromide. *Spectrochim. Acta A*, **72**: 577.
- [Chowdhury07] M. H. Chowdhury, S. K. Gray, J. Pond, C. D. Geddes, K. Aslan and J. R. Lakowicz (2007). Computational study of fluorescence scattering by silver nanoparticles. *J. Opt. Soc. Am. B*, **24**: 2259.
- [Chowdhury08] M. H. Chowdhury, K. Ray, C. D. Geddes and J. R. Lakowicz (2008). Use of silver nanoparticles to enhance surface plasmon-coupled emission (spce). *Chem. Phys. Lett.*, **452**: 162.
- [ChungI04] I. Chung and M. G. Bawendi (2004). Relationship between single quantum-dot intermittency and fluorescence intensity decays from collections of dots. *Phys. Rev. B*, **70**: 165304.
- [ChungS91] S. Chung and R. Kennedy (1991). Forward-backward non-linear filtering technique for extracting small biological signals from noise. *J. Neurosci. Meth.*, **40**: 71.
- [Cichos04] F. Cichos, J. Martin and C. von Borczyskowski (2004). Emission intermittency in silicon nanocrystals. *Phys. Rev. B*, **70**: 115314.
- [Cichos07] F. Cichos, C. von Borczyskowski and M. Orrit (2007). Power-law intermittency of single emitters. *Curr. Opin. Colloid. In.*, **12**: 272.
- [Cremer08] G. D. Cremer, Y. Antoku, M. B. J. Roeflaers, M. Sliwa, J. V. Noyen, S. Smout, J. Hofkens, D. E. D. Vos, B. F. Sels and T. Vosch (2008). Photoactivation of silver-exchanged zeolite a. *Angew. Chem. Int. Ed.*, **47**: 2813.
- [Durisic07] N. Durisic, A. I. Bachir, D. L. Kolin, B. Hebert, B. C. Lagerholm, P. Grutter and P. W. Wiseman (2007). Detection and correction of blinking bias in image correlation transport measurements of quantum dot tagged macromolecules. *Biophys. J.*, **93**: 1338.
- [Emory98a] S. R. Emory, W. E. Haskins and S. Nie (1998). Direct observation of size-dependent optical

- enhancement in single metal nanoparticles. *J. Am. Chem. Soc.*, **120**: 8009.
- [Emory06] S. R. Emory, R. A. Jensen, T. Wenda, M. Hanb and S. Nie (2006). Re-examining the origins of spectral blinking in single-molecule and single-nanoparticle SERS. *Faraday Discuss.*, **132**: 249.
- [Emory98b] S. R. Emory and S. Nie (1998). Screening and enrichment of metal nanoparticles with novel optical properties. *J. Phys. Chem. B*, **102**: 493.
- [Empedocles97] S. A. Empedocles and M. G. Bawendi (1997). Quantum-confined stark effect in single CdSe nanocrystallite quantum dots. *Science*, **278**: 2114.
- [Fleischmann81] M. Fleischmann, P. J. Hendra, I. R. Hill and M. E. Pemble (1981). Enhanced Raman spectra from species formed by the coadsorption of halide ions and water molecules on silver electrodes. *J. Electroanal. Chem.*, **117**: 243.
- [Ford84] G. W. Ford and W. H. Weber (1984). Electromagnetic interactions of molecules with metal surfaces. *Phys. Rep.*, **113**: 195 .
- [Freedman81] D. Freedman and P. Diaconis (1981). On the histogram as a density estimator - l_2 theory. *Z. Wahrscheinlichkeit*, **57**: 453.
- [Futamata07] M. Futamata and Y. Maruyama (2007). Electromagnetic and chemical interaction between Ag nanoparticles and adsorbed rhodamine molecules in surface-enhanced Raman scattering. *Anal. Bioanal. Chem.*, **388**: 89.
- [Futamata04] M. Futamata, Y. Maruyama and M. Ishikawa (2004). Adsorbed sites of individual molecules on Ag nanoparticles in single molecule sensitivity–surface-enhanced Raman scattering. *J. Phys. Chem. B*, **108**: 13119.
- [Geddes03] C. D. Geddes, A. Parfenov, I. Gryczynski and J. R. Lakowicz (2003). Luminescent blinking from silver nanostructures. *J. Phys. Chem. B*, **107**: 9989.
- [Godreche01] C. Godreche and J. M. Luck (2001). Statistics of the occupation time of renewal processes. *J. Stat. Phys.*, **104**: 489.
- [Gaertner08] M. Gärtner (2008). *Fluoreszenz-Lebensdauer-Analyse zur funktionalen Charakterisierung von Biomembranen*. Master’s thesis, Technische Universität Dresden.
- [Gwinn08] E. G. Gwinn, P. O’Neill, A. J. Guerrero, D. Bouwmeester and D. K. Fygenson (2008). Sequence-dependent fluorescence of DNA-hosted silver nanoclusters. *Adv. Mater.*, **20**: 279.
- [Haase04] M. Haase, C. G. Hu1bner, E. Reuther, Herrmann, K. Müllen and T. Basché (2004). Exponential and power-law kinetics in single-molecule fluorescence intermittency. *J. Phys. Chem. B*, **108**: 10445.
- [Hansen07] P. C. Hansen (2007). Regularization tools. A Matlab package for analysis and solution of discrete ill-posed problems. *Numer. Algorithms*, **46**: 103.
- [Hildebrand84] P. Hildebrandt and M. Stockburger (1984). Surface-enhanced resonance Raman-spectroscopy of Rhodamine-6G adsorbed on colloidal silver. *J. Phys. Chem.*, **88**: 5935.
- [Hoogenboom06] J. P. Hoogenboom, W. K. den Otter and H. L. Offerhaus (2006). Accurate and unbiased estimation of power-law exponents from single-emitter blinking data. *J. Chem. Phys.*, **125**: 204713.
- [Hoogenboom08] J. P. Hoogenboom, J. Hernando, M. F. García-Parajó and N. F. van Hulst (2008). Memory in single emitter fluorescence blinking reveals the dynamic character of nanoscale charge tunneling. *J. Phys. Chem. C*, **112**: 3417.
- [Hoogenboom07] J. P. Hoogenboom, J. Hernando, E. M. H. P. van Dijk, N. F. van Hulst and M. F. García-Parajó (2007). Power-law blinking in the fluorescence of single organic molecules. *ChemPhysChem*, **8**: 823.
- [Horimoto08] N. N. Horimoto, K. Imura and H. Okamoto (2008). Dye fluorescence enhancement and quenching by gold nanoparticles: Direct near-field microscopic observation of shape dependence. *Chem. Phys. Lett.*, **467**: 105.

- [Ievlev00] D. Ievlev, I. Rabin, W. Schulze and G. Ertl (2000). Light emission in the agglomeration of silver clusters. *Chem. Phys. Lett.*, **328**: 142.
- [ItohK05] K. Itoh, I. Kudryashov, J. Yamagata, T. Nishizawa, M. Fujii and N. Osaka (2005). Raman microspectroscopic study on polymerization and degradation processes of a diacetylene derivative at surface enhanced Raman scattering active substrates. 2. Confocal Raman microscopic observation of polydiacetylene adsorbed on active sites. *J. Phys. Chem. B*, **109**: 271.
- [ItohT06a] T. Itoh, V. Biju, M. Ishikawa, Y. Kikkawa, K. Hashimoto, A. Ikehata and Y. Ozaki (2006). Surface-enhanced resonance Raman scattering and background light emission coupled with plasmon of single Ag nanoaggregates. *J. Chem. Phys.*, **124**: 134708.
- [ItohT06b] T. Itoh, K. Hashimoto, V. Biju, M. Ishikawa, B. R. Wood and Y. Ozaki (2006). Elucidation of interaction between metal-free tetraphenylporphine and surface Ag atoms through temporal fluctuation of surface-enhanced resonance Raman scattering and background-light emission. *J. Phys. Chem. B*, **110**: 9579.
- [Izenman91] A. J. Izenman (1991). Recent developments in nonparametric density estimation. *J. Am. Stat. Assoc.*, **86**: 205.
- [Jacobson05] M. L. Jacobson and K. L. Rowlen (2005). Photo-dynamics on thin silver films. *Chem. Phys. Lett.*, **401**: 52.
- [Jacobson06] M. L. Jacobson and K. L. Rowlen (2006). The role of O₂ in SERS-active thin metal film photodynamics. *J. Phys. Chem. B*, **110**: 19491.
- [JiangJ03] J. Jiang, K. Bosnick, M. Maillard and L. Brus (2003). Single molecule Raman spectroscopy at the junctions of large Ag nanocrystals. *J. Phys. Chem. B*, **107**: 9964.
- [JiangZ05] Z. Jiang, W. Yuan and H. Pan (2005). Luminescence effect of silver nanoparticle in water phase. *Spectrochim. Acta A*, **61**: 2488.
- [Klaus99] T. Klaus, R. Joerger, E. Olsson and C.-G. Granqvist (1999). Silver-based crystalline nanoparticles, microbially fabricated. *Proc. Natl. Acad. Sci. USA*, **96**: 13611.
- [KneippJ06] J. Kneipp, H. Kneipp and K. Kneipp (2006). Two-photon vibrational spectroscopy for biosciences based on surface-enhanced hyper-Raman scattering. *Proc. Natl. Acad. Sci. USA*, **103**: 17149.
- [KneippK99] K. Kneipp, H. Kneipp, I. Itzkan, R. R. Dasari and M. S. Feld (1999). Ultrasensitive chemical analysis by Raman spectroscopy. *Chem. Rev.*, **99**: 2957.
- [KneippK97] K. Kneipp, Y. Wang, H. Kneipp, L. T. Perelman, I. Itzkan, R. Dasari and M. S. Feld (1997). Single molecule detection using surface-enhanced Raman scattering (SERS). *Phys. Rev. Lett.*, **78**: 1667.
- [Konig96] L. König, I. Rabin, W. Schulze and G. Ertl (1996). Chemiluminescence in the agglomeration of metal clusters. *Science*, **274**: 1353.
- [Kooij06] E. S. Kooij and B. Poelsema (2006). Shape and size effects in the optical properties of metallic nanorods. *Phys. Chem. Chem. Phys.*, **8**: 3349.
- [Kreibig95] U. Kreibig and M. Vollmer (1995). *Optical Properties of Metal Clusters*. Springer, Berlin.
- [Krichevsky02] O. Krichevsky and G. Bonnet (2002). Fluorescence correlation spectroscopy: the technique and its applications. *Rep. Prog. Phys.*, **65**: 251.
- [Krutyakov08] Y. A. Krutyakov, A. A. Kudrinskiy, A. Y. Olenin and G. V. Lisichkin (2008). Synthesis and properties of silver nanoparticles: Achievements and prospects. *Uspekhi Khimii*, **77**: 242.
- [Kuno01a] M. Kuno, D. P. Fromm, A. Gallagher, D. J. Nesbitt, O. I. Micic and A. J. Nozik (2001). Fluorescence intermittency in single InP quantum dots. *Nano Lett.*, **1**: 557.
- [Kuno00] M. Kuno, D. P. Fromm, H. F. Hamann, A. Gallagher and D. J. Nesbitt (2000). Nonexponential "blinking" kinetics of single CdSe quantum dots: A universal power law behavior. *J. Chem. Phys.*, **112**: 3117.

- [Kuno01b] M. Kuno, D. P. Fromm, H. F. Hamann, A. Gallagher and D. J. Nesbitt (2001). "on"/"off" fluorescence intermittency of single semiconductor quantum dots. *J. Chem. Phys.*, **115**: 1028.
- [Lakowicz05] J. R. Lakowicz (2005). Radiative decay engineering 5: metal-enhanced fluorescence and plasmon emission. *Anal. Biochem.*, **337**: 171.
- [Lakowicz06] J. R. Lakowicz (2006). Plasmonics in biology and plasmon-controlled fluorescence. *Plasmonics*, **1**: 5.
- [Larkin04] I. A. Larkin, M. I. Stockman, M. Achermann and V. I. Klimov (2004). Dipolar emitters at nanoscale proximity of metal surfaces: Giant enhancement of relaxation in microscopic theory. *Phys. Rev. B*, **69**: 121403.
- [Laven08] P. Laven (2008). *MiePlot*. The software can be obtained from www.philiplaven.com.
- [LeeK07] K. J. Lee, P. D. Nallathamby, L. M. Browning, C. J. Osgood and X.-H. N. Xu (2007). In vivo imaging of transport and biocompatibility of single silver nanoparticles in early development of zebrafish embryos. *ACS Nano*, **1**: 133.
- [LeeP82] P. C. Lee and D. Meisel (1982). Adsorption and surface-enhanced Raman of dyes on silver and gold sols. *J. Phys. Chem.*, **86**: 3391.
- [Link00] S. Link and M. A. El-Sayed (2000). Shape and size dependence of radiative, non-radiative and photothermal properties of gold nanocrystals. *Int. Rev. Phys. Chem.*, **19**: 409.
- [Mafune00] F. Mafune, J. Kohno, Y. Takeda, T. Kondow and H. Sawabe (2000). Formation and size control of silver nanoparticles by laser ablation in aqueous solution. *J. Phys. Chem. B*, **104**: 9111.
- [Mahoney80] M. R. Mahoney, M. W. Howard and R. P. Cooney (1980). Carbon-dioxide conversion to hydrocarbons at silver electrode surfaces - Raman-spectroscopic evidence for surface carbon intermediates. *Chem. Phys. Lett.*, **71**: 59.
- [Maliwal03] B. P. Maliwal, J. Malicka, I. Gryczynski, Z. Gryczynski and J. R. Lakowicz (2003). Fluorescence properties of labeled proteins near silver colloid surfaces. *Biopolymers*, **70**: 585.
- [Margolin04] G. Margolin and E. Barkai (2004). Aging correlation functions for blinking nanocrystals, and other on-off stochastic processes. *J. Chem. Phys.*, **121**: 1566.
- [Margolin06] G. Margolin and E. Barkai (2006). Nonergodicity of a time series obeying Lévy statistics. *J. Stat. Phys.*, **122**: 137.
- [Maruyama04] Y. Maruyama, M. Ishikawa and M. Futamata (2004). Thermal activation of blinking in SERS signal. *J. Phys. Chem. B*, **108**: 673.
- [Messin01] G. Messin, J. P. Hermier, E. Giacobino, P. Desbiolles and M. Dahan (2001). Bunching and antibunching in the fluorescence of semiconductor nanocrystals. *Opt. Lett.*, **26**: 1891.
- [Mueller05] J. Müller, J. M. Lupton, A. L. Rogach, J. Feldmann, D. V. Talapin and H. Weller (2005). Monitoring surface charge migration in the spectral dynamics of single CdSe/CdS nanodot/nanorod heterostructures. *Phys. Rev. B*, **72**: 205339.
- [Mooradian69] A. Mooradian (1969). Photoluminescence of metals. *Phys. Rev. Lett.*, **22**: 185.
- [Moyer00] P. J. Moyer, J. Schmidt, L. M. Eng and A. J. Meixner (2000). Surface-enhanced Raman scattering spectroscopy of single carbon domains on individual Ag nanoparticles on a 25 ms time scale. *J. Am. Chem. Soc.*, **122**: 5409.
- [Mukherjee01] P. Mukherjee, A. Ahmad, D. Mandal, S. Senapati, S. R. Sainkar, M. I. Khan, R. Parishcha, P. V. Ajaykumar, M. Alam, R. Kumar and M. Sastry (2001). Fungus-mediated synthesis of silver nanoparticles and their immobilization in the mycelial matrix: A novel biological approach to nanoparticle synthesis. *Nano Lett.*, **1**: 515.
- [Murray84] C. A. Murray and S. Bodoff (1984). Depolarization effects in raman scattering from monolayers on surfaces: The classical microscopic local field. *Phys. Rev. Lett.*, **52**: 2273.

- [Narayanan08] S. S. Narayanan and S. K. Pal (2008). Structural and functional characterization of luminescent silver-protein nanobioconjugates. *J. Phys. Chem. C*, **112**: 4874.
- [Nie97] S. Nie and S. Emery (1997). Probing single molecules and single nanoparticles by surface-enhanced Raman scattering. *Science*, **275**: 1102.
- [OConnor84] D. V. O'Connor and D. Phillips (1984). *Time Correlated Single Photon Counting*. Academic Press, London.
- [Otto02] A. Otto (2002). What is observed in single molecule SERS, and why? *J. Raman Spectrosc.*, **33**: 593.
- [Pelton04] M. Pelton, D. Grier and P. Guyot-Sionnest (2004). Characterizing quantum-dot blinking using noise power spectra. *Appl. Phys. Lett.*, **85**: 819.
- [Petrov09] E. P. Petrov, C. Bläul and P. Schwill (2009). Memory in blinking dynamics of silver nanoparticles. In V. E. Borisenko, V. S. Gurin and S. V. Gaponenko, editors, *Physics, Chemistry and Application of Nanostructures*. World Scientific, Singapore.
- [Pettinger81] B. Pettinger, M. R. Philpott and I. Joseph G. Gordon (1981). Contribution of specifically adsorbed ions, water, and impurities to the surface enhanced Raman spectroscopy (SERS) of Ag electrodes. *J. Chem. Phys.*, **74**: 934.
- [Peysers02] L. A. Peysers, T.-H. Lee and R. M. Dickson (2002). Mechanism of Ag_n nanocluster photoproduction from silver oxide films. *J. Phys. Chem. B*, **106**: 7725.
- [Peysers01] L. A. Peysers, A. E. Vinson, A. P. Bartko and R. M. Dickson (2001). Photoactivated fluorescence from individual silver nanoclusters. *Science*, **291**: 103.
- [Rabin98] I. Rabin, W. Schulze and G. Ertl (1998). Light emission during the agglomeration of silver clusters in noble gas matrices. *J. Chem. Phys.*, **108**: 5137.
- [Richards08] C. I. Richards, S. Choi, J.-C. Hsiang, Y. Antoku, T. Vosch, A. Bongiorno, Y.-L. Tzeng, and R. M. Dickson (2008). Oligonucleotide-stabilized Ag nanocluster fluorophores. *J. Am. Chem. Soc.*, **130**: 5038.
- [Righini05] G. C. Righini and M. Ferrari (2005). Photoluminescence of rare-earth-doped glasses. *Riv. Nuovo Cimento*, **28**: 1.
- [Schaefer06] S. Schäfer (2006). *Fluorescence imaging microscopy studies on single molecule diffusion and photophysical dynamics*. Ph.D. thesis, Technische Universität Dresden.
- [Schrieffer05] J. Schrieffer, M. C. D. Carpentier and P. Degiovanni (2005). Dephasing by a nonstationary classical intermittent noise. *Phys. Rev. B*, **72**: 035328.
- [Schwill01a] P. Schwill (2001). Personal communication to E. P. Petrov.
- [Schwill01b] P. Schwill (2001). Fluorescence correlation spectroscopy and its potential for intracellular applications. *Cell. Biochem. Biophys.*, **34**: 383.
- [Sengupta08] B. Sengupta, C. M. Ritchie, J. G. Buckman, K. R. Johnsen, P. M. Goodwin and J. T. Petty (2008). Base-directed formation of fluorescent silver clusters. *J. Phys. Chem. C*, **112**: 18776.
- [Shalaev98] V. M. Shalaev and A. K. Sarychev (1998). Nonlinear optics of random metal-dielectric films. *Phys. Rev. B*, **57**: 13265.
- [Shang08] L. Shang and S. Dong (2008). Silver nanocluster-based fluorescent sensors for sensitive detection of Cu(II). *J. Mater. Chem.*, **18**: 4636.
- [Sharaabi05] Y. Sharaabi, T. Shegai and G. Haran (2005). Two-state analysis of single-molecule Raman spectra of crystal violet. *Chem. Phys.*, **318**: 44.
- [Shiavi07] R. Shiavi (2007). *Applied statistical signal analysis*. Academic Press.
- [Shimizu01] K. T. Shimizu, R. G. Neuhauser, C. A. Leatherdale, S. A. Empedocles, W. K. Woo and M. G. Bawendi (2001). Blinking statistics in single semiconductor nanocrystal quantum dots. *Phys. Rev. B*,

- [Siwach08] O. P. Siwach and P. Sen (2008). Fluorescence properties of Ag nanoparticles in water. *Spectrochim. Acta A*, **69**: 659.
- [Slistan08] A. Slistan-Grijalva, R. Herrera-Urbina, J. F. Rivas-Silva, M. Ávalos Borja, F. F. Castellón-Barraza and A. Posada-Amarillas (2008). Synthesis of silver nanoparticles in a polyvinylpyrrolidone (PVP) paste, and their optical properties in a film and in ethylene glycol. *Mat. Res. Bull.*, **43**: 90.
- [Smitha08] S. Smitha, K. Nissamudeen, D. Philip and K. Gopchandran (2008). Studies on surface plasmon resonance and photoluminescence of silver nanoparticles. *Spectrochim. Acta A*, **71**: 186.
- [Stefani05a] F. D. Stefani, W. Knoll, M. Kreiter, X. Zhong and M. Y. Han (2005). Quantification of photoinduced and spontaneous quantum-dot luminescence blinking. *Phys. Rev. B*, **72**: 125304.
- [Stefani05b] F. D. Stefani, X. Zhong, W. Knoll, M. Han and M. Kreiter (2005). Memory in quantum-dot photoluminescence blinking. *New J. Phys.*, **7**: 197.
- [Steinmann63] W. Steinmann (1963). Optical plasma resonances in solids. *Phys. Stat. Sol.*, **28**: 437.
- [Tang05] J. Tang and R. A. Marcus (2005). Single particle versus ensemble average: From power-law intermittency of a single quantum dot to quasistretched exponential fluorescence decay of an ensemble. *J. Chem. Phys.*, **123**: 204511.
- [Treguer05] M. Treguer, F. Rocco, G. Lelong, A. L. Nestour, T. Cardinal, A. Maali and B. Lounis (2005). Fluorescent silver oligomeric clusters and colloidal particles. *Solid State Sci.*, **7**: 812.
- [Trukhin04] A. Trukhin, J. Jansons and K. Truhins (2004). Luminescence of silica glass containing aluminum oxide. *J. Non-Cryst. Solids*, **347**: 80.
- [Valeur06] B. Valeur (2006). *Molecular Fluorescence*. Wiley-VCH.
- [Verberk03] R. Verberk and M. Orrit (2003). Photon statistics in the fluorescence of single molecules and nanocrystals: Correlation functions versus distributions of on- and off-times. *J. Chem. Phys.*, **119**: 2214.
- [Verberk02] R. Verberk, A. van Oijen and M. Orrit (2002). Simple model for the power-law blinking of single semiconductor nanocrystals. *Phys. Rev. B*, **66**: 233202.
- [Vosch07] T. Vosch, Y. Antoku, J.-C. Hsiang, C. I. Richards, J. I. Gonzalez and R. M. Dickson (2007). Strongly emissive individual DNA-encapsulated Ag nanoclusters as single-molecule fluorophores. *Proc. Natl. Acad. Sci. USA*, **104**: 12616.
- [Vosgroene05] T. Vosgröne, A. Meixner, A. Anders, H. Dietz, G. Sandmann and W. Plieth (2005). Electrochemically deposited silver particles for surface enhanced Raman spectroscopy. *Surface Sci.*, **597**: 102.
- [Wang05] Z. J. Wang and L. J. Rothberg (2005). Origins of blinking in single-molecule Raman spectroscopy. *J. Phys. Chem. B*, **109**: 3387.
- [Weiss01] A. Weiss and G. Haran (2001). Time-dependent single-molecule Raman scattering as a probe of surface dynamics. *J. Phys. Chem. B*, **105**: 12348.
- [Weisstein06] E. W. Weisstein (2008). *Random Number*. From MathWorld—A Wolfram Web Resource.
- [Weitz83] D. A. Weitz, S. Garoff, J. I. Gersten and A. Nitzan (1983). The enhancement of Raman scattering, resonance Raman scattering, and fluorescence from molecules adsorbed on a rough silver surface. *J. Chem. Phys.*, **78**: 5324.
- [West97] R. W. West and R. T. Ogden (1997). Continuous-time estimation of a change-point in a Poisson process. *J. Stat. Comput. Simulation*, **56**: 293.
- [Wu08] X. Wu and E. K. L. Yeow (2008). Fluorescence blinking dynamics of silver nanoparticle and silver nanorod films. *Nanotechnology*, **19**: 035706.
- [Wustholz08] K. L. Wustholz, E. D. Bott, B. Kahr and P. J. Reid (2008). Memory and spectral diffusion in

- single-molecule emission. *J. Phys. Chem. C*, **112**: 7877.
- [Xu00] H. X. Xu, J. Aizpurua, M. Kall and P. Apell (2000). Electromagnetic contributions to single-molecule sensitivity in surface-enhanced Raman scattering. *Phys. Rev. E*, **62**: 4318.
- [Yang09] W. Yang, C. Shen, Q. Ji, H. An, J. Wang, Q. Liu and Z. Zhang (2009). Food storage material silver nanoparticles interfere with DNA replication fidelity and bind with DNA. *Nanotechnology*, **20**: 085102.
- [Yeow06] E. K. L. Yeow, S. M. Melnikov, D. M. Bell, F. C. D. Schryver and J. Hofkens (2006). Characterizing the fluorescence intermittency and photobleaching kinetics of dye molecules immobilized on a glass surface. *J. Phys. Chem. A*, **110**: 1726.
- [Yin03] B. Yin, H. Ma, S. Wang and S. Chen (2003). Electrochemical synthesis of silver nanoparticles under protection of poly(N-vinylpyrrolidone). *J. Phys. Chem. B*, **107**: 8898.
- [Yip98] W. Yip, D. Hu, J. Yu, D. Vanden Bout and P. Barbara (1998). Classifying the photophysical dynamics of single- and multiple-chromophoric molecules by single molecule spectroscopy. *J. Phys. Chem. A*, **102**: 7564.
- [YuJ08] J. Yu, S. Choi, C. I. Richards, Y. Antoku and R. M. Dickson (2008). Live cell surface labeling with fluorescent Ag nanocluster conjugates. *Photochem. Photobiol.*, **84**: 1435.
- [YuM06] M. Yu and A. V. Orden (2006). Enhanced fluorescence intermittency of CdSe-ZnS quantum-dot clusters. *Phys. Rev. Lett.*, **97**: 237402.
- [Zeman87] E. J. Zeman, K. T. Carron, G. C. Schatz and R. P. V. Duyne (1987). A surface enhanced resonance raman study of cobalt phthalocyanine on rough ag films: Theory and experiment. *J. Chem. Phys.*, **87**: 4189.
- [ZhangA08] A. Zhang, J. Zhang and Y. Fangb (2008). Photoluminescence from colloidal silver nanoparticles. *J. Lum.*, **128**: 1635.
- [ZhangK06] K. Zhang, H. Chang, A. Fu, A. P. Alivisatos and H. Yang (2006). Continuous distribution of emission states from single CdSe/ZnS quantum dots. *Nano Lett.*, **6**: 843.
- [Zhu97] Y. Zhu, Y. Qian, X. Li and M. Zhang (1997). γ -radiation synthesis and characterization of polyacrylamide-silver nanocomposites. *Chem. Commun.*, p. 1081.

Acknowledgements

First of all I would like to thank Prof. Petra Schwille for accepting me as diploma student in her group. I have enjoyed the freedom and the many possibilities in the group.

I want to thank Dr. Eugene Petrov for countless contributions to my development. He successfully grew me into a physicist.

Also, I thank Prof. Lukas Eng for the interest in my work.

Furthermore, I want to express my gratitude to Mr. Kevin Manygoats and Dr. Wolfgang Tirschler for donating their time and letting my use their electron microscopes.

I am grateful for the support and the interest from all members of the Schwille group, especially Dr. Zdenek Petrášek, Dipl. phys. Markus Burkhardt but also Karin Crell, Ellen Sieber and Anke Borrmann for their patience.

Selbstständigkeitserklärung

Hiermit erkläre ich, dass ich die von mir am heutigen Tage dem Prüfungsausschuss der Fakultät Physik eingereichte Diplomarbeit zum Thema “Fluorescence microscopy of colloidal silver nanoparticles immobilized on a glass surface: Emission spectra, power-law blinking and memory in the intermittent emission intensity” vollkommen selbstständig verfasst und keine anderen als die angegebenen Quellen und Hilfsmittel benutzt, sowie Zitate kenntlich gemacht habe.

Dresden, den 23. 4. 2009

Unterschrift

I herewith declare that I have produced this thesis without the prohibited assistance of third parties and without making use of aids other than those specified; notions taken over directly or indirectly from other sources have been identified as such.

This thesis has not been previously presented in identical or similar form to any other German or foreign examination board.

Printed April 23, 2009.